EVOLUTION OF ECLOGITE FACIES METAMORPHISM IN THE ST. CYR KLIPPE, YUKON-TANANA TERRANE, YUKON, CANADA

by

Meredith Blair Petrie

A thesis submitted in partial fulfillment
of the requirements for the Doctor of
Philosophy degree in Geoscience
in the Graduate College of
The University of Iowa

May 2014

Thesis Supervisor: Professor Jane A. Gilotti

Graduate College
The University of Iowa
Iowa City, Iowa

CERTIFICATE OF APPROVAL

_____

PH.D. THESIS

_____

This is to certify that the Ph.D. thesis of

Meredith Blair Petrie

has been approved by the Examining Committee
for the thesis requirement for the Doctor of Philosophy
degree in Geoscience at the May 2014 graduation.

Thesis Committee: _____
Jane A. Gilotti, Thesis Supervisor

_____
William C. McClelland

_____
Ingrid Ukstins Peate

_____
Cees R. van Staal

_____
David A. Bennett

To my dad, Philip Petrie, for inspiring my love of science

ACKNOWLEDGMENTS

I would like to thank the following individuals and research groups for all the assistance that made my research possible: My committee members; Dr. Sarah Roeski and Nick Botto, University of California, Davis, Microprobe Facility; Dr. Joseph Wooden of the SUMAC SHRIMP RG lab; Dr. Hans-Joachim Massonne and Dr. Thomas Theye at the Institute for Mineralogy and Crystal Chemistry at the University of Stuttgart, Stuttgart, Gemany; my field assistants Jacob Stewart and Dylan Cook; Siarra Isard for XRD analyses and her beautiful map; my fellow graduate students at the University of Iowa; my family for supporting me through these many years of school; and my husband, Jaime Ricci, for all of his encouragement, support, and love over the last 10 years.

I would also like to acknowledge the following sources of logistical and financial support that made my research possible: Dr. Maurice Colpron and staff at the Yukon Geological Survey, the Geological Survey of Canada, The National Science Foundation, Geological Society of America, the Alliances for Graduate Education and the Professoriate Fellowship, and the Department of Earth and Environmental Sciences, University of Iowa.

ABSTRACT

The St. Cyr klippe hosts well preserved to variably retrogressed eclogites found as sub-meter to hundreds of meter scale lenses within quartzofeldspathic schists in the Yukon-Tanana terrane, Canadian Cordillera. The St. Cyr area consists of structurally imbricated, polydeformed, and polymetamorphosed units of continental arc and oceanic crust. The eclogite-bearing quartzofeldspathic schists form a 30 by 6 kilometer thick, northwest-striking, coherent package. The schists consist of metasediments and felsic intrusives that are intercalated on the tens of meter scale. The presence of phengite and Permian age zircon crystallized under eclogite facies metamorphic conditions indicates that the eclogite was metamorphosed *in situ* with its quartzofeldspathic host.

I investigated the metamorphic evolution of the eclogite-facies rocks in the St. Cyr klippe using isochemical phase equilibrium thermodynamic (pseudosection) modeling. I constructed *P–T* pseudosections in the system Na_2O-K_2O-CaO-FeO-O_2-MnO-MgO-Al_2O_3-SiO_2-TiO_2-H_2O for the bulk-rock composition of an eclogite and a host metatonalite. In combination with petrology and mineral compositions, St. Cyr eclogites followed a five-stage clockwise *P–T* path. Peak pressure conditions for the eclogites and metatonalites reached up to 3.2 GPa, well within the coesite stability field, indicating the eclogites reached ultrahigh-pressure conditions. Decompression during exhumation occurred with a corresponding temperature increase.

SHRIMP-RG zircon dating shows that the protolith of the eclogites formed within the Yukon-Tanana terrane during early, continental arc activity, between 364 and 380 Ma, while the metatonalite protolith formed at approximately 334 Ma, during the Little Salmon Cycle of the Klinkit phase of Yukon-Tanana arc activity. Both the eclogites and

the metatonalites were then subducted to mantle depths and metamorphosed to ultrahigh-pressure conditions during the late Permian, between 266 and 271 Ma. The results of our study suggest portions of the Yukon-Tanana terrane were subducted to high-pressure and ultrahigh-pressure conditions. This is the first report of ultrahigh-pressure metamorphism in the accreted terranes of the North American Cordillera. Petrological, geochemical, geochronological, and structural relationships link the eclogites at St. Cyr to other eclogite localities in Yukon, indicating the high-pressure assemblages form a larger lithotectonic unit within the Yukon-Tanana terrane.

TABLE OF CONTENTS

LIST OF TABLES

LIST OF FIGURES

CHAPTER 1.

INTRODUCTION

High-pressure (HP) and ultrahigh-pressure (UHP) metamorphic rocks occur in many collisional orogenic belts throughout the world (e.g. Chopin, 2003; Agard et al. 2009; Liou et al., 2009). They form within the subduction channel during ocean-continent collisions (Pacific-Type; Fig. 1-1a) or continent-continent (Alpine-type; Fig. 1-1b) collisions, and thus provide insight into subduction zone processes (Ernst, 2005). HP rocks are those that have reached a minimum of ± 1.2 GPa and (±) 400 °C (approximately 40 km; Ernst, 2010), while UHP rocks are those that contain coesite, and/or microdiamonds as index minerals, commonly preserved as inclusions in garnet or zircon (Gilotti, 2013 and references therein). The presence of coesite and microdiamond is evidence that the rocks reached minimum pressures of 3 to 4 GPa at depths of 100 km or more. HP and UHP assemblages may follow a variety of different pressure-temperature (*P–T*) paths during their evolution, as shown by Fig. 1-2. HP and UHP rocks are found as blocks within tectonic mélange (e.g. Franciscan; Ernst, 1988; Aalto, 2014), ductilely deformed, relatively thin nappes (e.g. Sanbagawa; Enami, 1998; Matsumoto et al., 2003) and massive, coherent slices of continental crust (e.g. Dabie-Sulu belt, China; Zhang et al., 2009; Liou et al., 2012).

HP and UHP metamorphism are evidenced by the occurrence of eclogite, a garnet and pyroxene-bearing rock that is mainly formed from a basaltic protolith at high pressure conditions (see Godard, 2001 for a retrospective). Eclogite *sensu stricto* is a rock composed of omphacite (Na-rich clinopyroxene) + almandine-pyrope-grossular-garnet (Coleman et al., 1965; Carswell, 1990). At eclogite facies *P–T* conditions, plagioclase is not stable and the albite (Na) component substitutes for Ca in pyroxene (Harley and Carswell, 1990). Accessory phases may include rutile, clinozoisite, kyanite, phengite and titanite (Coleman et al., 1965). In general, the recrystallization of a

metabasite under HP-UHP conditions can be expressed as: plagioclase + clinopyroxene ± olivine ± orthopyroxene = omphacite + garnet ± quartz (Mottana et al., 1990).

The protolith metabasite for subduction-related eclogites (i.e. Pacific-type) can be derived from multiple sources: (1) the downgoing oceanic slab (including attached seamounts and overlying pelagic sediments; Maruyama et al., 1996; Agard et al. 2009; Anderson and Moecher, 2009), (2) basaltic dikes and/or underplated basaltic material from the overriding plate that was scraped, plucked, or eroded from the hanging wall and incorporated into the subduction channel (Clift and Vannucchi, 2004; von Huene et al., 2004), and (3) island arc, microcontinent, and/or passive margin rocks situated on the downgoing slab entrained into the subduction channel (Ernst, 2001, 2006, 2010; Chopin, 2003; Agard et al., 2009).

Large, coherent areas of continental crust can be involved in HP and UHP metamorphism (Chopin, 2003; Gilotti, 2013). Detailed *in situ* U-Pb zircon dating, trace element and stable isotope data have shown that many, typically more felsic host-rocks share the same metamorphic history as that of the HP and UHP rocks (e.g. Rumble et al., 2000; Liu et al., 2009; Schertl and Sobolev, 2013). Coesite- and microdiamond-bearing zircons from felsic host-rocks show that these rocks have also seen HP and UHP conditions, even though they are now composed of much lower-grade mineral assemblages (Liu et al., 2009). These data suggest that large coherent metamorphic terrane can be subjected to the same HP or UHP conditions, and that they are seldom a mixture of UHP and lower-pressure rocks. An outstanding example is the Sulu terrane in China, where all lithologies from a 5 km long drill core contain coesite and, thus, demonstrate that the entire section reached UHP conditions (Liu et al., 2009).

Eclogite-Facies Assemblages in the St. Cyr Klippe, Yukon-Tanana Terrane, Yukon, Canada

HP metamorphic assemblages formed during Pacific-type convergence occur from Alaska to Mexico along the western North American margin (Fig. 1-3; Erdmer et al., 1998). Most of these HP assemblages are found as blocks within tectonic mélanges, i.e. a large, mappable body consisting of a disordered mixture of rocks of various sizes, ages, lithologies, and origins, tumbled together within a fine-grained deformed matrix (Blake and Jones, 1974; Silver and Beutner, 1980). Mélanges are created from materials scraped off the top of the downward moving oceanic plate in a subduction zone, and contain mostly deformed marine sediments and ocean-floor basalts (Silver and Beutner, 1980; Aalto, 1981).

The St. Cyr klippe of the Yukon-Tanana terrane (YTT) preserves eclogite-facies assemblages that record Pacific-type subduction in the Canadian Cordillera (Tempelman-Kluit, 1977; 1979; Creaser et al., 1997; Erdmer et al., 1998). The eclogites in the St. Cyr klippe are different from the majority of eclogites found within the Cordillera because they primarily reside in coherent continental crust. Previous studies concluded that St. Cyr eclogites document the subduction of the Slide Mountain Ocean back-arc basin beneath the eastern margin of the Yukon-Tanana arc in the Late Permian (Templeman-Kluit, 1977; 1979). Yet their association with continental rocks suggests that the St. Cyr eclogites are derived from the Yukon-Tanana arc. Therefore, the relationships between the St. Cyr eclogite-facies rocks and the arc and back-arc remain unclear due to the lack of unambiguous evidence tying the St. Cyr eclogites to either the overriding or the subducting plate.

The Yukon-Tanana Terrane

The YTT represents a major peri-Laurentian cratonic block of the Canadian Cordillera in Yukon and Alaska (Fig. 1-3). In western and southern Yukon, the YTT

consists of a variably metamorphosed and deformed, Mid- to Late Paleozoic arc-forearc system built upon a sliver(s) of continental crust rifted from western North America (Tempelman-Kluit, 1979; Nelson et al., 2006; Berman et al., 2007; Colpron et al., 2007; Nelson et al., 2013). Three Late Devonian to Late Permian, distinct volcanic and volcaniclastic assemblages—the Finlayson, Klinkit, and Klondike—are built upon Neoproterozoic to pre-Early Devonian metasedimentary basement known as the Snowcap assemblage (Fig. 1-4; Mortensen 1992; Colpron et al., 2006a; 2006b; Piercey et al. 2002; Piercey et al., 2006; Piercey and Colpron, 2009; Piercey et al., 2012). The Yukon-Tanana composite arc is thought to have co-evolved with the opening of a back-arc basin, or basins, represented by an oceanic assemblage of chert, argillite, and mafic volcanic rocks, referred to as the Slide Mountain Ocean terrane (Fig. 1-4; Mortensen, 1992; Nelson, 1993; Nelson et al., 2006; Colpron et al., 2006a; Piercey et al., 2006; Piercey et al., 2012).

Several localities in the YTT preserve eclogite facies assemblages (Fig. 1-5; Erdmer et al., 1998). These assemblages were interpreted to record either multiple subduction zone complexes or episodic exhumation of deeply subducted rocks above a single subduction zone during continuous convergence (Erdmer et al., 1998). The Simpson Range and Stewart Lake areas contain eclogite or retrogressed eclogite that record evidence of Mid-Mississippian eclogite-facies metamorphism (Creaser et al, 1999; Devine et al., 2006). These HP mafic bodies are interpreted to have formed within a tectonic mélange with serpentinized ultramafic and gabbroic rocks and low-grade basalt, chert, limestone, chlorite-schist (Erdmer, 1987; Erdmer et al., 1998; Devine et al., 2006). Permian age eclogites occur in pre-metamorphic contact with their quartzofeldspathic hosts in the St. Cyr klippe, Ross River, Faro, and Last Peak (Erdmer and Armstrong, 1989; Creaser et al., 1997; Erdmer et al., 1998). These enigmatic eclogites, particularly in the St. Cyr area, are the focus of this study.

The St. Cyr Klippe

Eclogite, garnet amphibolite and low-grade mafic and ultramafic rocks in the St. Cyr klippe were originally characterized as part of a tectonic mélange (Tempelman-Kluit, 1979; Wheeler and McFeely, 1991). This mélange was postulated to have formed within subducting back-arc basin crust. However, the high pressures attained by metabasites and the penetrative fabrics they share with their quartzofeldspathic host rocks contrast with the weak deformation and low metamorphic grade that generally characterize the Slide Mountain Ocean assemblage (Colpron et al., 2006a). Eclogite in the St. Cyr klippe is found as lenses within quartzofeldspathic schists that share lithological and metamorphic relationships with the YTT. This discrepancy has led to the hypothesis that the Permian eclogites comprise a crustal component of the Yukon-Tanana composite arc. Uncertainty in the origin of the eclogite-facies assemblage hampers efforts to place the St. Cyr klippe into its regional tectonic context. If the St. Cyr eclogite-facies assemblage is derived from the Yukon-Tanana composite arc, then it was part of the overriding plate in a subduction margin, and a mechanism for generating eclogite-facies rocks in the overriding Yukon-Tanana arc (rather than the downgoing oceanic crust) is required.

Purpose of the Study

The overarching goal of this study is to test the hypothesis that the St. Cyr area is a fragment of the YTT subducted to eclogite-facies conditions. The objectives of this study are to (1) determine if the eclogite facies assemblages in the St. Cyr klippe are part of a tectonic mélange or are coherent slices of hanging wall Yukon-Tanana arc crust, (2) document the extent of eclogite-facies metamorphism in the St. Cyr klippe and determine the protoliths of eclogites and quartzofeldspathic host rocks, (3) establish the metamorphic and geochronologic evolution of eclogite in the St. Cyr klippe in an effort to reconstruct the evolution of subduction and exhumation within the YTT, and (4) to

elucidate the *P–T* evolution of eclogite-bearing quartzofeldspathic schists in the St. Cyr klippe.

Defining the relationships between the St. Cyr area eclogites and their host rocks in terms of *P–T*–time history will help determine whether these rocks belong to the YTT or not. The data generated by this study will allow us to place the St. Cyr klippe into its larger regional context and test tectonic models for the evolution of the YTT (e.g. Devine et al., 2006; Berman et al., 2007). If the St. Cyr klippe is a portion of deeply subducted YTT crust, the results of this study will lead to the reevaluation of preexisting models of the deep subduction and exhumation of the overriding plate.

Thesis Outline

Chapter 2 presents the results of field mapping in an effort to document the spatial extent of eclogites and their quartzofeldspathic host rocks in the St. Cyr klippe, and the structural relationships among the eclogites, quartzofeldspathic host rocks, and other lithologies within the klippe. Whole rock geochemistry demonstrates the protolith of the eclogites, and petrology and mineral chemistry show that the eclogites and their hosts are part of a coherent unit derived from the YTT. The crystallization and metamorphic ages of the metaigneous rocks are determined by U-Pb zircon geochronology to identify their provenance and show that they were metamorphosed in the eclogite facies. The results show that the St. Cyr eclogite-bearing unit forms slices of Yukon-Tanana arc material subducted as coherent crustal slices. Chapter 3 focuses on the mineral chemistry, petrological observations, metamorphic phase equilibrium calculations, and U-Pb zircon ages for the eclogites in the St. Cyr klippe. Peak and retrograde metamorphic conditions of the eclogites are determined by isochemical phase equilibrium modeling, while U-Pb zircon geochronology is used to document the Permian age of eclogite-facies metamorphism. These results establish the metamorphic and geochronologic evolution of the eclogites in the St. Cyr klippe, the first Permian eclogite locality to be studied in

the YTT in this detail. Chapter 4 presents a petrological and mineralogical study of the eclogite-bearing quartzofeldspathic schists, which are used in concert with metamorphic phase equilibrium calculations to document the *P–T* evolution in the host rocks of the St. Cyr klippe. Comparison of the results with the eclogites leads to a better understanding of the evolution of Yukon-Tanana arc subduction. The results and conclusions of the study, as well as a regional model for eclogite formation and evolution in the YTT, are presented in Chapter 5.

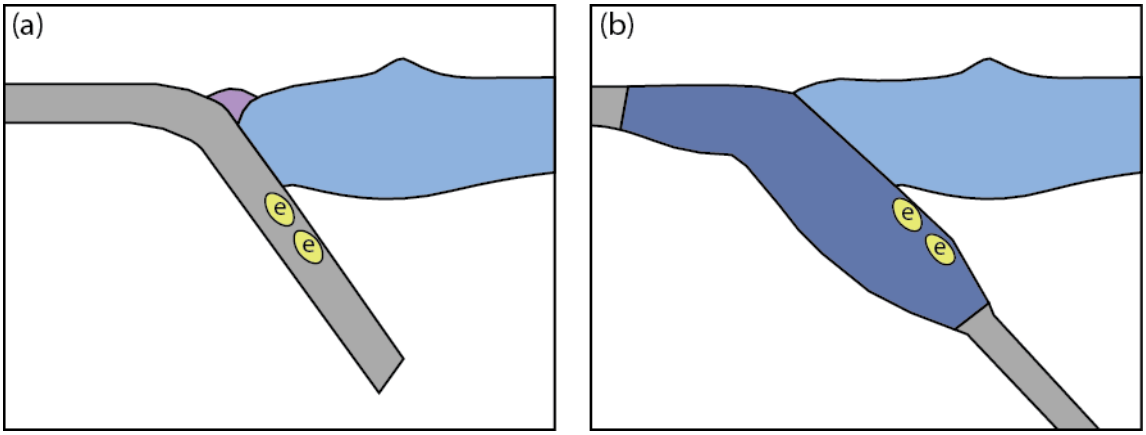

Figure 1-1 Simplified diagrams of convergent margins. (a) Pacific-type, accretionary orogen where eclogites are formed in the subducting slab and returned to the surface within a tectonic mélange. (b) Alpin-type orogen showing eclogites forming within the subducting continental crust.

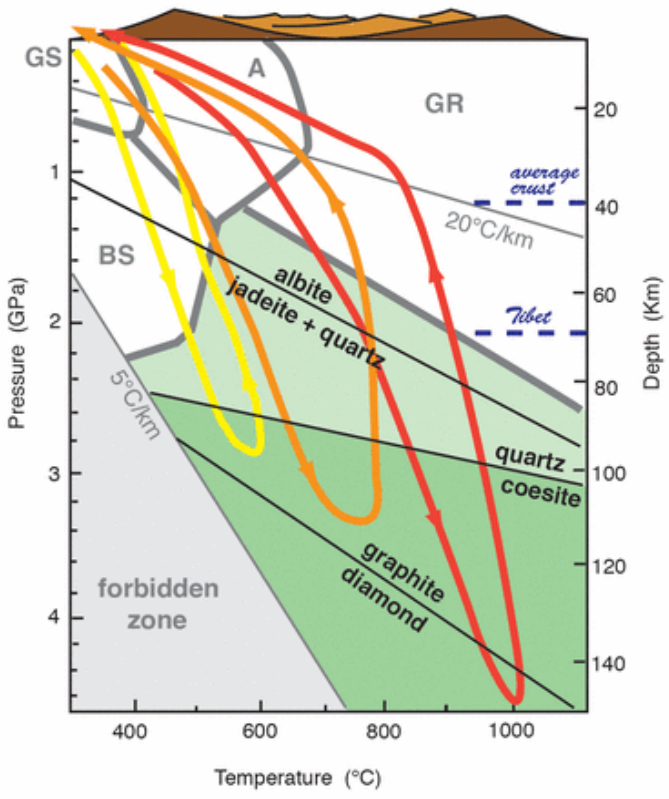

Figure 1-2 Pressure and temperature (*P–T*) space for high-pressure (HP) and ultrahigh-pressure (UHP) metamorphism. From Gilotti (2013). The yellow, orange, and red lines show different *P–T* paths that HP and UHP rocks can follow during subduction and exhumation. Eclogite facies space is shown by the green colors. The light green color represents HP eclogites, while the dark green color represents UHP eclogites. The different metamorphic facies are shown by gray lines. GS, greenschist; BS, blueschist, A, amphibolite; GR granulite facies. The gray region represents the area below the 5 °C geotherm, which is generally not found on Earth.

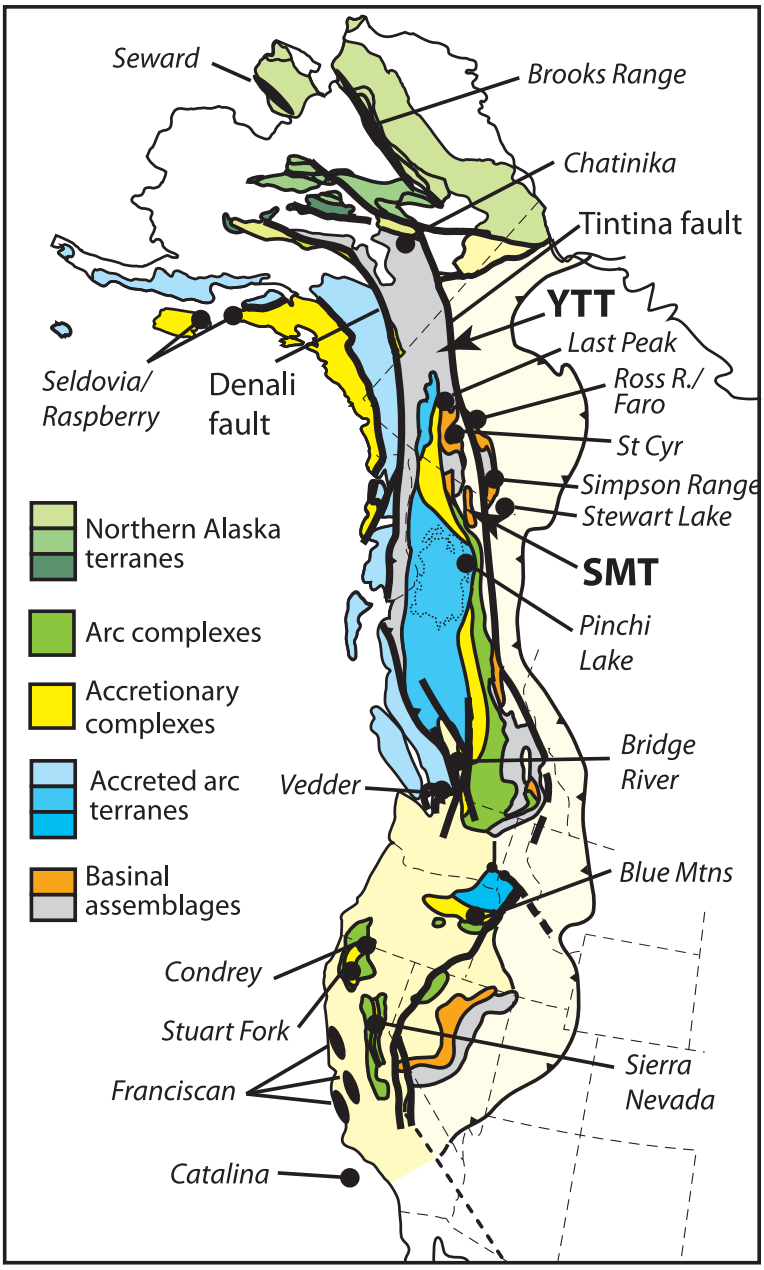

Figure 1-3 Terrane map of the North American Cordillera. Modified from Erdmer et al. (1998), Colpron et al. (2006), and Nelson et al. (2013). Black circles and ovals represent known eclogite facies assemblages along the western North America margin. SMT, Slide Mountain Ocean terrane; YTT, Yukon-Tanana terrane.

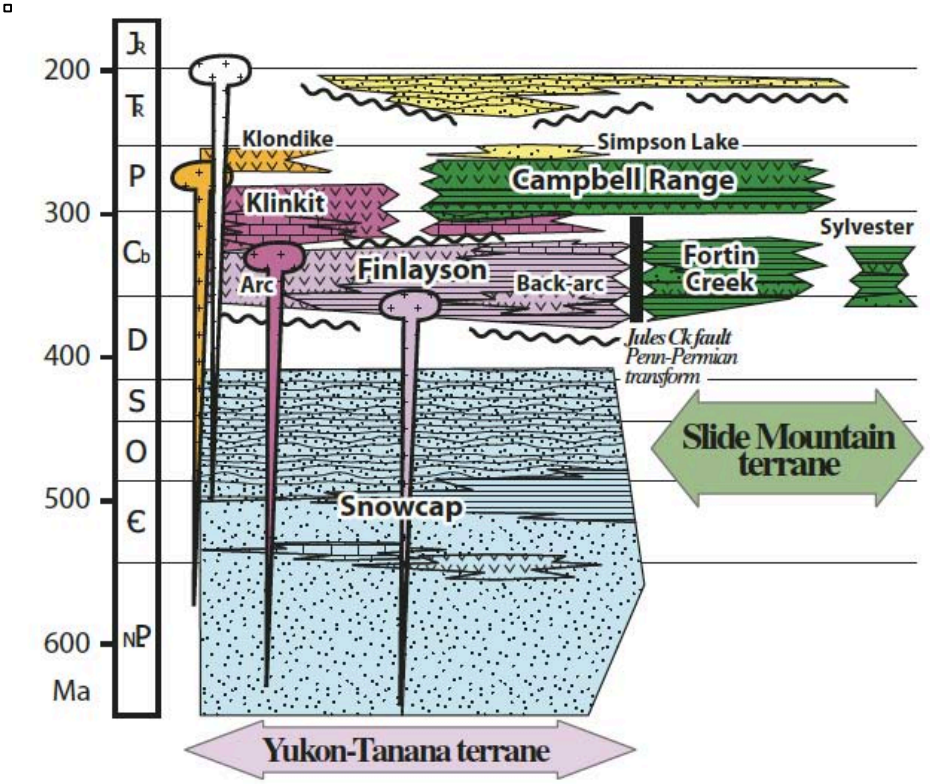

Figure 1-4 Schematic tectonostratigraphic relationships of the Yukon-Tanana and Slide Mountain terranes in the Canadian Cordillera. Modified after Colpron et al., 2007.

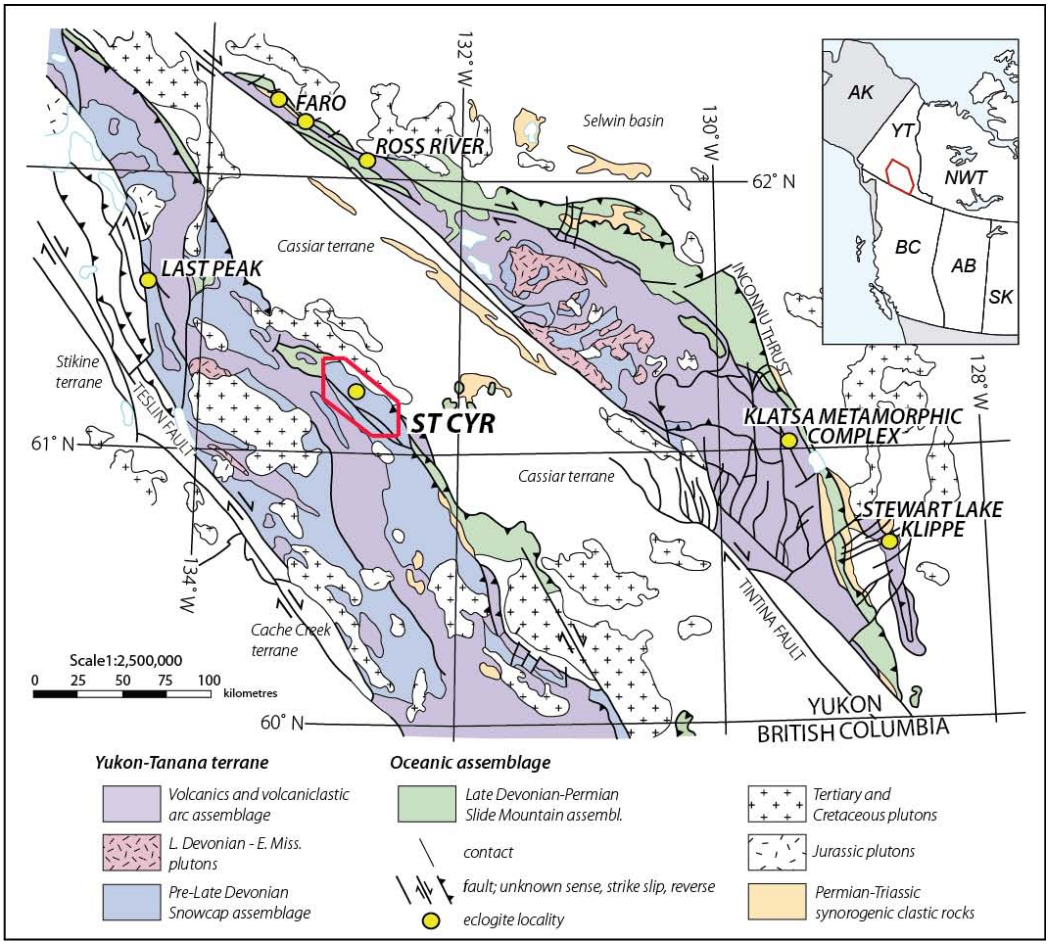

Figure 1-5 Regional geologic map of the Yukon-Tanana and Slide Mountain terrane in south-central Yukon. Modified from Colpron et al. (2006). The red box illustrates the locality of the St. Cyr klippe.

CHAPTER 2.
GEOLOGIC SETTING OF ECLOGITE-FACIES ASSEMBLAGES IN THE ST. CYR KLIPPE, YUKON-TANANA TERRANE, YUKON, CANADA

Abstract

The St. Cyr klippe hosts well preserved to variably retrogressed eclogites found as sub-meter to hundreds of meter scale lenses within quartzofeldspathic schists in Yukon, Canada. The St. Cyr area consists of structurally imbricated, polydeformed, and polymetamorphosed units of continental arc crust and oceanic crust. The eclogite-bearing quartzofeldspathic schists form a 30 by 6 km thick, northwest-striking, coherent package. The schists comprise metasedimentary rocks and felsic intrusives that are intercalated on the meter to tens of meter scale. Ultramafic rocks, serpentinites, and associated greenschist facies gabbros form imbricated tectonic slices within the eclogite-bearing quartzofeldspathic unit, which led to a previously held hypothesis that the eclogites were exhumed within a tectonic mélange. The presence of phengite and Permian age zircon crystallized under eclogite facies metamorphic conditions in the quartzofeldspathic host rocks indicate that the eclogite was metamorphosed *in situ* within a coherent unit. This indicates that the eclogites and their host schists were derived from arc crust of the Yukon-Tanana terrane, rather than the subducting oceanic crust of the Slide Mountain Ocean terrane. Petrological, geochemical, geochronological, and structural relationships link the St. Cyr eclogites to other high-pressure localities Yukon, indicating the high-pressure assemblages form a larger lithotectonic unit within the Yukon-Tanana terrane.

Introduction

High-pressure (HP) metamorphic assemblages formed in Pacific-type convergent margins are found along the western North American margin from Alaska to Mexico

(Erdmer et al., 1998). The Yukon-Tanana terrane (YTT) in the Canadian Cordillera preserves both Mississippian and Permian HP rocks. In southeastern Yukon (Fig. 2-1), strongly retrogressed, Early Mississippian eclogite facies rocks are preserved as pods within a tectonic mélange in the Klatsa metamorphic complex (Devine et al., 2006) and the Stewart Lake klippe (Erdmer, 1987, Erdmer et al., 1998). These HP rocks are inferred to have formed during east-directed subduction of Panthalassa beneath the Yukon-Tanana arc in the west and then transported eastward in Mesozoic thrust sheets (Erdmer et al., 1998; Devine et al., 2006). In contrast, in south-central Yukon, well-preserved, Late Permian eclogites and blueschists are exposed within quartzofeldspathic schists (Erdmer and Helmstaedt, 1983; Erdmer, 1987, 1992; Erdmer et al., 1998). Traditionally, these eclogites were assumed to have formed within Slide Mountain oceanic crust (e.g. Tempelman-Kluit, 1977; 1979). Unlike the Mississippian eclogitic rocks, the Permian eclogites are preserved as coherent units that were in contact with their quartzofeldspathic host prior to peak metamorphism (Erdmer et al., 1998), and thus are not part of a mélange. This discovery has led to the hypothesis that the Permian eclogites comprise a crustal component of the Yukon-Tanana composite arc.

The St. Cyr klippe is the least known of four localities that preserve Permian age eclogites in the YTT (Fig. 2-1, 2-2, and 2-3; Erdmer, 1992). Eclogite, garnet amphibolite, and low-grade mafic and ultramafic rocks in the St. Cyr klippe, previously mapped as part of a tectonic mélange, were considered to have formed within the Slide Mountain oceanic crust during subduction of the backarc (Tempelman-Kluit, 1979; Erdmer, 1992). However, Erdmer et al. (1998) recognized that the Permian eclogites, including the St. Cyr localities, are hosted by quartzofeldspathic schists and seem to share a common metamorphic history. Mafic and ultramafic rocks of the Slide Mountain Ocean terrane, in contrast, are of much lower metamorphic grade and lack the muscovite-quartz rich host rocks typical of the eclogite-bearing units at St. Cyr, Faro, Ross River, and Last Peak (Fig. 2-1; e.g., Wheeler et al., 1991; Colpron et al., 2006a).

This study documents the extent of HP metamorphism in the St. Cyr klippe and determines the protoliths of eclogites and quartzofeldspathic host rocks. This work is based primarily on fieldwork performed by Petrie during the 2010, 2011, and 2012 field seasons as part of a PhD research project. Field relationships, petrology, and mineral chemistry are used to document the widespread occurrence of eclogite in the St. Cyr klippe and to show that the eclogites are part of a coherent unit of quartzofeldspathic schists and mafic rocks that correlates with the YTT. The quartzofeldspathic host rocks surrounding the eclogites are metamorphosed igneous and sedimentary protoliths. U-Pb geochronology on zircon is used to determine the crystallization and metamorphic ages of the metaigneous rocks in the assemblage. The St. Cyr eclogite-bearing unit is tectonically imbricated with low-grade ultramafic rocks and associated gabbros that are commonly assigned to the Slide Mountain Ocean terrane (Colpron et al., 2006a). This study establishes the terrane affinity of eclogite-bearing unit in the St. Cyr klippe in an effort to place these rocks into their regional tectonic context.

Regional Geologic Setting

The Yukon-Tanana terrane (YTT) extends from Alaska to British Columbia, and constitutes a major component of the allochthons that form the northern Canadian Cordillera (Fig. 2-1). The YTT comprises a Mid- to Late Paleozoic arc-forearc system built upon a sliver(s) of continental crust rifted from western North America (Nelson et al., 2013 and references therein). Three Late Devonian to Late Permian, unconformity-bounded, geochronologically and geochemically distinct volcanic and volcaniclastic assemblages are built upon pre-Early Devonian metasedimentary basement (Fig. 2-1; Mortensen 1992; Colpron et al., 2006a; 2006b; Piercey et al. 2002; Piercey et al., 2006; Piercey and Colpron, 2009; Piercey et al., 2012). This substrate to the arc, the Snowcap assemblage, represents the rifted margin of Laurentia (Fig. 2-1; Colpron et al., 2006a; Piercey et al., 2006; Piercey and Colpron, 2009). The Snowcap assemblage is a

heterogeneous mix of psammitic, pelitic and calc-silicate schist, quartzite, marble, and amphibolite (Colpron et al., 2006a, 2006b; Berman et al., 2007; Piercey and Colpron, 2009). These rocks are typically polydeformed and polymetamorphosed at amphibolite facies conditions (Colpron et al., 2006a; Berman et al., 2007; Piercey and Colpron, 2009; Staples et al., 2013). Mafic amphibolites in the Snowcap assemblage display normal mid-ocean ridge basalt (N-MORB), enriched mid-ocean ridge basalt (E-MORB), or ocean island basalt (OIB) signatures consistent with emplacement in a continental rift setting (Nelson and Friedman, 2004; Colpron et al., 2006b; Piercey and Colpron, 2009). The Snowcap metasedimentary section is characterized by Precambrian detrital zircon populations consistent with a western North American provenance (Colpron et al., 2006a, 2006b, 2007; Nelson et al., 2006). Snowcap rocks are commonly intruded by deformed Late Devonian to Early Mississippian tonalite, granodiorite, and granite bodies, that represent subvolcanic intrusions to overlying arc rocks.

The Late Devonian to Early Mississippian Finlayson assemblage, the oldest arc assemblage, is characterized by mafic to felsic metavolcanic and metaplutonic rocks of arc and backarc affinities (Murphy et al., 2006; Piercey et al., 2006; Piercey et al., 2012). The assemblage also includes carbonaceous pelite, quartzite, volcaniclastic rocks and minor marbles (Mortensen, 1992; Colpron et al., 2006a). The Finlayson assemblage is unconformably overlain by the Mid-Mississippian to Early Permian Klinkit assemblage, consisting of variably metamorphosed mafic to intermediate calc-alkaline volcanic and volcaniclastic rocks with minor alkali basalt, limestone/marble, and conglomerate (Nelson, 1993; Simard et al., 2003; Murphy et al., 2006; Roots et al., 2006). The Klondike assemblage, the youngest assemblage in the YTT, consists of Middle to Late Permian felsic calc-alkaline metavolcanic and metaplutonic rocks, and minor mafic rocks (Mortensen, 1990; Nelson and Friedman, 2004; Dusel-Bacon et al., 2006; Murphy et al., 2006; Roots et al., 2006).

Yukon-Tanana arc rocks are thought to have co-evolved with the opening of a marginal basin represented by an oceanic assemblage of chert, argillite, and mafic volcanic rocks (Fig. 2-1; Mortensen, 1992; Nelson, 1993; Nelson et al., 2006; Colpron et al., 2006a; Piercey et al., 2006; Piercey et al., 2012). This marginal basin, originally termed the Anvil Ocean by Tempelman-Kluit (1979) and now referred to as the Slide Mountain Ocean terrane (Wheeler and McFeely, 1991), is preserved today in a discontinuous belt along the eastern edge of the YTT (Mortensen, 1992; Pigage, 2004; Piercey et al., 2012; Colpron, 2006a). In southeastern Yukon, the Slide Mountain Ocean terrane is found as fault bounded slivers of oceanic lithosphere and mélange preserved between the YTT and the underlying North American margin. Representative assemblages of the Slide Mountain Ocean terrane include fresh to greenschist facies basalt, gabbro, and leucogabbro, and variably serpentinized ultramafite, as well as deep-water sedimentary sequences such as chert and argillite (Tempelman-Kluit, 1979; Colpron, 2006; Colpron et al., 2006a; Murphy et al., 2006; Nelson et al., 2006; Piercey et al., 2012). Other sedimentary rocks found within the Slide Mountain Ocean terrane include siltstone, limestone, epivolcaniclastic sandstone and conglomerate, and phyllitic chert. Basalts typically display MORB geochemical signatures (Piercey et al., 2006), and together with the ultramafic rocks, these rocks are interpreted as units of oceanic crust and mantle (Piercey et al, 2012; Murphy et al., 2006). Two important characteristics of the Slide Mountain Ocean terrane are that metamorphic grade is usually greenschist facies or lower and there are no muscovite-quartz schists associated with these assemblages (Wheeler et al., 1991; Colpron et al., 2006a; Piercey et al., 2012).

Blueschist and eclogite facies rocks are known from several localities in the YTT (Fig. 2-1; Erdmer, 1992; Mortensen, 1992; Erdmer, 1987; Erdmer et al., 1998; Devine et al., 2006). The Simpson Range and Stewart Lake areas contain retrogressed eclogite that records evidence of Mid-Mississippian HP metamorphism (Creaser et al, 1999; Devine et al., 2006). In the Stewart Lake area, omphacite inclusions in zircon from garnet

amphibolites are the only conclusive evidence of HP metamorphism within the Klatza metamorphic complex (Devine et al., 2006). These HP mafic bodies are interpreted to have formed in a tectonic mélange with serpentinized ultramafic and gabbroic rocks and low-grade basalt, chert, limestone, chlorite-schist interpreted to be derived from YTT basement and early Yukon-Tanana arc rocks (Erdmer, 1987; Erdmer et al., 1998; Devine et al., 2006). In addition to the St. Cyr area, Permian age HP rocks are found at Ross River, Faro, and Last Peak (Erdmer and Armstrong, 1989; Creaser et al., 1997; Erdmer et al., 1998). At these localities, eclogite and their variably retrogressed equivalents, form meter- to tens of meter-sized boudins or structurally conformable layers hosted by greenschist-, blueschist-, or amphibolite-facies schists and quartzite (Erdmer and Helmstaedt, 1983; Erdmer, 1987; Erdmer et al., 1998). Structural fabrics shared by the eclogites and their host rocks led to the suggestion that they were in contact prior to peak metamorphism (Erdmer, 1987; Erdmer and Helmstaedt, 1983; Creaser et al., 1997; Erdmer et al., 1998).

Geology of the St. Cyr Klippe

The St. Cyr klippe lies 14 km northeast of Quiet Lake, Yukon, and is transected by the South Canol Road. The study area occupies a 15 km-wide by 40 km-long strip east of the Canol Road and southwest of the Nisutlin batholith (Fig. 2-1 and 2-3). The klippe west of the road does not contain the eclogite-bearing units, but has recently been mapped as part of a M.S. thesis (Isard, 2014; Isard and Gilotti, 2013). Eclogite, garnet amphibolite, and moderately metamorphosed mafic and ultramafic rocks in the St. Cyr klippe were originally mapped as large blocks within a tectonic mélange assigned to the Slide Mountain Ocean terrane (Tempelman-Kluit, 1979; Erdmer, 1992). Fallas (1997) later showed that eclogite and retrogressed eclogite in the St. Cyr klippe are intercalated with quartzofeldspathic tectonites of both sedimentary and igneous origin, and that HP metamorphism was much more widespread than previously known. Fallas (1997) also

recognized the shared penetrative fabric displayed by the quartzofeldspathic schists and eclogites. These observations contrast with the low-grade, weakly deformed oceanic strata typical of the Slide Mountain terrane (e.g., Wheeler et al., 1991; Colpron et al., 2006a; Piercey et al., 2012). Thus, we have mapped the different rock units in the St. Cyr klippe as distinct slices, unrelated to the Slide Mountain Ocean terrane (Fig. 2-3).

The eclogite-bearing unit is located in the central portion of the field area, forming northwest-striking slices bound by northeast-vergent thrust faults. The lowermost fault places HP rocks of the St. Cyr klippe above phyllites of the Finlayson assemblage (Fig. 2-3). The southwestern boundary of the eclogite-bearing unit is marked by a 600-m thick northwest-striking, southeast-dipping ductile shear zone. Two slices of amphibolite-facies garnet-mica schist, quartzite, and marble that correlate with the Snowcap assemblage of the YTT (Gilotti et al., 2013) overlie the shear zone.

The Snowcap assemblage, the St. Cyr eclogite-bearing unit, and the oceanic unit are interpreted to form a complex imbricate fan, as shown by the cross-section of A-A' in Fig. 3-3a and b. Within the imbricate fan, the eclogite-bearing unit defines two distinct slices separated by a sliver of the oceanic unit rather than a continuous belt of amphibolites as mapped by Tempelman-Kluit (1979, 2012). Fieldwork by Isard (2014) in the northwestern portion of the St. Cyr area, in combination with the fieldwork of this study, shows that the southeastern imbricates are cut by flat-lying klippen containing a mafic-ultramafic unit and metabasaltic rocks of the overlying Tower Peak assemblage (Fig. 3-2; Isard, 2014). These two units exhibit brittle structures including fault gouge and cataclasites, and are metamorphosed in the greenschist facies (Isard, 2014). The imbricates to the southeast and the mafic-ultramafic and Tower Peak klippen to the northwest are thrust above phyllites of the Finlayson assemblage. Small klippen of the mafic-ultramafic unit (which are probably unrelated to the oceanic unit imbricated with the eclogite-bearing unit) are preserved in the southeast portion of the St. Cyr area, thrust above the phyllites (Fig. 3-2).

The imbricates southeast of the South Canol Road were most likely juxtaposed during exhumation from within a subduction channel prior to the emplacement of the overlying units. The imbricates are characterized by medium- to high-pressure metamorphism, ductile fabrics, and steeply-dipping thrust contacts. In contrast, the Tower Peak and mafic-ultramafic units in the northwest are characterized by brittle deformation, low-grade metamorphism, and flat lying thrust faults. These contrasting structures and metamorphic signatures suggest that the imbricates to the southeast and the units to the northwest do not share primary relationships. Thus, the low-grade on high-grade relationship between the Tower Peak and mafic-ultramafic units and the underlying imbricates more likely represents out-of-sequence thrusting, rather than the roof thrust of a hinterland-dipping duplex (e.g. Boyer and Elliott, 1982).

Eclogite-Bearing Quartzofeldspathic Schists

Quartzofeldspathic schists hosting eclogites in the St. Cyr klippe comprise a 30 km long by 6 km wide, northwest-striking belt of metasedimentary and felsic metaigneous rocks that are intercalated on the meter to hundreds of meter scale. The quartzofeldspathic rocks were mapped as one unit regardless of their protolith. Eclogite and retrogressed eclogite are found as sub-meter to hundreds of meter scale lenses surrounded by the quartzofeldspathic schists (Fig. 2-3 and 2-4). Schistosity in the eclogites is defined by compositional layering and the grain-shape preferred orientation of omphacite and amphibole. Lenses are flattened parallel to schistosity and show a variety of internal fabrics. Most commonly, the schistosity in the mafic boudins is subparallel to the schistosity in the adjacent host rocks. In other cases, an eclogite-facies schistosity is discordant with the fabric in host rocks; some boudins are massive and unfoliated or display complex internal folding. Contacts between the eclogites and the surrounding host rocks range from sharp. Adjacent to contacts with the metasediments, the boudins preserve plagioclase melt stringers, which were either formed during

metamorphism of the metasedimentary rocks or are related to the boudinage of the eclogites.

Quartzofeldspathic schists with an igneous origin include meta-quartz diorites, metatonalites, and metatrondhjemites. Host rocks derived from sedimentary protoliths include mica- and garnet-bearing quartzites, garnet-mica schists, and feldspar-quartz-mica schists. The schists are fine-grained and variably retrogressed to amphibolite or greenschist facies assemblages. Contacts between the metaigneous rocks and the metasedimentary rocks do not show evidence of faulting or strain localization and are assumed to be pre-metamorphic.

The schistosity of the quartzofeldspathic rocks is defined by the alignment of micas and, less commonly, the grain-shape preferred orientation of quartz. Fabric intensity is moderate to strong throughout the schists with few areas of higher strain. Schistosity in the upper and lower eclogite-bearing thrust sheets is dominantly northwest striking and moderately to steeply southwest dipping (Fig. 2-5). The poles to foliation in the upper sheet form a great circle girdle are interpreted to represent a regional scale fold with an axis that plunges moderately to the northwest (Fig. 2-5a). Several macroscopic, open to isoclinal folds with moderate to steeply plunging, northwest trending fold axes were observed, parasitic to the larger-scale fold, however, the data are inconclusive as to whether they form part of a regional synform, like that mapped by Tempelman-Kluit (1979, 2012). Lineations plunge moderately to steeply in the down-dip direction of the foliation plane (Fig. 2-5a). Lineations in the lower thrust slice plunge shallowly to moderately toward the northwest or southeast (Fig. 2-5b).

Non-Eclogite-Bearing Metasedimentary Units

In the southwestern part of the St. Cyr klippe, rocks with lithologic, metamorphic, and detrital zircon signatures correlative with the Snowcap assemblage (Gilotti et al., 2013) are found in the hanging wall of a shear zone, structurally above the eclogite-

bearing quartzofeldspathic schists (Fig.2- 3). Tempelman-Kluit (1979, 2012) identified these rocks as part of the Nisutlin assemblage, parts of which are now attributed to the Snowcap assemblage. These rocks are divided into two lithostratigraphic units that are inferred to be separated by a northwest striking thrust fault (Fig. 2-3). From west to east these include: (1) interlayered garnet-white mica schist, chlorite schist, quartz-white mica schist, with minor biotite schist, quartzite, calc-silicate and carbonate and (2) garnet-white mica schist. The rocks are medium to coarse grained, variably deformed, and exhibit amphibolite-facies metamorphism locally retrograded to greenschist facies assemblages. The schistosity, defined by the planar alignment of micas, strikes northwest and dips moderately to steeply southwest (Fig. 2-5c). Quartz, mica, and plagioclase stretching lineations are variable, plunging shallowly to the southeast and moderately to the northwest and southeast (Fig. 2-5c). Some garnets within the schists show S-shaped spiral inclusion trails, a feature common to Snowcap rocks (e.g. Staples et al., 2013).

Shear zone between the eclogite-bearing and eclogite free schists

The eclogite-free metasedimentary rocks lie above a 600 m thick shear zone, separating this unit from the underlying eclogite-bearing quartzofeldspathic schists (Fig. 2-3). The northwest-striking shear zone contains a mixture of meter-sized blocks of variably metamorphosed mafic, ultramafic, carbonate, and undifferentiated quartzofeldspathic rocks in a matrix dominated by metapsammite. At least one block of eclogite of indeterminate size was identified within the shear zone. This eclogite is similar in mineralogy and grain size to the eclogite in the quartzofeldspathic schists. The ultramafics are pervasively serpentinized and mafic blocks are greenschist facies metagabbros. Quartzofeldspathic blocks contain garnet-bearing and garnet-free schists interpreted to be derived from sedimentary and felsic igneous protoliths. The

metapsammite matrix is composed of greenschist facies phyllite and quartzite (Fig. 2-6). Outcrop scale shear bands show a top-to-the-northeast thrust sense (Fig. 2-6a and b).

The foliation in the metapsammite matrix is defined by the planar alignment of phyllosilicates. Foliations strike northwest or northeast and dip moderately to steeply to the southwest, northwest, and northeast (Fig. 2-5d). Quartz, mica, and plagioclase stretching lineations plunge down-dip or moderately to steeply northwest, oblique to the foliation (Fig. 2-5d). These rocks are complexly folded on the centimeter to meter scale, with randomly oriented, but steeply plunging fold axes (Fig. 2-6c and d).

Oceanic Rocks

Mafic and ultramafic rocks of oceanic affinity form a structurally imbricated panel within the eclogite-bearing quartzofeldspathic unit (Fig. 2-3). The ultramafic rocks form prominent orange peaks on high ridges throughout the field area (Fig. 2-7a). These fault-bounded bodies range in size from a few square meters to several hundred square meters and include both greenschist facies gabbro to leucogabbro and intact, variably serpentinized ultramafics composed of olivine + clinopyroxene. Powder X-ray diffraction analysis of serpentinite sample 11-39 on a D8 Advance Bruker instrument housed within the Department of Chemistry, University of Iowa, shows that lizardite is the main serpentine mineral, and as such indicates metamorphic temperatures < 300 °C (Evans et al., 2013). Lizardite was also identified in the northwestern portion of the St. Cyr klippe, west of Canol Road (Isard and Gilotti, 2013). Within the center of the panels, metagabbros and leucogabbros are massive and may exhibit igneous textures (Fig. 2-7b), with leucogabbro intruding the surrounding gabbro and ultramafic rocks (Fig. 2-7c). Adjacent to the fault boundaries with the eclogite-bearing unit, ultramafic rocks are moderately to strongly foliated, dipping steeply to the southwest; the degree of deformation increases with the degree of serpentinization and proximity to the fault boundaries. Because there were no oceanic sediments associated with the ultramafic and

mafic rocks, a common characteristic of the Slide Mountain Ocean terrane, and the fact that the YTT can contain ultramafic rocks (Colpron et al., 2006a), we cannot unequivocally link these rocks to either the Slide Mountain Ocean terrane or the YTT.

Finlayson Assemblage and Nisutlin Batholith

The eclogite-bearing unit lies in the hanging wall of the basal thrust of the St. Cyr klippe (Fig. 2-3). This northwest striking thrust fault places eclogite-facies rocks of the YTT on top of siliciclastic rocks of the Finlayson assemblage, the oldest volcanic and volcaniclastic arc assemblage of the YTT (Colpron et al. 2006a). The contact with the overlying quartzofeldspathic schists is sharp, and both schists and clastic sedimentary rocks are brecciated. The siliciclastic rocks in the footwall comprise an interlayered package of phyllite, siltstone, shale, with minor psammite overlain by thickly bedded psammite, quartzite, marble, and minor siltstone. The low-grade metasedimentary rocks in the footwall contain a pervasive, moderately southwest-dipping cleavage.

The Early to Mid-Cretaceous Nisutlin batholith cuts rocks of both the Finlayson assemblage and St. Cyr klippe (Tempelman-Kluit, 1977; Colpron, 2006). Intrusion of medium to coarse-grained, biotite-quartz monzonite produced a 100-m-thick contact aureole that metamorphosed the Finlayson sedimentary rocks to andalusite bearing hornfels (Fallas et al., 1999). A small 1x1 km pluton, a satellite of the Nisutlin batholith, intrudes the quartzofeldspathic schists in the central eastern portion of the field area. The intrusion pins movement on the basal thrust of the St. Cyr klippe as pre-intrusion in age.

Petrology of Eclogite and Quartzofeldspathic Host Rocks

Eclogitic rocks from two localities near the South Canol Road within the St. Cyr klippe were first described by Erdmer (1992); additional localities were noted by Fallas et al. (1998). Here, we document the pervasive nature of HP metamorphism of both the mafic lenses and the quartzofeldspathic host rocks. Omphacite, garnet, quartz, and rutile comprise the representative HP assemblage for mafic rocks, while the presence of

phengite and garnet is the most compelling evidence of HP metamorphism in the quartzofeldspathic schists. Both assemblages display an amphibolite to greenschist-facies overprint.

Eclogites and Retrogressed Eclogites

Well-preserved eclogites contain a peak mineral assemblage of omphacite + garnet + quartz + rutile ± phengite ± amphibole, with epidote, apatite and zircon as accessory phases (Fig. 2-8). Omphacite forms pale green, 200-800 μm diameter equant grains or elongate porphyroblasts. Garnet is typically euhedral and fine-grained, ≤ 300 μm in diameter. When present as a peak phase, brownish-green amphibole constitutes subhedral, 300-900 μm grains in equilibrium with omphacite or euhedral inclusions in garnet (Fig. 2-8b). Rutile is present in the matrix and included within garnet. Other inclusions observed in garnet are omphacite, quartz, titanite, plagioclase, diopside, augite, phengite, muscovite, epidote, ilmenite, and calcite; these inclusions are generally confined to the cores of grains. Quartz occurs as either 100-300 μm diameter grains with undulose-extinction and subgrains or < 100 μm polycrystalline aggregates with undulose- to flat-extinction and 120° triple-junctions.

Eclogites show progressive retrogression from fresh eclogite to garnet amphibolite. In the transition zones between preserved eclogite and completely retrograde garnet amphibolite, omphacite-rich and amphibole-rich layers are often interleaved. In the least retrogressed samples, omphacite is replaced by fine-grained, lobate symplectites of diopside + plagioclase or amphibole + plagioclase (Fig. 2-8c and d). Phengite is commonly replaced by fine-grained, blocky symplectites of biotite and plagioclase. Other retrograde features include rutile rimmed by ilmenite, ilmenite surrounded by titanite, and garnet rimmed by biotite. In moderately retrogressed samples, garnet is subhedral, with embayed edges converted to biotite. These garnets preserve inclusions of quartz, amphibole, rutile, clinopyroxene, and phengite. In samples

with ≥ 10 modal percent clinopyroxene, amphibole forms medium, light greenish-brown, subhedral to euhedral grains, flattened parallel to the schistosity. In samples with trace amounts of clinopyroxene, the clinopyroxene is typically present as < 50 μm sized grains surrounded by extremely fine-grained amphibole + plagioclase symplectites. These symplectites create a cloudy appearance along the grain boundaries of larger amphiboles. Completely retrogressed eclogites consist of amphibole + garnet + plagioclase ± quartz ± biotite ± ilmenite ± titanite. Amphibole is pale bluish-green, 200-800 μm, flattened parallel to the foliation, and displays straight, clear grain boundaries. Quartz and amphibole are common inclusions in garnet.

Quartzofeldspathic Schists

The quartzofeldspathic schists are derived from both igneous and sedimentary protoliths. The mineral assemblage of the metaigneous schists is quartz, garnet, phengite, and plagioclase, with or without biotite, clinozoisite, or apatite (Fig. 2-9a and b). Rutile, apatite, ilmenite, and potassium-feldspar are common accessory phases. Metasedimentary protoliths are distinguished from metaigneous rocks by the higher modal percent of quartz, garnet, micas, and the lack of K-feldspar. In both metaigneous and metasedimentary rocks, quartz exhibits undulose extinction, subgrains, and lobate grain boundaries—evidence for its dynamic recrystallization over a range of temperatures (~300-500°C; e.g. Stipp et al., 2002). Coarse-grained biotite is pale reddish-brown to dark greenish-brown and is commonly altered to chlorite. Biotite is also a typical retrograde phase after phengite.

In metaigneous rocks (Fig. 2-9a and b), phengite grains are either 300-800 μm in diameter, isolated grains within the matrix, or < 50 μm, euhedral, randomly oriented crystals replacing plagioclase. Garnet is present as subhedral porphyroblasts with embayed boundaries altered to chlorite. Titanite forms inclusions in garnet or overgrowths on ilmenite or rutile. Clinozoisite is 100-400 μm in diameter, and exhibits

embayed grain boundaries. Epidote forms < 50 μm lobate blobs replacing clinozoisite and plagioclase, which exhibits 500-1000 μm diameter grains with embayed boundaries and multiple albite growth or deformation twins.

In metasedimentary rocks (Fig. 2-9c and d), 100-600 μm diameter phengite is a common matrix phase. Garnet forms isolated, subhedral to rounded porphyroblasts or aggregates of small, ≤ 100 μm, grains within plagioclase and contains inclusions of quartz, phengite, and biotite. In the most retrogressed samples, garnet is fractured and replaced by chlorite or biotite. In quartzites, the long axes of garnet lies in the schistosity defined by the grain-shape preferred orientation of micas. Titanite forms medium, euhedral grains within the matrix. Plagioclase is found as elliptical porphyroclasts with embayed or lobate grain boundaries. Quartz, in plagioclase-rich samples, is also preserved as porphyroclasts, surrounded by a finer-grained quartz + mica matrix.

Mineral Chemistry

Mineral chemistry data was collected from nine eclogites, three metatonalites, and three metasedimentary rocks in order to characterize the HP phases in both the eclogites and their host quartzofeldspathic schists. UTM coordinates for the analyzed samples are shown in Table 2-1, while selected mineral chemistry data are given in Tables 2-1 through 2-6. Mineral compositions were determined using a CAMECA SX-100 electron microprobe at the University of California, Davis, CA. Analytical conditions include 15 kV acceleration voltage, 5-20 nA beam current, and a beam diameter of 1-10 μm. Major element concentrations are shown as weight % oxides (wt.%). Amphibole nomenclature is after Hawthorne et al. (2012), pyroxene nomenclature is after Morimoto et al. (1988), and epidote nomenclature follows Armbruster et al. (2006). Mineral abbreviations are from Whitney and Evans (2010).

Clinopyroxene

Clinopyroxene compositions are plotted in Fig. 2-10 and representative pyroxene analyses are given in Table 2-2. Clinopyroxene analyses were normalized to four cations per formula unit ($M2M1Si_2O_6$) and the Fe^{2+}/Fe^{3+} ratio was obtained from the charge balance. Cations were assigned to the M1 and M2 sites according to the procedure described in Morimoto et al. (1988). Omphacite (i.e. sodic clinopyroxene with a jadeite component between 20-80 mol %) was confirmed in all nine eclogite samples. In general, Jd_{35-49} in grain cores decreases to Jd_{20-30} at grain rims, which are adjacent to symplectites. Diopside is found within symplectites or at grain rims adjacent to amphibole-plagioclase symplectites with a jadeite content ranging from Jd_{10-18}. Euhedral clinopyroxene inclusions in garnet are diopside (Jd_{2-8}) or omphacite (Jd_{20-43}).

Amphibole

Taramite, kataphorite, and winchite [Si = 6.16-7.21 atoms per formula unit (apfu), Ca = 1.13-1.49 apfu, $^{[A]}(Na+K)$ = 0.34-0.86 apfu] are found as matrix grains in equilibrium with omphacite (Fig. 2-11, Table 2-3). Symplectitic amphibole is more calcic than the matrix amphibole, and is pargasitic with Si = 6.30-7.19 apfu, Ca = 1.50-2.28 apfu, $^{[A]}(Na+K)$ = 0.48-0.90 apfu. Both Na-Ca and Ca amphiboles are included in garnet. These include taramite and katophorite [Si = 6.00-6.72 apfu, Ca = 1.50-1.31 apfu, $^{[A]}(Na+K)$ = 0.53-0.88 apfu] as sodic phases, and sadanagite, pargasite, and magnesiohornblende [Si = 5.87-6.89 apfu, Ca = 1.51-1.79 apfu, $^{[A]}(Na+K)$ = 0.34-0.81 apfu] as calcic phases.

Garnet

Garnet in eclogite exhibits a rather narrow range in composition. Garnets are almandine-pyrope-grossular solid solutions in the range $Alm_{50-61}Prp_{7-21}Grs_{17-34}Sps_{0.5-6.8}$ (Table 2-4). All garnets plot in the area typical of type C eclogites, which are defined by Coleman et al. (1965) as crustally derived, relatively low-temperature eclogite. Garnet

displays both prograde and sector zoning (Fig. 2-12). Prograde compositional zoning exhibits a core to rim decrease in Mn and Ca. In some cases, Ca zonation is more complex, rising during garnet growth before decreasing at the rim. Sector zoning is developed in the intermediate domain between a distinct core and outer rim, and is thought to be due to either the heterogeneous distribution of Mg and Fe on the {110} faces of garnet or a rapid increase in temperature (Shirahata and Hirajima, 1995; Kleinschmidt et al., 2008). Sector zoning is most pronounced in the Mg component, where Mg decreases early in growth history, only to steeply increase at the rim. Mn shows less well-defined sector variation in some samples. The ~30 μm at the rim of the grain is characterized by a slight increase in Mn, and decrease in Fe and Ca.

Garnet in the quartzofeldspathic schists is much more compositionally complex than those in the eclogites (Table 2-4). Grains display highly variable zoning patterns between sedimentary and igneous schists, and even between garnets in the same sample. This may reflect the original bulk rock composition or some of the garnets could be detrital. Zoning along the rims and cracks indicate that these garnets have been affected by element diffusion after peak metamorphism. In general, garnet in the metatonalite is an almandine-grossular solid solution in the range $Alm_{39-54}Prp_{1.2-25}Grs_{29-51}Sps_{2.7-7.1}$. Although pyrope content reaches 25 mol%, in the majority of cases it is less than 2 mol%. Metatonalite garnets display two types of zoning: (1) homogeneous cores with <20 μm wide retrograde rims where Fe and Mn increase and Mg decreases and (2) prograde zoning with a core to rim increase in Mg and decrease in Fe, Ca, and Mn without a retrograde rim. Garnet compositions in the metasediments are in the range $Alm_{54-69}Prp_{6-21}Grs_{10-29}Sps_{0.5-21}$. These garnets are irregularly zoned and tend to be more Mn-rich than garnet in the metatonalites. In the metasediments garnet generally exhibits a core to rim decrease in Fe and Mg and increase in Mn and Ca. At the outermost rims (<20 μm) Fe and Mg experience significant drops. For example, Fe decreases as much as 39 mol% from the adjacent analysis in the core of the grain. At the same time, Ca and

Mn substantially increase, 22 mol% in the case of Ca. Along cracks, Mg decreases, Ca and Mn increase and Fe remains unchanged.

Phengite

White mica is muscovite to phengite (Si apfu > 3.2) in chemical composition. Phengite was found in three eclogite samples as matrix grains and included in garnet. In the matrix, white mica compositions range from 3.12 to 3.67 Si apfu (Table 2-5). Inclusions in garnet have Si contents as high as 3.32 apfu. While the majority of phengite is homogeneous in composition, a few grains in each sample experience a decrease in Mg, Ba, and Si within 25-10 μm of the grain rim. Matrix phengite was identified in all six quartzofeldspathic host rocks. In the matrix, phengites are irregularly zoned, with the highest values of Si generally concentrated in grain cores. With decreasing Si, Ba and Mg also decrease. In metatonalites, matrix phengite contains 3.07 to 3.45 Si apfu, and the fine grains that replace plagioclase contain up to 3.48 Si apfu (Fig. 2-13; Table 2-5). In metasedimentary rocks, Si concentrations are 3.04 to 3.34 apfu, which is lower than the Si composition in the metatonalites, possibly a reflection of their differences in bulk composition. White mica included in garnet in metasedimentary rocks is muscovite, with Si values between 2.99 and 3.13 apfu.

Other Phases

Representative compositions of biotite, plagioclase, K-feldspar, and epidote are presented in Table 2-6. Biotite grains that have completely replaced phengite in the matrix of eclogite are relatively homogeneous (Si = 2.79-2.87 apfu, X_{Mg} [Mg/(Mg+Fe)] = 0.54-0.63, $Ti0_2$ = 2.70-3.74 wt.%). Biotite grains in garnet have a similar X_{Mg} (0.53-0.68), but are richer in Si (2.97-3.07 apfu) and much lower in TiO_2 (0.14-0.16 wt.%) than matrix grains. Biotite in symplectites with plagioclase shows much wider compositional variations with respect to Si (2.66-3.27 apfu) and TiO_2 (0.86-3.69 wt.%), but displays a similar X_{Mg} (0.48-0.49). In metatonalites, biotite matrix and symplectite grains are

homogeneous (Si = 2.75-2.80 apfu, X_{Mg} = 0.49-0.51, $Ti0_2$ = 1.63-1.76 wt.%). Biotite in metasedimentary rocks has a range of Si (2.72-2.89 apfu) and X_{Mg} (0.48-0.52) similar to metatonalite biotite, but with a wider range in TiO_2 (1.20-2.31 wt.%).

Plagioclase in eclogites is albite-oligoclase (An_{2-22}) in symplectites with clinopyroxene and included in garnet. In symplectites with phengite, plagioclase is oligoclase (An_{9-30}). Plagioclase in metatonalites and metasedimentary rocks is also albite-oligoclase, ranging between An_{2-26} and An_{3-32}, respectively. K-Feldspar was identified in one sample as fine grains adjacent to plagioclase in the range $An_{0.5-3}$. Epidote is found in both the eclogite and the metatonalites and clinozoisite is found in metasediments. In eclogite, the pistacite component [$Ca_2Al_2Fe^{3+}Si_3O_{12}(OH)$] in epidote in the matrix and included in garnet lies between 23-35 mol% and 10-34 mol%, respectively. In metatonalites, epidote that replaced plagioclase has a pistacite component of 20-29 mol%. Clinozoisite from one metasedimentary sample is 0.04 and 5 mol% in pistacite content.

Geochemistry

Whole rock major and trace element concentrations were analyzed by X-ray fluorescence and inductively coupled plasma mass spectrometry, respectively, at the GeoAnalytical Laboratory of Washington State University, Pullman, WA, following conventional procedures. Ten eclogite and retrogressed eclogite samples were chosen for whole rock geochemistry. Bulk compositions (Table 2-7) reveal that the eclogites are basaltic in composition. SiO_2 content is 45.2-51.1 wt %, with TiO_2 = 1.7-2.7 wt % and Na_2O = 2.5-4.0 wt %. Trace element discrimination diagrams (Fig. 2-14) show that most of the St. Cyr eclogites fall in the mid-ocean ridge basalt (MORB) field of the Ti-Zr-Y and the Ti-Zr plot (Pearce and Cann, 1973) and the normal type MORB (N-MORB) field in the Nb-Zr-Y plot (Meschede, 1986). The primitive-mantle trace element normalized

plot (Fig. 2-15) shows that the eclogites broadly correlate with N-MORB (Sun and McDonough, 1989).

Zircon U-Pb Geochronology and Trace Element Geochemistry of Metatonalites

U-Pb dates of zircon from two metatonalite samples were obtained in an effort to determine the age of the protolith and HP metamorphism of the eclogite-bearing felsic igneous rocks. The two samples were chosen because they were collected adjacent to eclogite lenses. Cathodoluminescence (CL) images of zircon (Fig. 2-16) guided the choice of analytical spots. U-Pb data is presented in Table 2-8 and Fig. 2-17 and trace element data is in Table 2-9 and Fig. 2-18.

Analytical Methods

U–Th–Pb isotopic data were measured using the sensitive high-resolution ion microprobe-reverse geometry (SHRIMP-RG) mass spectrometer at the U.S. Geological Survey – Stanford University ion probe facility, Stanford, California. Zircon grains were separated from 1-3 kg samples by standard physical separation techniques and mounted in 2.54 cm epoxy rounds, which were polished to expose grain interiors. CL, transmitted light, and reflected light images were used to characterize zircon domains, identify internal growth zones, and select spots for analysis (Fig. 2-16). Calibration of U was based on zircon standard Madagascar Green (MAD; 4196 ppm U; Barth and Wooden, 2010). Isotopic ratios were calibrated by replicate analyses of zircon standard R33 (421 Ma, Black et al., 2004; Mattinson, 2010), which was rerun after every fourth analysis. The analytical routine followed Barth and Wooden (2006, 2010). Uncertainties in the isotopic ratios are reported at the 1σ level. Ages are assigned based on the weighted mean of $^{206}Pb/^{238}U$ ages corrected for common Pb using the ^{207}Pb correction method. Uncertainties in the weighted mean ages discussed below are reported at the 95 % confidence level. The weighted mean ages are equivalent within uncertainty to concordia

ages calculated in Squid 1.13 (Ludwig, 2001). Age calculations and Tera-Wasserburg diagrams (Fig. 2-17) were generated with the Isoplot 3 program of Ludwig (2003).

Trace-element data for Y, REE, and Hf were collected simultaneously with the U, Th and Pb analyses. The following peaks were measured: ^{89}Y, ^{139}La, ^{140}Ce, ^{146}Nd, ^{147}Sm, ^{153}Eu, $^{157}Gd^{16}O$, $^{163}Dy^{16}O$, $^{166}Er^{16}O$, $^{172}Yb^{16}O$, $^{90}Zr_2{}^{16}O$, $^{180}Hf^{16}O$, ^{206}Pb, $^{232}Th^{16}O$, $^{238}U^{16}O$. Data reduction of elemental concentrations used zircon standards CZ3 and MAD (Mazdab and Wooden, 2006; Mazdab, 2009). Chondrite-normalised REE plots (Fig. 2-18) use the chondrite REE abundances of Anders and Grevesse (1989) multiplied by a factor of 1.36 (Korotev 1996). Chondrite-normalized values for Pr were calculated by interpolation ($Pr_{(N)} = La_{(N)}{}^{0.33} \times Nd_{(N)}{}^{0.67}$). Eu and Ce anomalies are based on $Eu_{(N)}/Eu^*$ and $Ce_{(N)}/Ce^*$ with Eu* and Ce* calculated as geometric means (e.g., $Eu^* = (Sm_{(N)} \times Gd_{(N)})^{0.5}$).

Metatonalite Sample 11-94

Sample 11-94 was collected several meters away from an approximately two meter diameter eclogite boudin in the south-central part of the field area (Fig. 2-3). It is a medium grained, moderately foliated metatonalite schist, with an estimated mode of 50% quartz, 30% plagioclase, 15% phengite, and 5% biotite. Accessory phases include epidote, apatite, and titanite. Plagioclase grains are replaced by very fine grains of phengite, epidote, and K-feldspar. Isolated garnet grains are replaced by chlorite along rims and fractures. Phengite is replaced by biotite, which is in turn overprinted by chlorite.

Zircons in 11-94 are elongate, euhedral to subrounded, with complex cores and rims (Fig. 2-16), common characteristics of high-grade metamorphic zircon (Corfu et al., 2003). Oscillatory zoned, subrounded cores are surrounded by CL-dark mantles and homogeneous CL-light gray rims (e.g. grain 7 in Fig. 2-16a). Grains with round, CL-dark, mottled cores display multiple euhedral rims, moderately luminescent in CL (Fig.

2-16a, grain 13). Analyses of cores give $^{206}Pb/^{238}U$ ages ranging from 303 to 349 Ma. Core and mantle domains have variable trace element patterns characterized by steep HREE (Yb/Gd = 6-41), ΣREE = 308-2136, and negative Eu and positive Ce anomalies (Eu/Eu* = 0.2-0.6 and Ce/Ce* = 2-35). Two cores that have elevated light REE (Fig. 2-18a), indicative of modification of the original trace element signature, give discordant U/Pb analyses (Fig. 2-17a). Th/U ratios of four oscillatory zoned and two dark mottled cores range from 0.1-0.3, typical of igneous zircon (Hoskin and Schaltegger, 2003). Seven cores give a weighted mean $^{206}Pb/^{238}U$ age of 334 ± 8 Ma, which we interpret as the igneous crystallization age.

Some oscillatory zoned zircon cores lack a CL-dark mantle, while other cores are patchy (e.g., Fig. 2-16a, grain 17). These cores display multiple metamorphic rims. Seven metamorphic rims show a strong depletion of ΣREE (32-61), a pronounced flattening of the HREE pattern (Yb/Gd = 2-13), and the disappearance of the Eu anomaly (Fig. 2-18a). The Th/U ratio of the rims ranges from 0.004 to 0.01. These are all characteristics consistent with the growth or recrystallization of zircon during HP metamorphism (Rubatto, 2002). Five oscillatory zoned or patchy cores and two metamorphic rims have elevated ΣREE (129-837) and steep HREE (Yb/Gd = 37-822) compared to the HP signatures, but low Th/U (0.002-0.003) values and no Eu anomaly, consistent with HP metamorphism (Fig. 2-18a). This likely reflects the low amount of garnet in sample 11-94, as garnet growth is the cause of the flattening of the HREE pattern associated with HP metamorphism (Rubatto, 2002; Rubatto and Hermann, 2007). Along with the rims on igneous cores, these cores and rims give $^{206}Pb/^{238}U$ ages ranging from 250 to 284 Ma, with most analyses clustering between 264 to 272 Ma. The scatter in the ages may reflect inherited material from the protolith, Pb-loss, or both. The weighted mean $^{206}Pb/^{238}U$ age of 266 ± 3 Ma is interpreted as the age of HP metamorphism (Fig. 2-17a).

Metatonalite Sample 11-114

Sample 11-114 was collected adjacent to an eclogite boudin in the south-central part of the field area (Fig. 2-3). It is a fine to medium grained, metatonalite schist composed of approximately 50% quartz, 20% plagioclase, and 30% white mica; titanite and apatite are accessory phases. Plagioclase is replaced by fine grains of white mica. Unlike sample 11-94, this sample lacks garnet altogether. Retrograde microstructures include white mica replaced by biotite, and biotite replaced by chlorite. A well-developed schistosity is defined by the planar alignment of phyllosilicates.

Zircon in sample 11-114 preserves CL-dark cores with faint oscillatory zoning overgrown by CL-bright rims (Fig. 2-16b). Seven cores with $^{206}Pb/^{238}U$ ages spanning 303-338 Ma have characteristic igneous trace element patterns, including steep HREE patterns (Yb/Gd = 7-17), ΣREE = 724-1170, Th/U = 0.1-0.4, a positive Ce anomaly (Ce/Ce* = 3-22), and a modestly developed Eu anomaly (Eu/Eu* = 0.3; Fig. 2-18b). Five of those cores give a $^{206}Pb/^{238}U$ concordia age of 333 ± 3 Ma, although only one of the cores is concordant (Fig. 2-17b) and two cores have elevated LREE patterns (Fig. 2-16b), indicating a partial resetting of the protolith U/Pb systematics. The age of CL-dark cores is interpreted as the age of the protolith, which is within error of the 334 ± 8 Ma age of oscillatory zoned and patchy cores in sample 11-94.

Cl-bright rims give $^{206}Pb/^{238}U$ ages between 243-356 Ma, overlapping the ages of the cores. The rims have highly variable trace element signatures with generally elevated ΣREE (49-832), steep HREE (Yd/Gd = 6-39) patterns and Th/U ratios (0.004-0.3) that vary between HP and igneous signatures. The rims show the lack of or shallow Eu anomalies and a depressed Ce anomaly (Fig. 2-18b). The wide variability of trace elements and Th/U ratios suggests modification of the original metamorphic signature and/or inheritance from the protolith cores. The elevated HREE most likely reflect the lack of garnet in the sample. All of the rim ages are discordant; six homogeneous rims range in $^{206}Pb/^{238}U$ age from 279 to 243 Ma and define a lower intercept age of 248 ± 8

Ma or a weighted mean age of 251 ± 11 Ma. These analyses may reflect the disturbance in the U-Pb systematics after original zircon growth or, more likely, continued zircon growth with compositional changes during exhumation.

Discussion

The St. Cyr klippe comprises structurally imbricated units that record contrasting geologic histories. The imbricate panels include a slice of greenschist facies oceanic-like crust and serpentinized mantle rocks and different units of the YTT. Two imbricates consisting of undifferentiated, amphibolite facies quartzofeldspathic schists sit in the structurally highest position of the klippe. These units form part of the Snowcap assemblage, which constitutes part of the substrate of the Yukon-Tanana arc (e.g. Colpron et al., 2006a). Snowcap rocks are thrust on top of at least two slices of eclogite-bearing quartzofeldspathic schists that are dominated by Yukon-Tanana arc material. Igneous crystallization ages for metatonalites (333 ± 3 and 334 ± 8 Ma) fall within the Little Salmon Cycle (as defined by Piercey et al., 2006) of the Klinkit phase of Yukon-Tanana arc activity (342 to 314 Ma; Nelson et al., 2006 and references therein). Felsic metaigneous and metavolcanic rocks of similar age are found in the YTT in the Fortymile River assemblage in eastern Alaska, and the Ram Creek and Big Salmon complexes in the Wolf Lake-Jennings river area of southern Yukon-northern British Colombia (Nelson and Friedman, 2004; Dusel-Bacon et al., 2006; Roots et al., 2006). Whole-rock composition of the eclogites indicates that their protolith was oceanic tholeiitic basalt, which falls into the N-MORB field. Primitive basalts are found throughout the Yukon-Tanana arc, from initial arc formation in the Mid- to Late Devonian through the Late Permian (Colpron et al., 2006a; Nelson et al., 2006).

The eclogite-bearing quartzofeldspathic rocks at St. Cyr record evidence of HP metamorphism consistent with that of other Permian age HP rocks in the YTT (e.g. Hansen, 1992). Trace element signatures of metamorphic zircon in metatonalite sample

11-94 indicate their formation under garnet-present, plagioclase absent pressure-temperature conditions, consistent with eclogite facies paragenesis. These zircon record a HP metamorphic age of 266 ± 3 Ma, which is not only identical to the U-Pb TIMS zircon age of 266 ± 0.6 Ma derived from an eclogite sample from the St. Cyr area (Fallas et al., 1998), but is also within error of a U-Pb zircon age interpreted to record the HP metamorphism of eclogite at Last Peak (269 ± 2 Ma; Creaser et al., 1997). This corroboration not only solidifies the age of HP metamorphism at St. Cyr, but also provides a link to other Permian eclogite-facies assemblages attributed to the YTT.

The younger zircon rims on zircons from sample 11-114 lack Eu anomalies yet display elevated HREE (Fig. 2-18b). These rims are also highly discordant (Fig. 2-17). One explanation for these U-Pb and trace element characteristics is that that the zircon grew during eclogite facies, but retained the HREE signature because garnet is only a minor component of the assemblage in sample 11-114. However, this does not explain why the ages are discordant. A more likely scenario is that the rims record continued zircon growth during exhumation. The absence of a pronounced Eu anomaly can persist under garnet amphibolite-facies metamorphic conditions (Liu and Liou, 2011; Gilotti et al., 2014). The addition of new fluids during decompression, combined with the lack of garnet in the sample, could attest to both the lack of a Eu anomaly and the discordance of the analyses, provided the new fluid composition was depleted in U, giving the impression that the sample incorporated common Pb. The fact that the younger rims truncate compositional zoning in the cores is suggestive of the dissolution/reprecipitation of zircon during metamorphism.

The St. Cyr klippe is significant in that it represents a window into Late Permian HP metamorphism in the YTT. Taken as a whole, the YTT is a complex polymetamorphic terrane, recording multiple ages and pressure-temperature ranges of peak metamorphism. For example, in the Stewart River area, titanite and monazite ages suggest that Yukon-Tanana arc and Snowcap rocks were metamorphosed during

deformation at low-pressure conditions between 365-350 Ma and at medium-pressure conditions at ~ 265 Ma (Berman et al., 2007). These rocks were further overprinted by regional Cretaceous plutonism and Jurassic-Cretaceous metamorphism during deformation and exhumation (Berman et al., 2007; Staples et al., 2013). In the St. Cyr area, the majority of $^{40}Ar/^{39}Ar$ muscovite cooling ages (Fallas et al., 1998) fall between 263 Ma to 235 Ma demonstrating that HP rocks in the St. Cyr klippe escaped the regionally pervasive Jurassic and Cretaceous metamorphic overprint recorded in other YTT rocks.

Eclogites in the St. Cyr klippe are remarkably well preserved, and comparison of the petrological and chemical signatures of the eclogites at St. Cyr suggest a genetic link to the three other Permian age eclogites in the YTT. At St. Cyr, omphacite ranges from Jd_{20-49} and phengite contains as much as 3.67 Si apfu. These values overlap with those of omphacite and phengite from eclogites in Ross River, Faro, and Last Peak (Erdmer, 1987; Erdmer et al., 1998; Perchuk et al., 1999; Perchuk and Gerya, 2005; Ghent and Erdmer, 2011). Phengite in the host quartzofeldspathic schists contain values of Si between 3.20 and 3.48. These values are consistent with, but slightly higher than, phengite Si content of white mica in garnet mica schists at Last Peak, which record 3.20 to 3.38 Si apfu (Hansen, 1992). Eclogite at Ross River is hosted by quartzofeldspathic garnet-mica and glaucophane-bearing schists (Erdmer, 1987; Erdmer and Armstrong, 1988; Ghent and Erdmer, 2011), at Faro by glaucophane-bearing and garnet-mica schists that contain phengite (Perchuk et al., 1999; Perchuk and Gerya, 2005), and at Last Peak, by hornblende-, biotite-, and phengite-bearing schists (Erdmer and Helmstaedt, 1983; Erdmer et al., 1998). These rocks bear a resemblance to the host rocks in the St. Cyr klippe, although the amphibole is less sodic at St. Cyr. Petrographically, eclogite and retrogressed eclogite at St. Cyr looks remarkably like those at Ross River, Faro, and Last Peak. At each of the three other localities, the peak eclogite facies assemblage is omphacite + garnet + quartz, which is the dominant peak assemblage at St. Cyr (Creaser

et al., 1997; Erdmer et al., 1998). Phengite is confirmed in Ross River and Faro eclogites (Erdmer, 1987; Perchuk et al., 1999). Like eclogite at St. Cyr, during the transition from eclogite to garnet amphibolite, omphacite is replaced primarily by calcic amphibole, such as pargasite, and albitic plagioclase (Erdmer and Helmstaedt, 1983; Erdmer, 1987; Creaser et al., 1997; Perchuk et al., 1999). Geochemically, eclogites like those at St. Cyr are also found at Last Peak and the MORB signature recorded in the major and trace element geochemistry of the St. Cyr eclogites is consistent with the geochemical signatures of eclogites at all three localities (Erdmer and Helmstaedt, 1983; Creaser et al., 1999; Ghent and Erdmer, 2011). Thus, the Permian age eclogites in the YTT are not isolated occurrences, but form part of a regional HP lithotectonic assemblage.

When eclogite was first identified at St. Cyr, the HP mafic rocks were assumed to have formed at depth and returned to the surface as part of a tectonic mélange (e.g. Erdmer, 1987). The results of our investigation show that the eclogite and quartzofeldspathic host rocks were juxtaposed within the Yukon-Tanana arc prior to subduction and experienced the same metamorphic history. Thus, the HP assemblage in the St. Cyr klippe represents slices of coherent continental arc crust subducted to HP conditions. The idea of exotic versus *in situ* metamorphism of HP rocks was something of a controversy in HP and ultrahigh-pressure (UHP) terranes, such as the Western Gneiss Region in Norway and the Dabie-Sulu UHP terrane in China (e.g., Smith, 1984; Wang and Liou, 1991). The argument was largely due to the rare preservation of the pre- versus post-metamorphic field relationships between eclogites and their host rocks, as well as retrograde overprinting of the host rocks that erased the evidence of UHP metamorphism (Andersen et al., 1991; Zhang et al., 1995). Numerous studies on the eclogite-bearing host rocks in these localities have shown that those rocks have in fact been subjected to coeval HP and UHP metamorphism (Wang and Liou, 1991; Zhang et al., 1995; Wain, 1997; Carswell et al., 2003; Liu et al., 2005; Butler et al., 2013) and hence they represent coherent slices of continental crust. Eclogite in the St. Cyr klippe

also formed *in situ* with their enveloping HP, Yukon-Tanana derived schists and do not constitute a tectonic mélange, but rather coherent slices of Yukon-Tanana arc rocks.

Conclusions

The St. Cyr klippe consists of variably metamorphosed and deformed, structurally imbricated units of Yukon-Tanana continental arc crust and oceanic crust. Quartzofeldspathic schists derived from the YTT host sub-meter to hundreds of meter scale lenses of well-preserved eclogite and retrogressed eclogite. The presence of phengite and HP zircon show that the eclogite was metamorphosed *in situ* within the quartzofeldspathic host during the Late Permian. This confirms that the eclogite-bearing unit consists of slices of coherent arc crust, and that the eclogites are not part of a tectonic mélange. The petrological, geochemical, geochronological, and structural relationships between the eclogite and the host rocks in the St. Cyr klippe are shared with similar HP assemblages found in the YTT at Faro, Ross River, and Last Peak. These mutual relationships suggest that Permian age HP assemblages form part of a larger HP lithotectonic assemblage within the YTT.

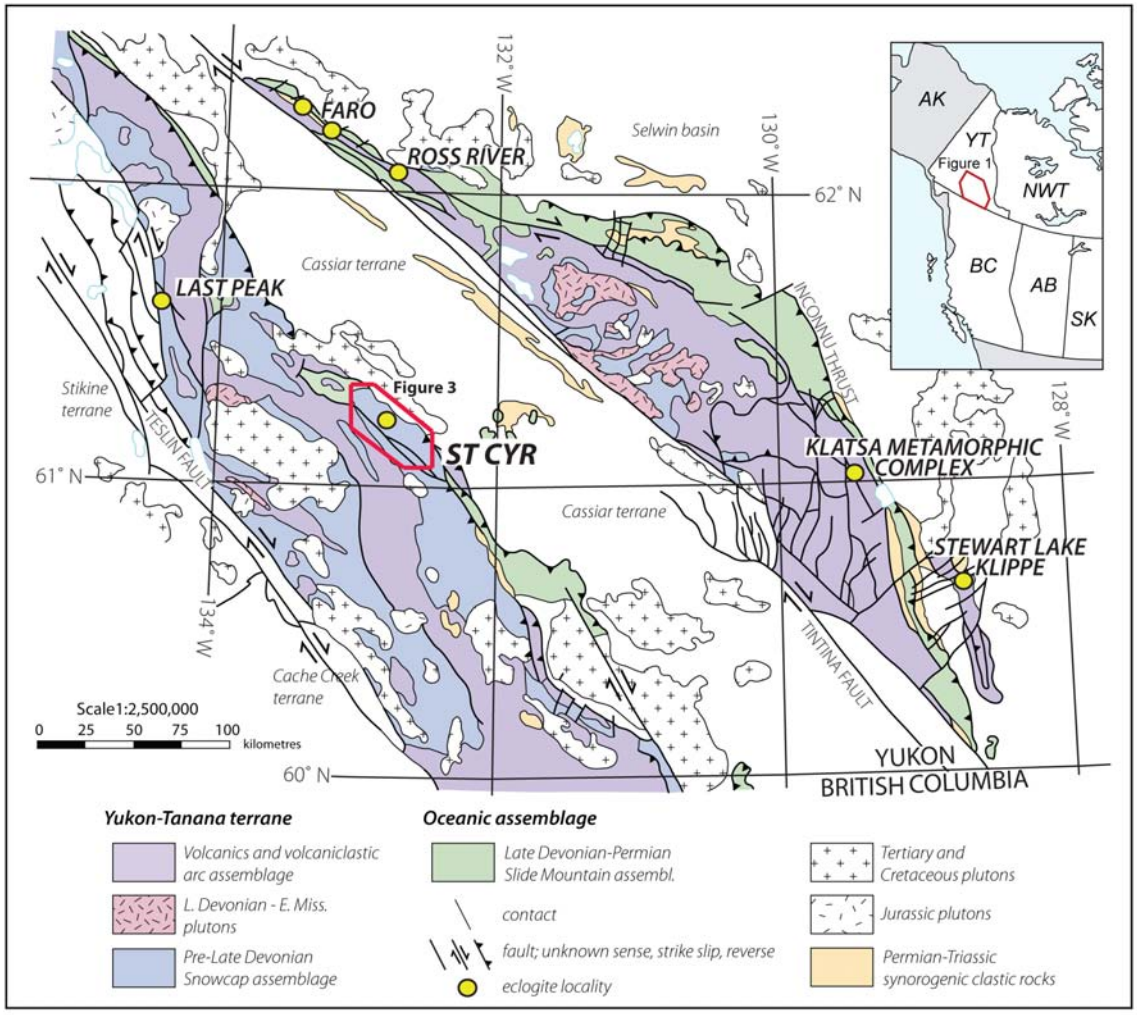

Figure 2-1 Regional geologic map of the Yukon-Tanana and Slide Mountain terrane in south-central Yukon. Modified from Colpron et al. (2006).

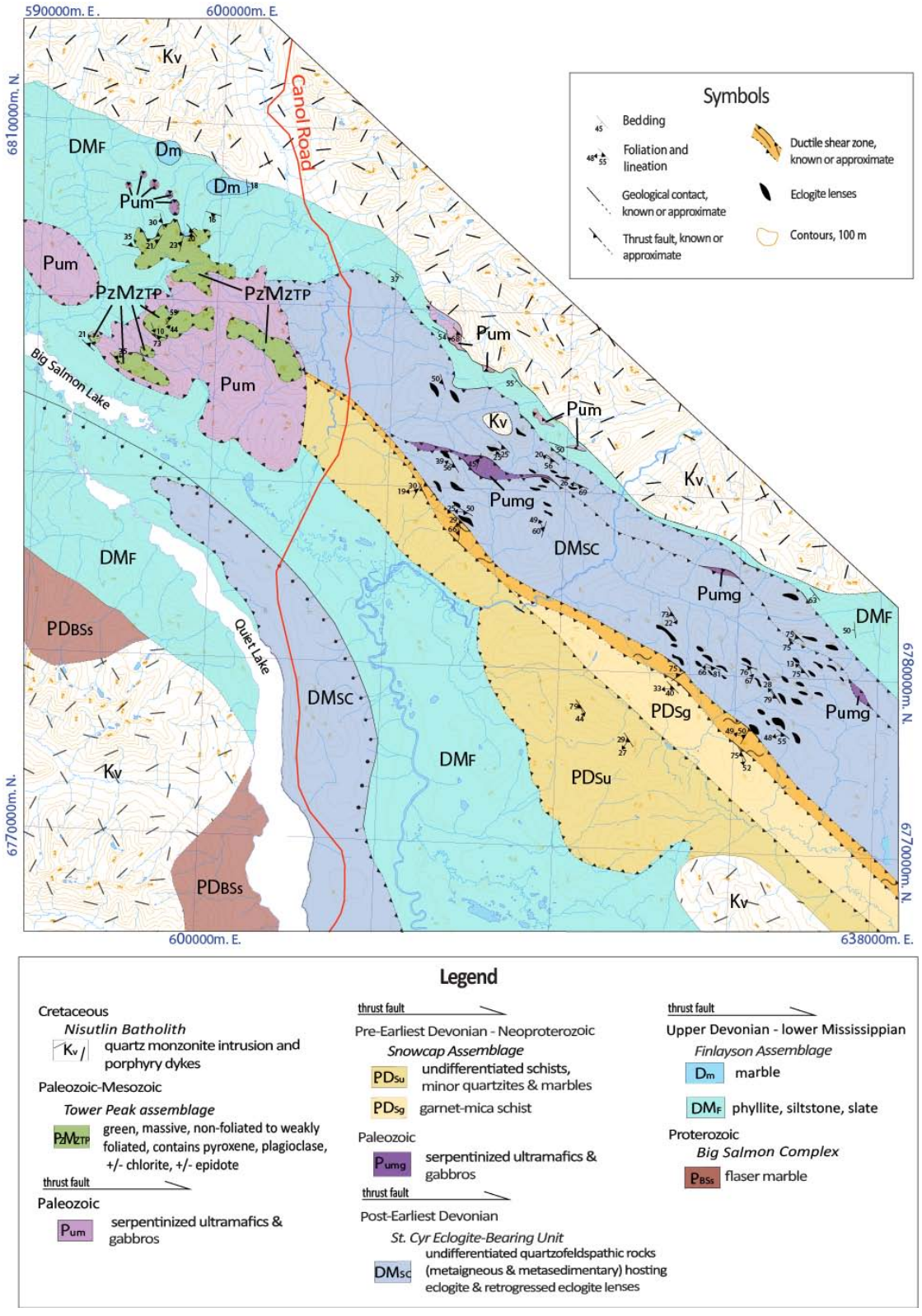

Figure 2-2 Geologic map of the St. Cyr klippe and surrounding region. Modified from Tempelman-Kluit (2012) and Colpron (2006). Based on mapping Isard (2014), this study.

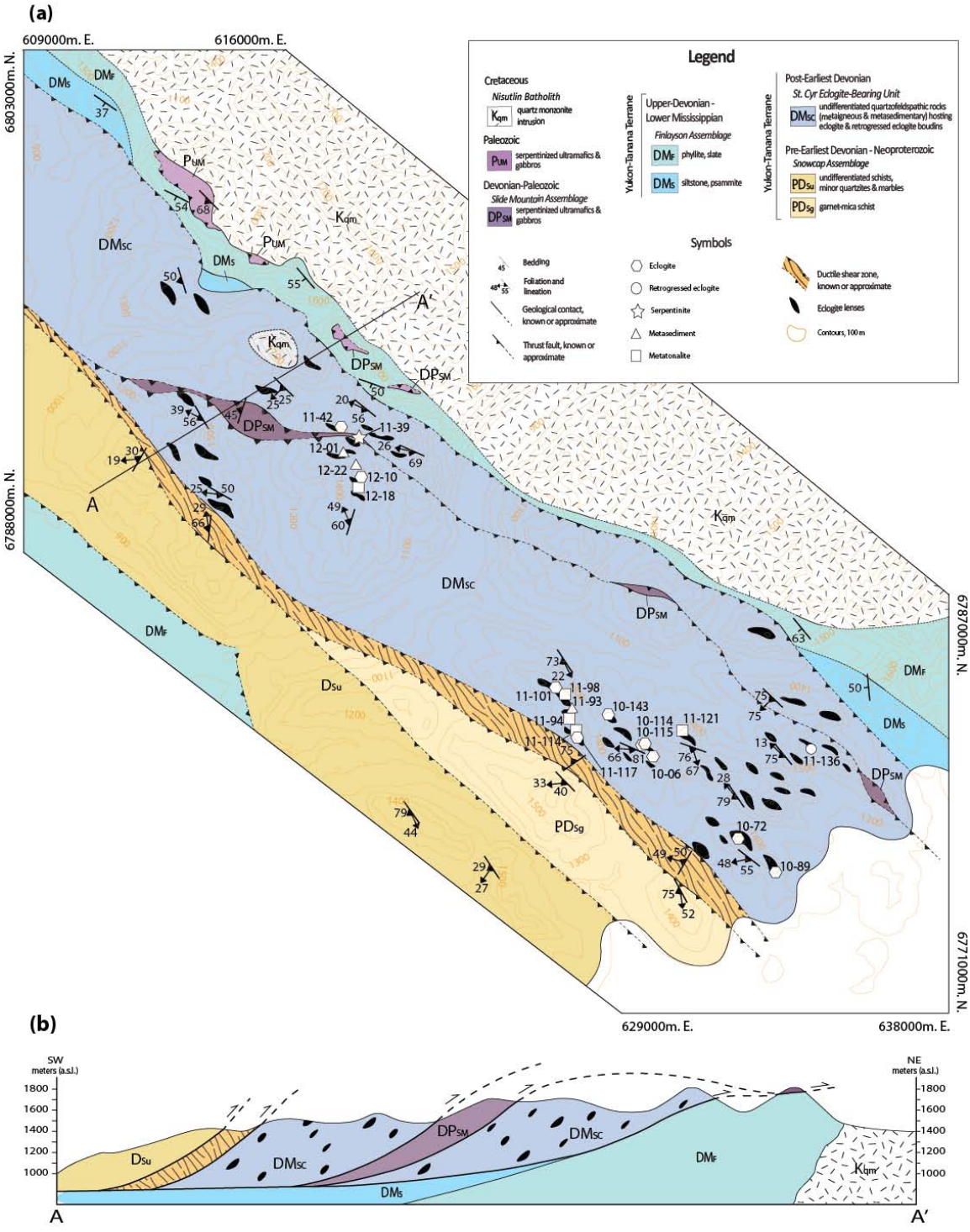

Figure 2-3 Geologic setting of eclogite in the St. Cyr klippe. (a) Geologic map. (b) Cross-section of the eclogite-rich study area. UTM coordinates for samples identifies on the map are shown in Table 2-1.

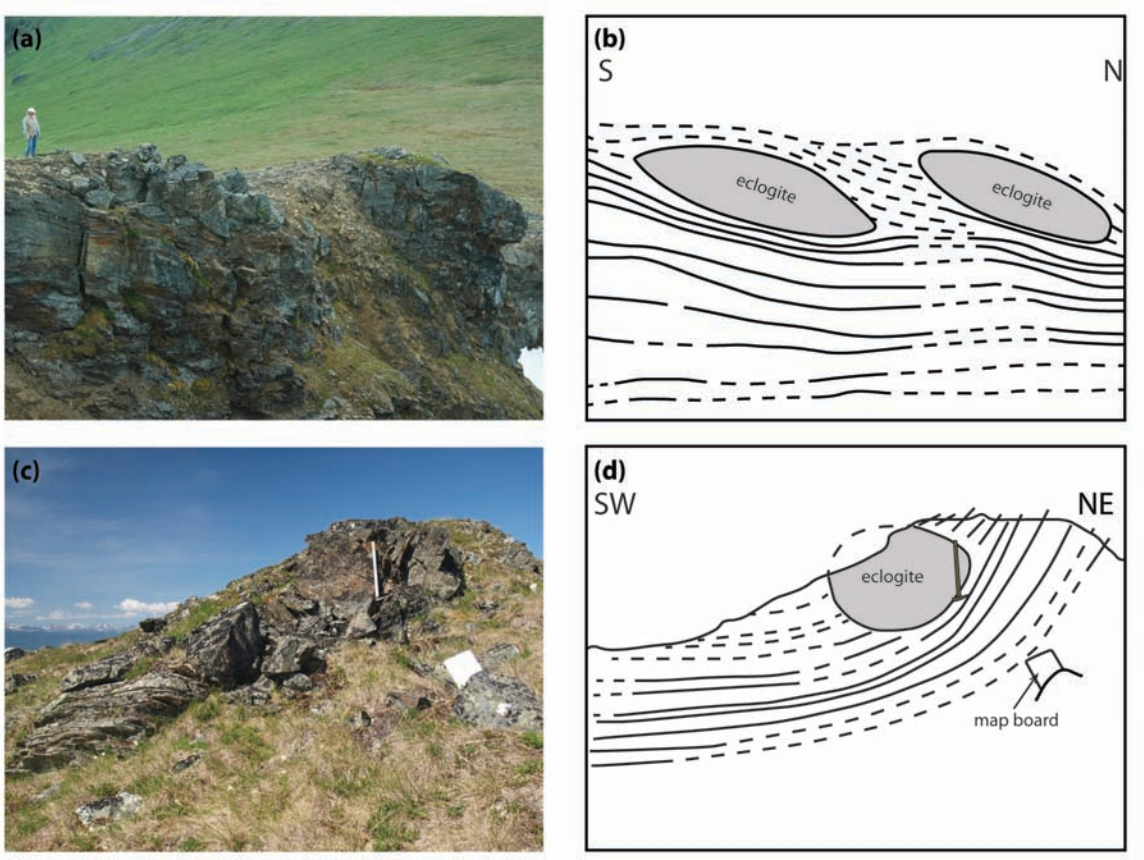

Figure 2-4 Field photographs and simplified illustrations of eclogite boudins within the quartzofeldspathic host rocks. (a) and (c) Field photographs. (b) and (d) Line drawings showing the eclogite boudins and the trace of the foliation of the host rocks. (a) person for scale. (c) Hammer for scale is 80 cm long.

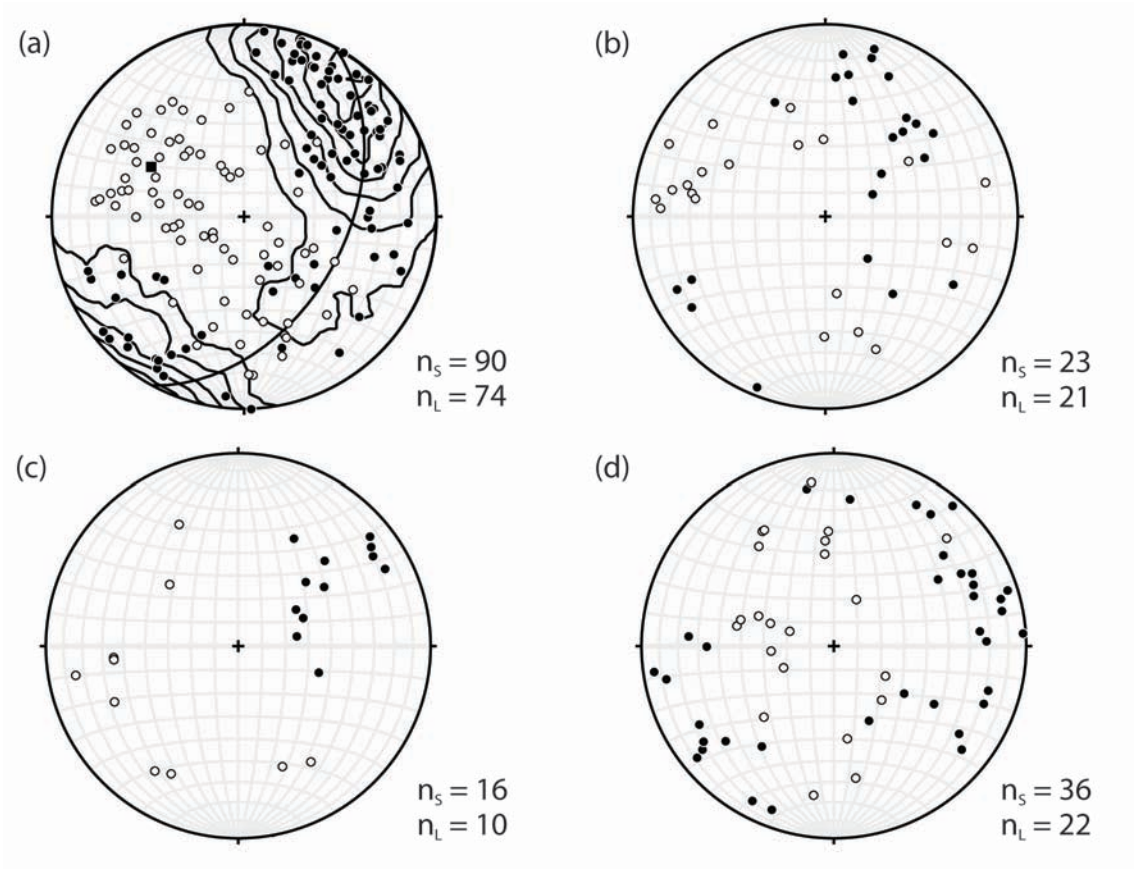

Figure 2-5 Lower hemisphere, equal area stereonet of poles to foliations and lineations in the field area. Filled circles = poles to foliations; open circles = lineations. (a) Upper thrust sheet of eclogite-bearing quartzofeldspathic schists. Poles to foliation measurements plot along a girdle; pole to the girdle (black square) is oriented 45, 298. (b) Lower thrust sheet of eclogite-bearing quartzofeldspathic schists. (c) Snowcap, non-eclogite-bearing schists. (d) Shear zone between eclogite- and non-eclogite-bearing schists.

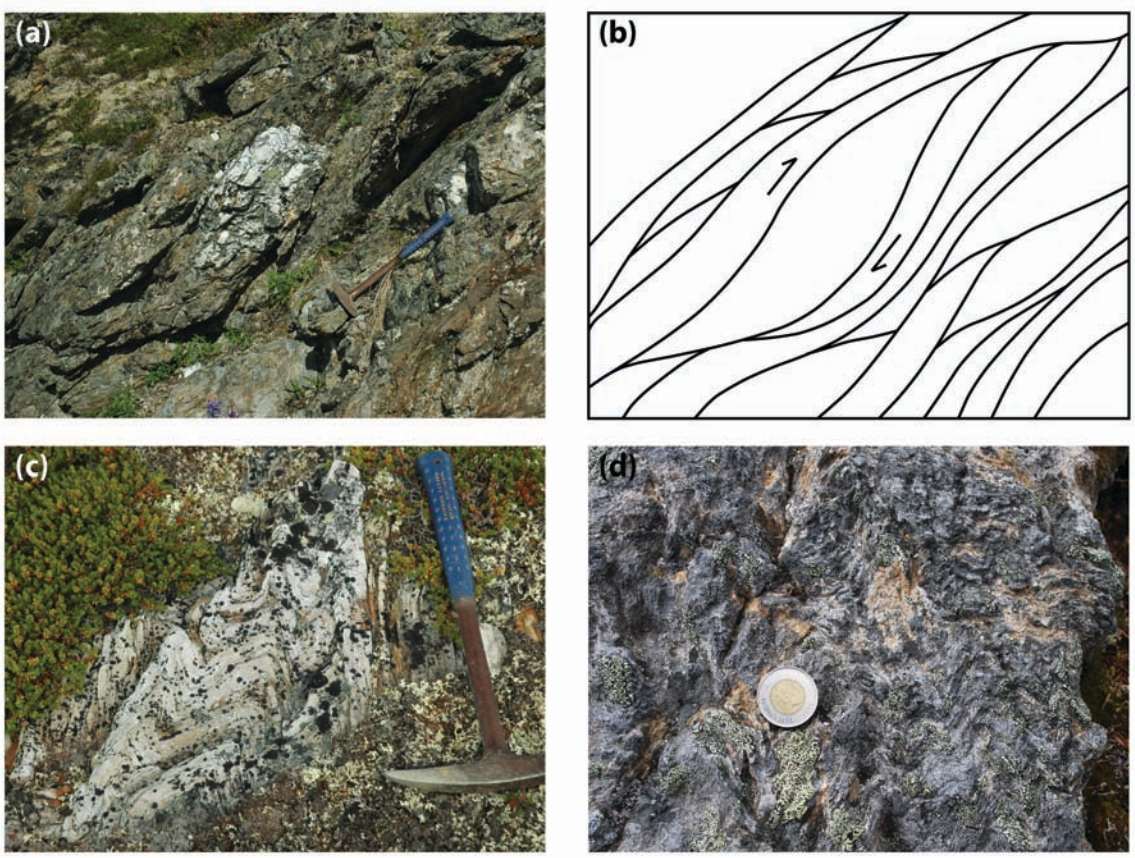

Figure 2-6 Field photographs of the metapsammite matrix of the shear zone. (a) View of the southwest dipping foliation from the northwestern portion of the field area. Hammer for scale is 42 cm long. (b) Line drawing illustrating an anastomosing foliation and direction of movement from (a). (c) Folded quartzite; hammer is 42 cm long. (d) Crenulations within a micaceous quartzite. Coin for scale is 2.8 cm in diameter.

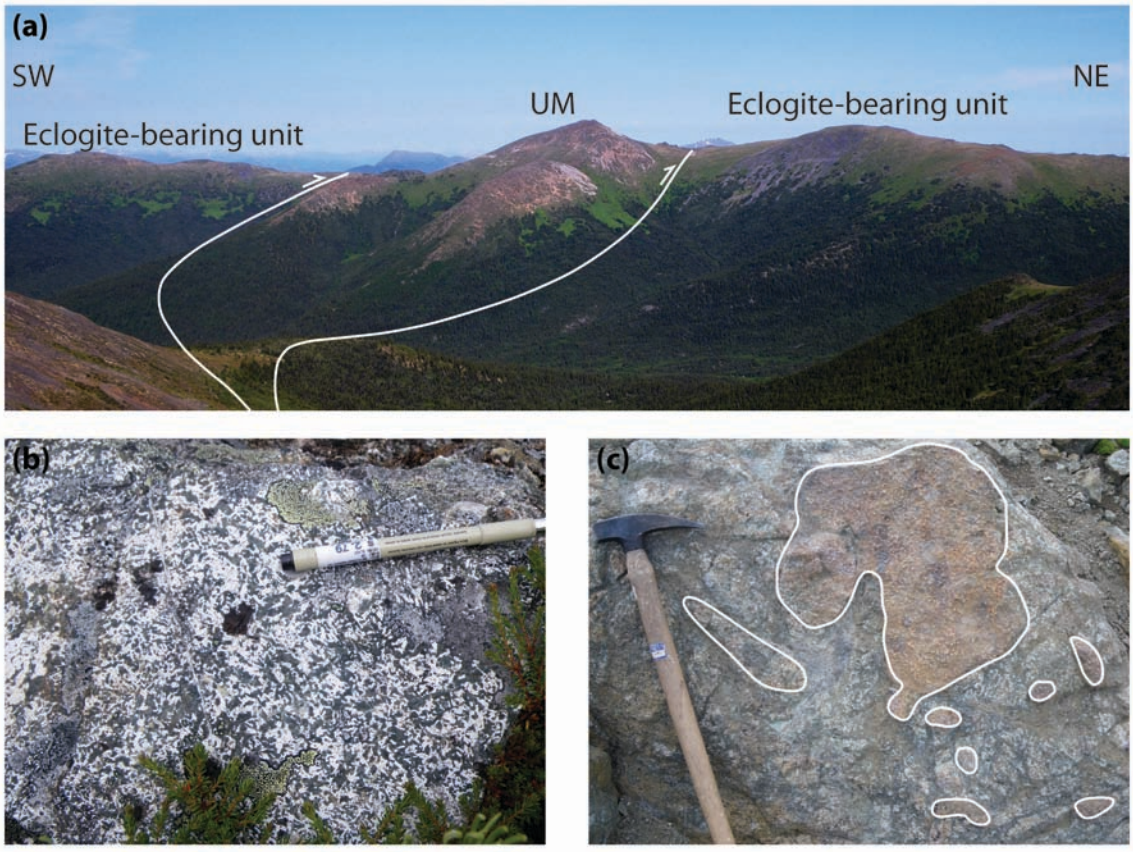

Figure 2-7 Field photographs of low-grade mafic and ultramafic rocks imbricated within the St. Cyr eclogite-bearing unit. a) View of a large, orange-weathering ultramafic body (UM) in the central portion of the field area. White lines mark thrust boundaries. b) Outcrop of leucogabbro preserving intrusive igneous texture. Pen for scale is 13.5 cm long. c) Outcrop of leucogabbro intrusion with ultramafic enclaves (outlined in white). Hammer for scale is 80 cm long.

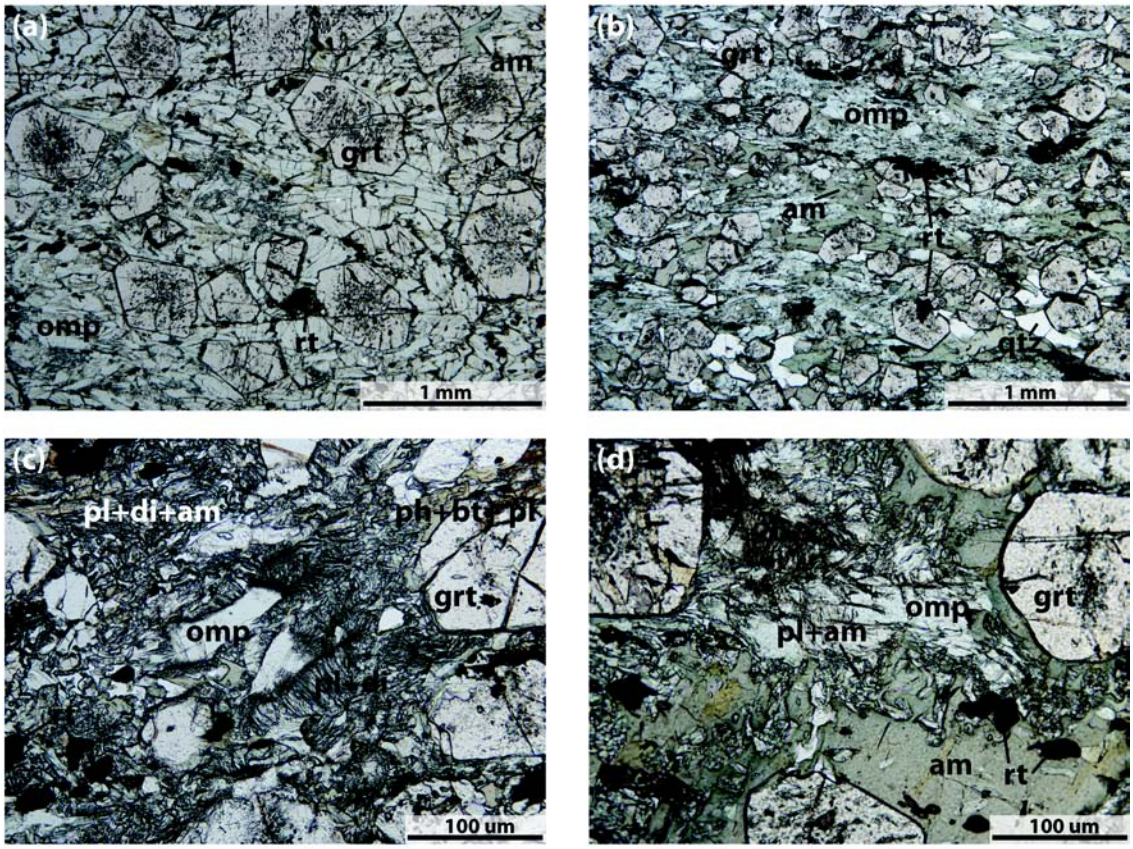

Figure 2-8 Photomicrographs of eclogite in the St. Cyr klippe. (a) Well-preserved eclogite sample 11-101 with a peak assemblage of omphacite, garnet, and rutile. b) Well-preserved eclogite sample 10-89 with a peak assemblage of omphacite, garnet, quartz, amphibole, and rutile. c) Retrogressed eclogite sample 12-10 showing omphacite altering to lobate symplectite of plagioclase + diopside, which is intern replaced by amphibole. d) Retrogressed eclogite sample 10-06 with omphacite converting to plagioclase + amphibole. Plane polarized light.

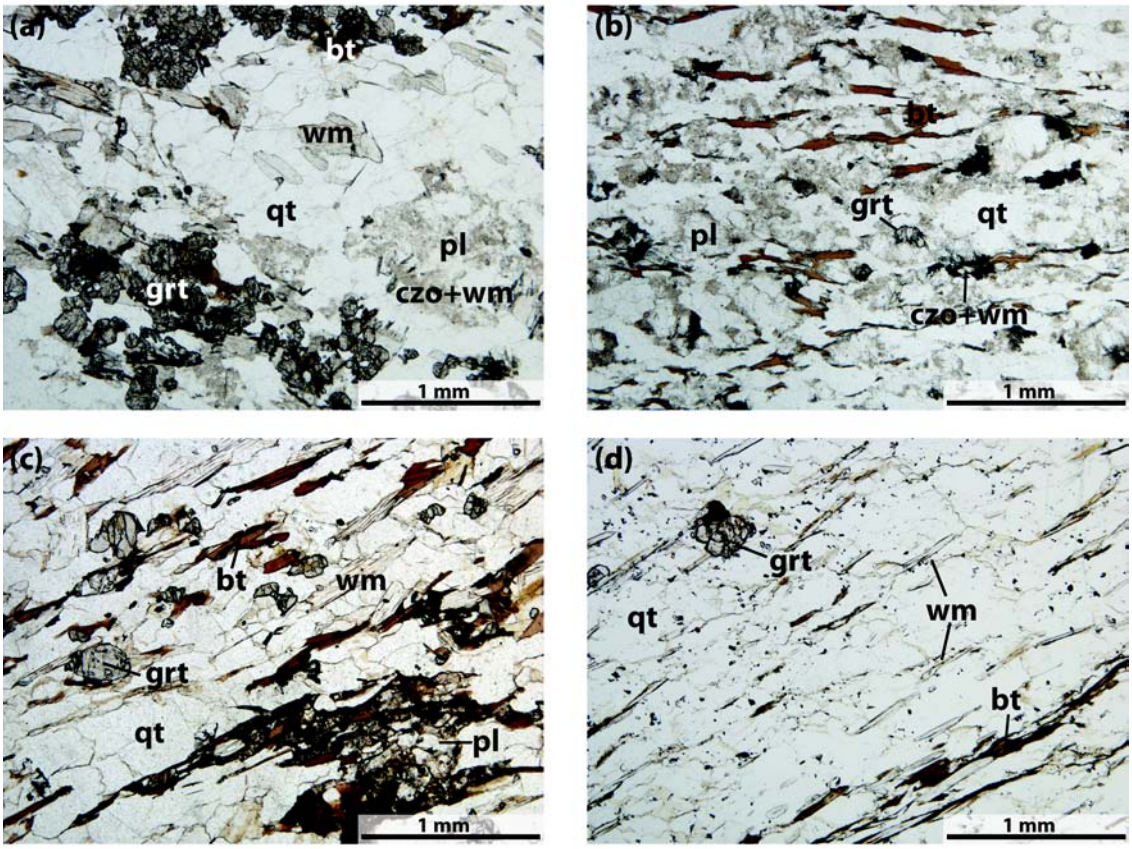

Figure 2-9 Photomicrographs of quartzofeldspathic host rocks. (a) Garnet-bearing, phengite + biotite-bearing metatonalite sample 11-121. Plagioclase is replaced by fine-grained phengite and clinozoisite. (b) Foliated metatonalite sample 11-98. This sample has more biotite and phengite is generally associated with plagioclase. (c) Garnet-phengite + biotite-schist sample 11-93. (g) Garnet-white mica quartzite sample 12-01. Plane polarized light.

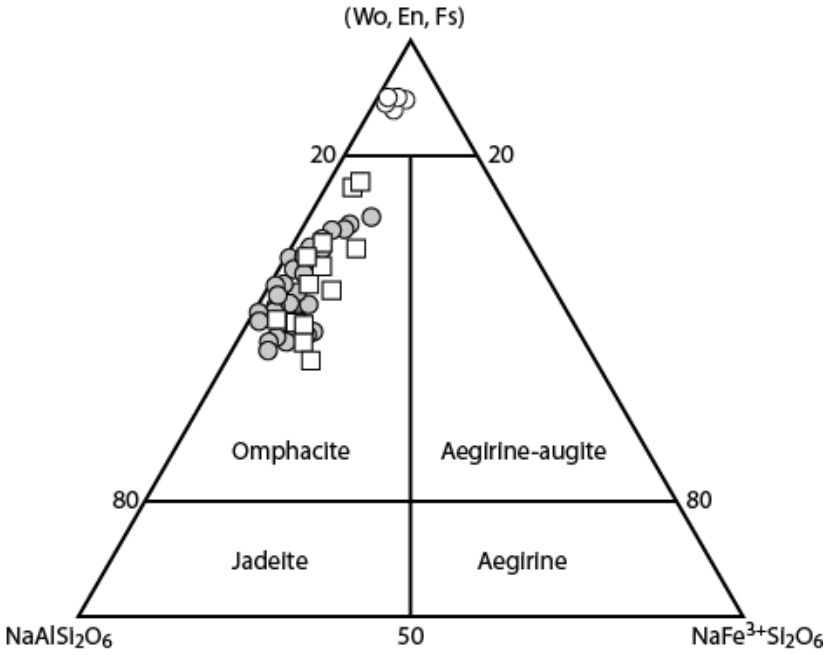

Figure 2-10 Ternary plot of omphacite compositions in the matrix. After Morimoto et al. 1989. Wo, En, Fs = wollastonite (Fe: $CaSiO_3$) + entatite (En: $MgSiO_3$) + ferrosilite (Fs: $FeSiO_3$). Matrix grains = gray circles, garnet inclusion = open squares, diopside in symplectites = open circles.

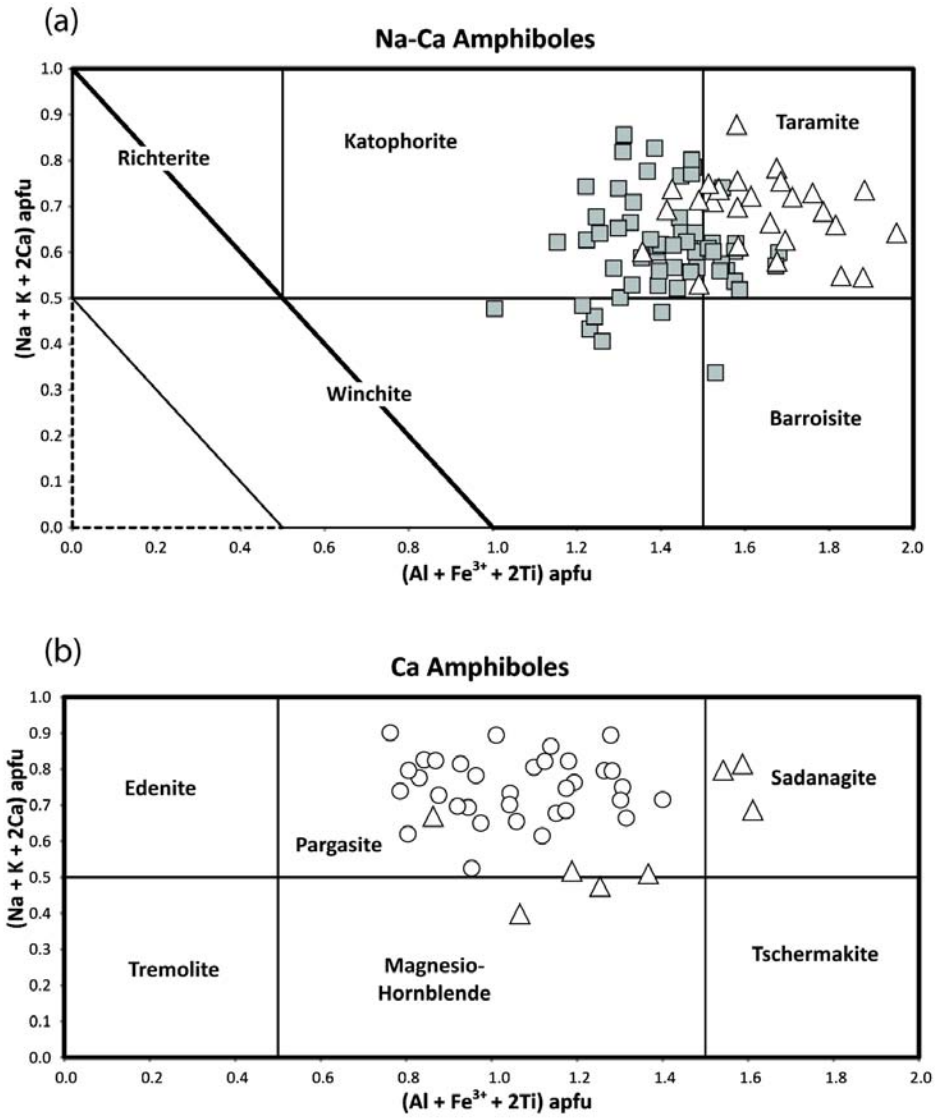

Figure 2-11 Compositional variations of amphibole diagram. Modified after Hawthorne et al. (2012). (a) Na-Ca amphibole in the matrix (gray squares) and included in garnet (open triangles). (b) Ca amphiboles in symplectites (open circles) and as garnet inclusions (symbol as above).

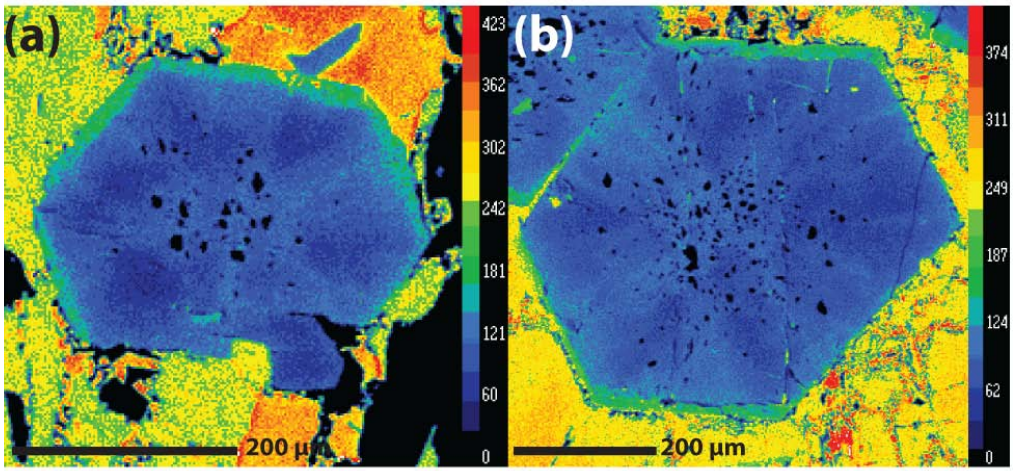

Figure 2-12 Mg X-ray maps in sector zoned garnet from the St. Cyr klippe. Samples (a) 10-143 and (b) 10-06. Warm colors represent higher elemental concentrations and cool colors, lower concentrations.

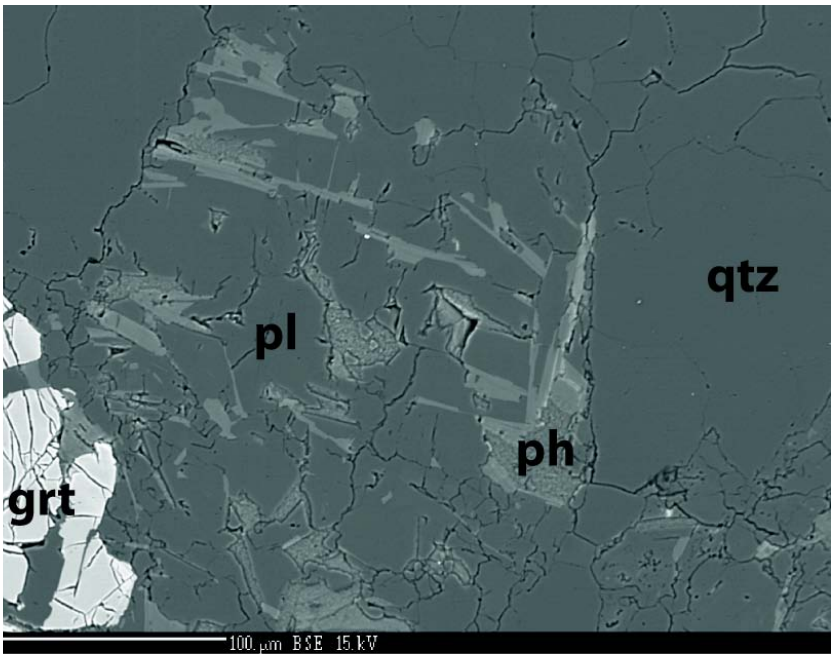

Figure 2-13 Backscattered electron image of fine-grained phengite replacing plagioclase within metatonalite sample 12-18.

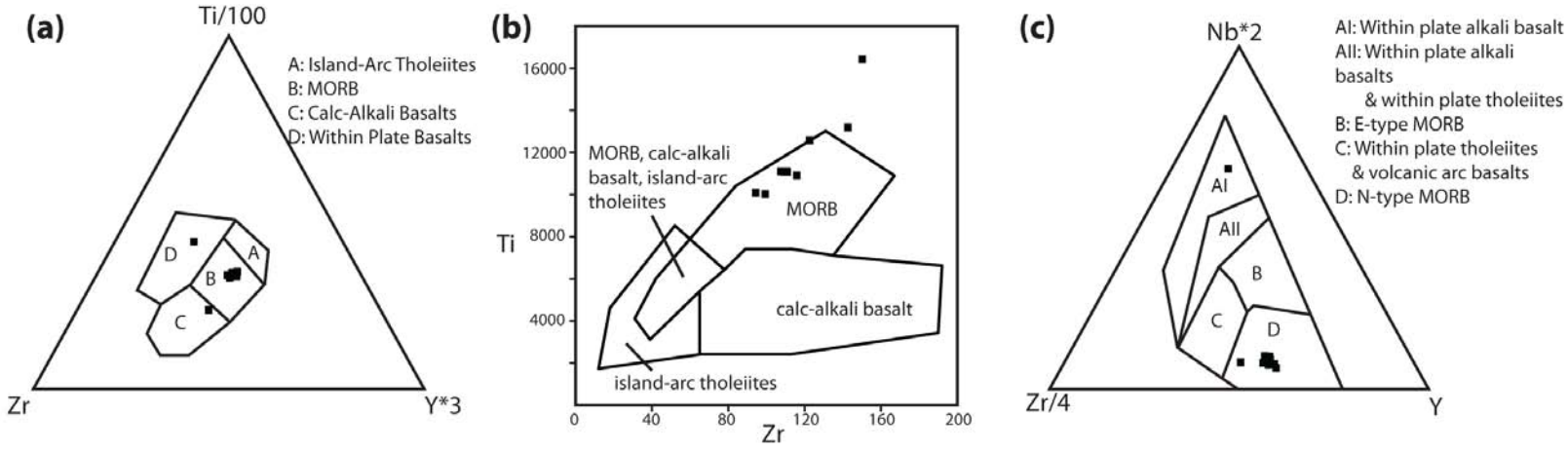

Figure 2-14 Trace element discrimination diagrams for eclogite to identify the protolith and its tectonic setting in the St. Cyr klippe. The protolith is normal mid-oceanic ridge basalt (N-MORB).

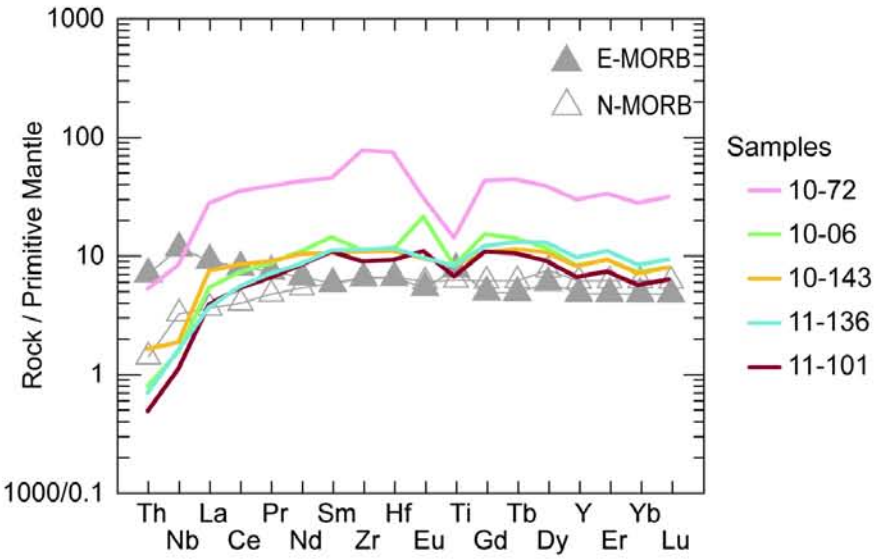

Figure 2-1 Primitive-mantle normalized plot for eclogites and retrogressed eclogites in the St. Cyr klippe. Normal mid-ocean ridge basalt (N-MORB) and enriched mid-ocean ridge basalt (E-MORB) are shown for reference (Sun and McDonough, 1989).

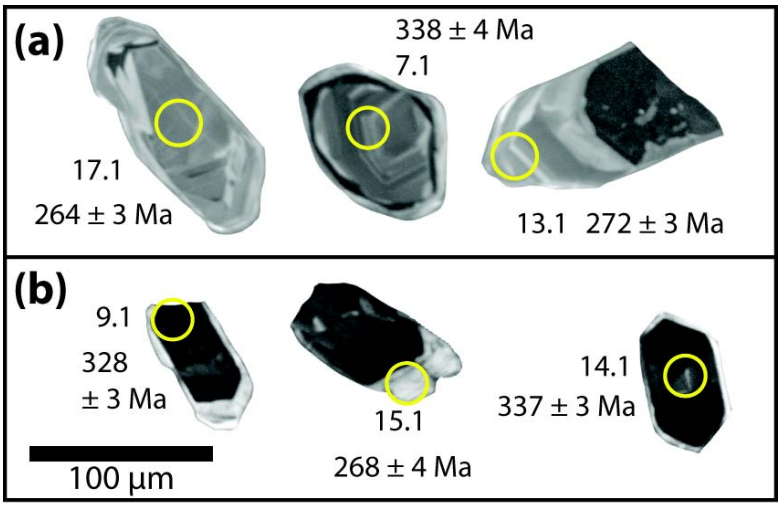

Figure 2-2 Representative cathodoluminescence (CL) images of metatonalites from the St. Cyr klippe. (a) 11-94 and (b) 11-114. Ellipses indicate SHRIMP-RG U-Pb and trace element analysis spots labeled by grain and spot number.

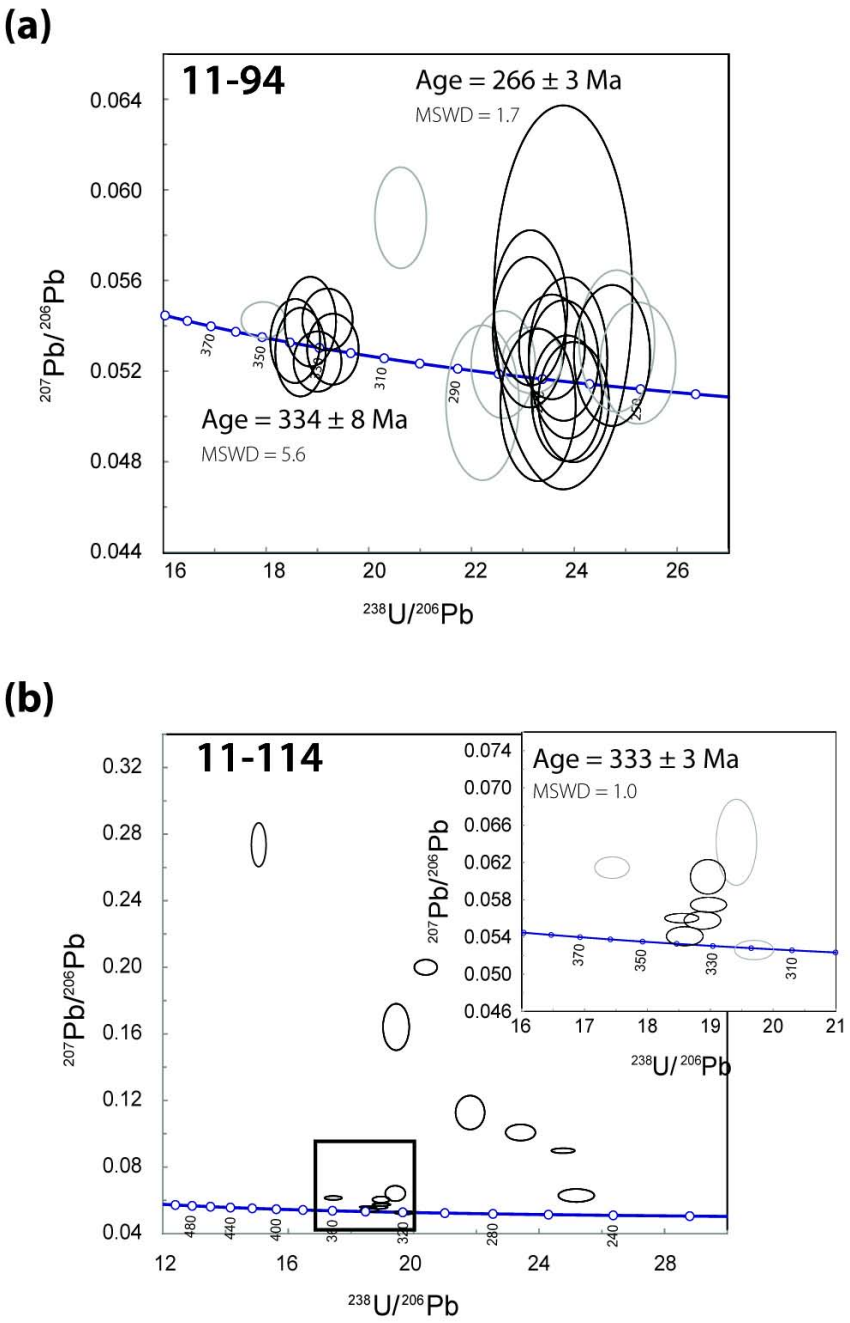

Figure 2-17 Terra–Wasserburg plots of sensitive high-resolution ion microprobe reverse-geometry (SHRIMP-RG) U/Pb data from metatonalites from the St. Cyr klippe. Samples 11-94 (a) and 11-114 (b). Data are 1σ error ellipses uncorrected for common Pb. Black ellipses are used in calculating concordia ages. Errors are reported at the 95% confidence level. Weighted mean ages were calculated for 11-94 (a). A weighted mean age was calculated for the crystallization age of sample 11-114 (b) and an intercept age of 248 ± 8 Ma was calculated for the metamorphic age.

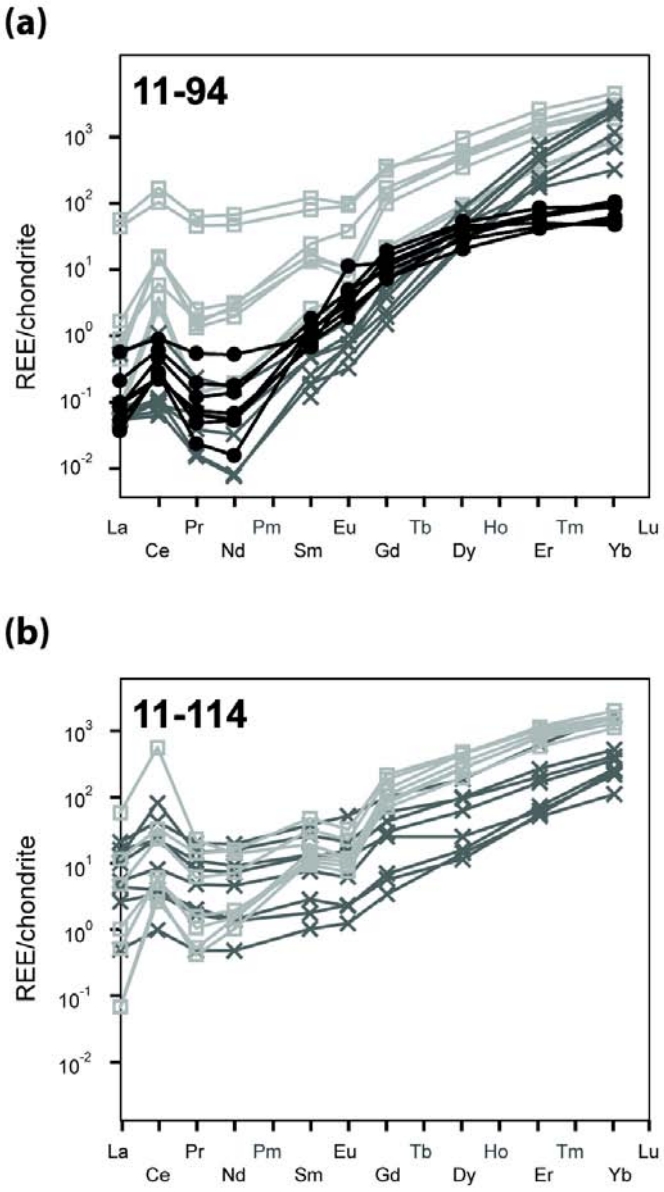

Figure 2-18 Chondrite-normalized REE patterns for different age populations of zircon grains from metatonalites from the St. Cyr klippe. Samples 11-94 (a) and 11-114 (b). Normalization uses chondrite abundances from Anders and Grevesse (1989) multiplied by 1.36 (Korotev, 1996). Ages are divided into igneous crystallization ages (lightest gray) and metamorphic ages (medium gray – without garnet; black – HP with garnet) as discussed in the text.

Table 2-1 Sample locations

Sample	UTM Coordinates (Zone 8N)
Eclogites	E N
10-06	0629189, 6780367
10-72	0632445, 6777476
10-89	0633667, 6776599
10-114	0629167, 6780409
10-115	0629167, 6780409
10-143	0628260, 6781208
11-42	0618451, 6790935
11-101	0626171, 6782297
11-117	0626764, 6780873
12-10	0619035, 6789751
Retrogressed eclogite	
11-136	0634779, 6780635
Serpentinite	
11-39	0618349, 6790941
Metasedimentary rocks	
11-93	0626547, 6781336
12-01	0618526, 6790306
12-22	0618848, 6790004
Metatonalites	
11-94	0626543, 6781389
11-98	0626445, 6781946
11-114	0626570, 6781168
11-121	0630776, 6780456
12-18	0618918, 6788995

Table 2-2 Representative clinopyroxene compositions in eclogite

Sample	10-115	12-10	11-42	12-10	11-117	11-42	11-117
Mineral	Omp (m)	Omp (m)	Omp (m)	Cpx (s)	Cpx (s)	Cpx (a)	Omp (i)
Anal.	3/1	2/1	12/1	6/1	5/1	9/1	4/1
SiO_2 wt%	55.866	54.393	53.995	51.107	53.655	53.150	55.152
TiO_2	0.060	0.203	0.082	0.322	0.075	0.187	0.178
Al_2O_3	10.262	9.723	4.726	7.697	1.679	3.960	9.981
Cr_2O_3		0.045		0.033	0.009		
FeO	5.520	5.189	7.108	6.441	11.260	7.441	6.436
MnO	0.000	0.048	0.175	0.048	0.177	0.173	0.078
MgO	8.049	9.334	11.433	12.757	10.673	12.043	8.142
CaO	13.457	16.073	19.398	18.837	21.570	20.841	13.560
Na_2O	6.780	5.207	2.865	2.296	1.416	2.290	6.398
K_2O	0.000		0.005			0.017	0.001
Total	99.994	100.215	99.787	99.538	100.514	100.102	99.926
Si	1.992	1.949	1.980	1.867	2.005	1.949	1.977
Ti	0.002	0.005	0.002	0.009	0.002	0.005	0.005
Al	0.431	0.411	0.204	0.331	0.074	0.171	0.422
Cr		0.001		0.001	0.000		
Fe^{3+}	0.050	0.041	0.036	0.080	0.014	0.084	0.059
Fe^{2+}	0.114	0.114	0.182	0.117	0.338	0.145	0.134
Mn	0.000	0.001	0.005	0.001	0.006	0.005	0.002
Mg	0.428	0.499	0.625	0.695	0.595	0.658	0.435
Ca	0.514	0.617	0.762	0.737	0.864	0.819	0.521
Na	0.469	0.362	0.204	0.163	0.103	0.163	0.445
K	0.000		0.000			0.001	0.000
Quad	0.50	0.60	0.76	0.75	0.88	0.77	0.51
Jd	0.45	0.35	0.20	0.17	0.10	0.15	0.43
Ae	0.05	0.04	0.04	0.08	0.01	0.08	0.06
Wo				0.45	0.48	0.48	
En				0.43	0.33	0.39	

m, matrix; s, symplectite; a, adjacent to am+pl symplectite; i, inclusion in garnet

Calculation based on 6 O

Table 2-1 Representative amphibole compositions in eclogite

Sample	12-10	12-10	12-10	10-115	10-115	10-115	11-117	11-117	11-117
Mineral	m	i	i	m	s	i	m	i	i
Analysis	4/1	3/1	1/1	5/1	8/1	1/1	5/1	3/1	8/1
SiO_2 wt%	43.555	43.157	45.969	51.394	45.248	44.240	43.784	45.343	39.331
TiO_2	0.749	0.899	0.890	0.380	0.953	0.358	0.881	0.420	1.471
Al_2O_3	16.179	16.749	11.266	10.107	11.458	15.539	15.151	11.625	16.815
FeO	12.082	11.311	12.024	10.899	12.343	15.595	13.986	14.847	17.075
MnO	0.067	0.057	0.127	0.085	0.059	0.104	0.023	0.096	0.045
MgO	11.175	11.604	13.418	13.330	13.320	9.018	10.160	10.928	8.378
CaO	9.243	9.544	10.595	7.485	11.137	9.001	8.984	11.270	11.215
Na_2O	3.675	3.565	2.606	4.561	2.915	4.351	4.340	3.107	3.052
K_2O	0.757	0.879	0.583	0.374	0.576	0.586	0.731	0.000	0.631
Total	97.482	97.765	97.478	98.615	98.009	98.792	98.040	97.636	98.013
Mineral formulas and names based on 23 oxygens and sum of cations - (Ca + Na + K) = 13									
Si	6.291	6.208	6.634	7.211	6.558	6.433	6.384	6.687	5.873
Ti	0.081	0.097	0.097	0.040	0.104	0.039	0.097	0.047	0.165
Al	2.754	2.839	1.916	1.671	1.957	2.663	2.603	2.021	2.959
Fe^{3+}	0.472	0.454	0.510	0.268	0.335	0.252	0.267	0.062	0.373
Fe^{2+}	0.987	0.907	0.941	1.011	1.161	1.645	1.438	1.769	1.759
Mn	0.008	0.007	0.016	0.010	0.007	0.013	0.003	0.012	0.006
Mg	2.406	2.488	2.887	2.788	2.878	1.955	2.208	2.403	1.865

Table 2-3 Continued

Sample	12-10	12-10	12-10	10-115	10-115	10-115	11-117	11-117	11-117
Ca	1.430	1.471	1.638	1.125	1.729	1.402	1.403	1.781	1.794
Na	1.029	0.994	0.729	1.241	0.819	1.227	1.227	0.888	0.884
K	0.139	0.161	0.107	0.067	0.106	0.109	0.136	0.000	0.120
Name	taramite	taramite	magnesio-hornblende	winchite	pargasite	katophorite	katophorite	pargasite	sadanagaite

m, matrix; i, inclusion in garnet; s, symplectite

Table 2-2 Representative garnet compositions

Rock type	Eclogite					Metatonalite		Metasediment		
Sample	10-143	10-143	10-143	12-10	12-10	12-18	12-18	12-22	12-22	12-22
Analysis	core	interm.	rim	core	rim	core	rim	core	interm.	rim
Analysis	10/1	6/1	1/1	2/16	2/1	1/10	1/1	1/9	1/4	1/1
SiO_2 wt%	38.513	38.313	38.751	38.675	39.548	38.369	39.017	37.878	39.325	37.789
TiO_2	0.265	0.155	0.040	0.195	0.034	0.070	0.122	0.046	0.066	0.250
Al_2O_3	21.855	21.762	22.083	21.473	22.103	21.564	21.753	21.013	21.505	20.951
FeO	24.196	26.673	26.831	25.116	21.739	24.276	23.628	26.648	26.087	16.548
MnO	1.705	0.947	0.647	0.901	0.420	2.570	1.326	6.856	6.807	12.033
MgO	3.810	2.154	6.138	4.257	6.999	1.940	3.827	3.300	2.973	0.430
CaO	10.848	11.400	6.490	9.422	8.741	11.299	10.280	4.194	3.654	11.802
Total	101.192	101.404	100.979	100.039	99.584	100.088	99.953	99.935	100.417	99.803
Mineral formulas based on 12 oxygens										
Si	2.978	2.987	2.984	3.023	3.043	3.030	3.050	3.025	3.126	3.024
Ti	0.015	0.009	0.002	0.011	0.002	0.004	0.007	0.003	0.004	0.015
Al	1.992	2.000	2.004	1.978	2.005	2.007	2.004	1.978	2.015	1.976
Fe^{3+}	0.020	0.008	0.024	0.000	0.000	0.000	0.000	0.000	0.000	0.000
Fe^{2+}	1.544	1.731	1.704	1.642	1.399	1.603	1.544	1.779	1.734	1.107
Mn	0.112	0.063	0.042	0.060	0.027	0.172	0.088	0.464	0.458	0.815
Mg	0.439	0.250	0.705	0.496	0.803	0.228	0.446	0.393	0.352	0.051
Ca	0.899	0.952	0.535	0.789	0.721	0.956	0.861	0.359	0.311	1.012

Table 2-4 Continued

Sample	10-143	10-143	10-143	12-10	12-10	12-18	12-18	12-22	12-22	12-22
Endmembers										
X_{Alm}	0.52	0.58	0.57	0.55	0.47	0.54	0.53	0.59	0.61	0.37
X_{Sps}	0.04	0.02	0.01	0.02	0.01	0.06	0.03	0.15	0.16	0.27
X_{Prp}	0.15	0.08	0.23	0.17	0.27	0.08	0.15	0.13	0.12	0.02
X_{Grs}	0.30	0.32	0.18	0.26	0.24	0.32	0.29	0.12	0.11	0.34
X_{Mg}	0.22	0.13	0.29	0.23	0.36	0.12	0.22	0.18	0.17	0.04

Table 2-3 Representative phengite compositions

Rock type	Eclogite			Metatonalite		Metasediment		
Sample	11-117	10-115	10-115	11-94	12-18	11-93	11-93	12-22
Mineral	mc	mr	i	m	r	m	i	r
Analysis	1/13	3/1	1/1	1/5	1/1	7/1	1/1	7/1
SiO_2 wt%	49.642	48.466	49.049	47.900	50.863	48.283	46.879	48.283
TiO_2	0.879	0.974	0.995	0.811	0.054	1.310	1.518	0.000
Al_2O_3	27.241	27.593	28.004	30.459	27.479	29.088	32.298	28.680
FeO	2.356	2.274	2.488	1.683	2.188	3.416	1.746	2.035
MnO	0.011	0.011	0.000	0.000	0.000	0.034	0.000	0.069
MgO	3.319	3.374	3.556	2.278	2.325	2.730	2.064	2.940
CaO	0.011	0.030	0.014	0.029	0.128	0.000	0.003	0.077
Na_2O	0.630	0.524	0.688	0.307	2.104	0.496	0.717	0.739
K_2O	10.289	9.945	9.853	10.506	8.482	9.892	9.826	9.721
BaO		0.876		0.630	0.617	0.610	0.856	0.683
Total	94.378	94.067	94.647	94.603	94.240	95.859	95.907	93.227
Mineral formulas based on 11 oxygens								
Si	3.353	3.304	3.301	3.234	3.422	3.240	3.127	3.306
Ti	0.045	0.050	0.050	0.041	0.003	0.066	0.076	0.000
Al	2.168	2.217	2.221	2.423	2.179	2.300	2.538	2.314
Fe^{2+}	0.133	0.130	0.140	0.095	0.123	0.192	0.097	0.116
Mn	0.001	0.001	0.000	0.000	0.000	0.002	0.000	0.004

Table 2-5 Continued

Sample	11-117	10-115	10-115	11-94	12-18	11-93	11-93	12-22
Mg	0.334	0.343	0.357	0.229	0.233	0.273	0.205	0.300
Ca	0.001	0.002	0.001	0.002	0.009	0.000	0.000	0.006
Na	0.082	0.069	0.090	0.040	0.274	0.065	0.093	0.098
K	0.886	0.865	0.846	0.905	0.728	0.847	0.836	0.849
Ba		0.023		0.017	0.016	0.016	0.022	0.018
mc, matrix-core; mr, matrix-rim; m, matrix; i, inclusion in garnet; r, replacing plagioclase								

Table 2-4 Representative biotite, clinozoisite-epidote, plagioclase, and K-feldspar compositions

Rock type	eclogite	meta-tonalite	meta-sediment	eclogite	meta-tonalite	meta-sediment	eclogite	meta-tonalite	meta-sediment	meta-tonalite
Sample	11-117	11-94	11-93	10-06	12-18	12-22	10-143	11-94	12-22	11-94
Mineral	Bt	Bt	Bt	Ep	Ep	Czo	Pl	Pl	Pl	Kfs
Analysis	s	m	m	i	r	r	i	m	m	r
Analysis	3/1	4/1	6/1	5/1	2/1	5/1	11/1	1/1	14/1	6/1
SiO_2 wt%	46.183	35.981	36.620	38.202	38.283	38.873	64.967	63.572	65.973	62.760
TiO_2	1.391	1.668	2.243	0.053	0.086	0.000				0.027
Al_2O_3	20.167	18.073	19.103	28.463	28.723	33.018	21.732	23.140	21.472	19.317
FeO	9.187	18.420	18.818	7.125	6.223	0.663	0.397	0.012	0.000	0.135
MnO	0.000	0.339	0.053	0.176	0.054	0.548	0.032			0.000
MgO	7.259	10.052	9.842	0.111	0.028	0.000	0.000			0.008
CaO	0.815	0.000	0.000	23.288	23.797	23.497	2.537	3.858	1.527	0.033
Na_2O	3.977	0.080	0.259				10.560	9.396	10.818	0.679
K_2O	5.543	9.368	8.940				0.021	0.133	0.104	15.179
BaO										1.889
Total	94.522	93.981	95.878	97.418	97.194	96.599	100.245	100.111	99.894	100.027
Oxygen	11	11	11	12.5	12.5	12.5	8	8	8	8
Si	3.238	2.765	2.744	2.810	2.837	2.974	2.861	2.804	2.898	2.937
Ti	0.073	0.096	0.126	0.003	0.005	0.000				0.001
Al	1.667	1.637	1.687	2.467	2.509	2.976	1.128	1.203	1.112	1.065

Table 2-6 Continued

Sample	11-117	11-94	11-93	10-06	12-18	12-22	10-143	11-94	12-22	11-94
Fe^{2+}	0.539	1.184	1.179	0.876	0.771	0.085	0.015	0.000	0.000	0.005
Mn	0.000	0.022	0.003	0.011	0.003	0.036	0.001			0.000
Mg	0.759	1.152	1.100	0.012	0.003	0.000	0.000			0.001
Ca	0.061	0.000	0.000	1.835	1.889	1.926	0.120	0.182	0.072	0.002
Na	0.541	0.012	0.038				0.902	0.803	0.921	0.062
K	0.496	0.918	0.855				0.001	0.007	0.006	0.906
Ba										0.035
X_{Mg}	0.58	0.49	0.48							
X_{Fe3+}				0.26	0.24	0.03				
X_{Ca}							0.88	0.82	0.93	0.03

m, matrix; i, inclusion in garnet; r, replacing plagioclase; s, symplectite

Table 2-5 Whole-rock geochemical data for eclogite

Sample	10-06	10-72	10-143	11-101	11-136	10-114[a]	10-115[a]	11-42[a]	11-117[a]	12-10[a]
SiO_2 wt. %	48.17	49.73	51.14	50.40	50.36	48.97	50.36	45.16	49.31	48.77
TiO_2	1.85	2.40	1.85	1.67	1.85	2.10	1.85	2.74	2.20	1.82
Al_2O_3	14.02	13.10	13.44	13.50	14.04	13.66	13.89	14.18	14.24	15.04
FeO_{tot}	12.25	14.95	12.14	11.11	10.80	13.71	13.16	12.88	14.32	11.66
MnO	0.22	0.29	0.21	0.20	0.16	0.26	0.21	0.47	0.25	0.20
MgO	6.08	4.99	6.48	6.91	6.87	6.74	6.84	8.74	6.47	7.25
CaO	12.78	8.86	10.51	11.72	11.17	10.37	10.20	8.40	10.15	11.43
Na_2O	2.92	3.99	3.62	3.11	2.49	3.27	3.13	2.61	3.19	2.91
K_2O	0.28	0.14	0.11	0.24	0.08	0.27	0.32	2.77	0.19	0.29
P_2O_5	0.32	0.27	0.14	0.23	0.16	0.15	0.14	0.46	0.16	0.13
Total	98.90	98.70	99.65	99.09	97.98	99.50	100.10	98.41	100.46	99.49
Sc (ppm)	43.9	40.9	44.4	43.3	40.1	48.3	46.0	29.1	48.4	47.7
Pb	2.65	0.77	0.62	1.54	0.36	1.00	0.70	3.30	0.80	1.50
Rb	13.1	1.5	1.8	7.3	1.9	3.9	5.8	90.5	1.9	3.8
Cs	0.53	0.02	0.06	0.23	0.55					
Ba	196	51	26	159	15	76	119	1495	34	75
Sr	384	88	257	152	108	124	148	251	185	85
Ta	0.19	0.44	0.21	0.17	0.21					
Nb	2.70	6.13	2.96	2.30	2.75	3.50	3.50	58.00	4.50	2.80
Hf	3.05	7.66	3.03	2.78	3.11					

Table 2-7 Continued

Sample	10-06	10-72	10-143	11-101	11-136	10-114[a]	10-115[a]	11-42[a]	11-117[a]	12-10[a]
Zr	110	283	109	99	111	122	109	149	142	115
Y	38.87	72.37	38.60	34.86	41.90	44.30	39.10	26.60	48.10	37.80
Th	0.23	0.58	0.33	0.18	0.22	0.00	1.10	5.00	0.40	0.60
U	0.29	0.23	0.10	0.09	0.07	0.00	0.00	2.90	0.00	0.00
La	4.76	10.56	5.57	4.07	3.95	5.90	3.70	36.50	2.00	4.10
Ce	14.24	30.57	15.32	12.26	12.43	17.80	11.50	65.10	14.80	11.20
Pr	2.41	4.98	2.45	2.10	2.18					
Nd	13.20	25.60	12.90	11.63	11.73	13.70	10.80	30.80	12.60	10.80
Sm	4.95	8.64	4.27	4.32	4.38					
Eu	2.28	2.72	1.53	1.64	1.55					
Gd	6.83	11.33	5.76	5.80	6.11					
Tb	1.19	2.08	1.08	1.03	1.15					
Dy	7.43	13.31	7.12	6.58	7.82					
Ho	1.57	2.89	1.57	1.40	1.68					
Er	4.32	8.07	4.34	3.87	4.70					
Tm	0.64	1.23	0.64	0.56	0.68					
Yb	3.96	7.59	3.90	3.50	4.24					
Lu	0.62	1.21	0.62	0.55	0.67					

[a] Trace element data collected via X-ray fluorescence, not included in ig. 13

Table 2-6 U-Pb SHRIMP geochronologic data and apparent ages

Spot[a]	U[b] (ppm)	Th (ppm)	Th/U	$^{206}Pb*$[b] (ppm)	$f^{206}Pb_c$[b]	$^{238}U/^{206}Pb$[c]		$^{207}Pb/^{206}Pb$[c]		$^{206}Pb/^{238}U$[d] (Ma)	
Sample 11-94											
1.1	1567	6	0.004	55	0.05	24.355	(1.2)	.05179	(1.2)	259	(3)
2.1	275	0.6	0.002	10	0.39	23.194	(1.4)	.05482	(2.6)	271	(4)
3.1	1243	220	0.18	56	0.17	19.247	(1.2)	.05428	(1.0)	326	(4)
4.1	242	0.5	0.002	9	0.14	23.925	(1.5)	.05260	(2.8)	264	(4)
5.1	3295	472	0.15	157	0.10	18.004	(1.2)	.05427	(0.6)	348	(4)
6.1	46	0.1	0.002	2	0.47	23.831	(2.4)	.05528	(6.3)	264	(6)
6.2	276	2	0.01	9	0.15	25.310	(1.4)	.05240	(2.1)	249	(3)
7.1	712	128	0.19	33	0.02	18.619	(1.3)	.05335	(1.4)	337	(4)
8.1	617	90	0.15	28	<0.01	18.726	(1.3)	.05286	(1.5)	336	(4)
9.1	377	2	0.004	14	<0.01	23.908	(1.4)	.05081	(2.2)	264	(4)
10.1	243	1	0.004	9	<0.01	22.262	(1.5)	.05061	(2.8)	284	(4)
12.1	544	1	0.002	20	0.19	23.612	(1.3)	.05308	(1.8)	267	(3)
13.1	278	1	0.004	10	0.26	23.173	(1.4)	.05374	(2.5)	272	(4)
14.1	1349	3	0.002	50	0.10	23.239	(1.2)	.05248	(1.1)	271	(3)
15.1	1639	322	0.20	74	<0.01	19.053	(1.2)	.05242	(1.0)	330	(4)
16.1	310	1	0.004	11	0.18	24.803	(1.4)	.05274	(2.4)	254	(4)
17.1	402	1	0.002	14	<0.01	24.034	(1.3)	.05064	(2.2)	263	(4)
18.1	400	5	0.013	14	0.12	23.840	(1.3)	.05249	(2.1)	265	(4)
19.1	605	209	0.36	27	0.14	18.913	(1.3)	.05419	(1.5)	332	(4)
20.1	242	1	0.005	9	<0.01	23.343	(1.4)	.05052	(2.7)	271	(4)
21.1	1832	187	0.11	76	0.80	20.669	(1.2)	.05881	(1.6)	302	(4)

Table 2-8 Continued

Spot[a]	U[b] (ppm)	Th (ppm)	Th/U	$^{206}Pb^{*b}$ (ppm)	$f^{206}Pb_c$[b]	$^{238}U/^{206}Pb$[c]		$^{207}Pb/^{206}Pb$[c]		$^{206}Pb/^{238}U$[d] (Ma)	
22.1	504	3	0.005	19	0.06	22.665	(1.3)	.05229	(1.9)	278	(4)
23.1	282	1	0.004	10	0.26	24.896	(1.4)	.05337	(2.4)	253	(3)
Sample 11-114											
1.1	931	151	0.17	40	<0.01	19.741	(1.2)	.05260	(1.3)	319	(4)
2.1	134	1	0.004	5	1.47	25.245	(1.6)	.06292	(4.1)	247	(4)
3.1	411	57	0.14	17	18.57	20.432	(1.4)	.20002	(1.5)	252	(4)
4.1	259	6	0.02	9	6.18	23.462	(1.5)	.10078	(3.2)	253	(4)
5.1	536	154	0.30	24	1.42	19.459	(1.3)	.06416	(4.8)	319	(4)
6.1	1126	187	0.17	51	0.34	18.917	(1.2)	.05578	(1.1)	331	(4)
7.1	221	1	0.005	10	14.00	19.485	(1.6)	.16417	(5.6)	278	(6)
8.1	3907	1563	0.41	181	0.35	18.589	(1.2)	.05601	(0.6)	337	(4)
9.1	3208	1217	0.39	145	0.93	19.005	(1.2)	.06046	(2.0)	328	(4)
10.1	2004	62	0.03	69	4.85	24.821	(1.2)	.08983	(1.1)	243	(3)
11.1	819	90	0.11	47	27.53	15.093	(1.2)	.27360	(3.2)	302	(6)
12.1	1550	285	0.19	70	0.55	19.014	(1.2)	.05745	(0.9)	329	(4)
13.1	846	171	0.21	42	0.97	17.477	(1.2)	.06144	(1.2)	355	(4)
14.1	872	167	0.20	40	0.11	18.636	(1.2)	.05408	(1.2)	337	(4)
15.1	177	4	0.02	7	7.63	21.849	(1.6)	.11277	(6.0)	267	(5)

Table 2-8 Continued

Note: All analyses were performed on the SHRIMP-RG ion microprobe at the United States Geological Survey-Stanford University Microanalytical Center, Stanford, CA. Calibration concentrations and isotopic compositions were based on replicate analyses of CZ3 and R33 (419 Ma; Black et al., 2004), respectively. Analytical routine followed Williams (1998). Data reduction utilized Ludwig (2001).

[a] 1.1 = grain1, spot 1.

[b] Pb* denotes radiogenic Pb; Pb_c denotes common Pb; $f^{206}Pb_c = 100*(^{206}Pb_c/^{206}Pb_{total})$.

[c] Reported ratios are not corrected for common Pb. Errors are reported in parentheses as percent at the 1 σ level.

[d] Ages calculated from ratios corrected for common Pb using ^{207}Pb for the $^{206}Pb/^{238}U$ ages and ^{204}Pb for the $^{207}Pb/^{206}Pb$ ages. Uncertainties in millions of years reported as 1 σ.

Table 2-7 Zircon trace element data

Spot[a]	CL	Y	La	Ce	Nd	Sm	Eu	Dy	Er	Yb	Hf	Ce/Ce*	Eu/Eu*	$Yb_{(N)}/Gd_{(N)}$	T (°C)
Sample 11-94															
1.1	c	482	0.02	0.1	0.02	0.1	0.08	1.2	19	117	628	12,089	0.68	2	503
2.2	r	245	0.17	0.9	0.10	0.2	0.13	1.9	16	38	72	12,798	0.71	3	37
3.1	c	1,776	0.51	13	2.0	3.4	0.80	37	161	298	511	11,728	0.22	8	14
4.1	o	225	0.02	0.1	-	0.0	0.04	0.5	9	53	258	12,507	1.01		492
5.1	c	3,163	14.12	88	29.2	15.9	7.14	87	319	560	1,017	17,569	0.58	2	12
6.1	r	191	0.02	0.1	0.005	0.0	0.02	0.4	7	43	157	15,004	0.61	3	392
7.1	o	118	0.02	0.2	0.010	0.2	0.28	3.0	12	14	21	12,965	1.01	7	7
8.1	o	428	0.03	3.1	0.11	0.5	0.28	6	32	81	204	9,396	0.50	35	36
9.1	r	387	0.02	2	0.12	0.4	0.23	5	28	75	198	9,809	0.50	29	41
10.1	r	171	0.03	0.4	0.08	0.3	0.35	5	17	18	19	13,799	0.80	5	4
11.1	c	70	0.03	0.2	0.03	0.2	0.15	2	7	9	14	14,086	0.81	3	7
12.1	o	1,256	0.28	5	1.5	2.6	0.60	26	112	220	424	10,533	0.22	5	16
13.1	r	484	0.02	0.1	0.005	0.1	0.05	1	18	115	596	11,264	0.73	2	599
14.1	p	110	0.18	1	0.3	0.2	0.19	2	10	14	24	12,864	0.98	2	13
15.1	r	675	0.03	0.1	0.04	0.1	0.06	2	27	158	650	13,531	0.46	1	412
16.1	r	2,142	0.20	13	1.2	2.9	0.84	36	190	401	794	11,019	0.25	17	22
17.1	p	123	0.01	0.2	0.03	0.2	0.22	4	15	11	10	13,935	0.67	7	2
18.1	p	393	0.02	0.1	0.00	0.0	0.06	1	14	97	504	12,121	1.17		822
19.1	o	123	0.07	1	0.11	0.2	0.86	3	13	15	20	12,628	2.86	3	6

Table 2-9 Continued

20.1	r	1,848	0.14	14	1.7	4.9	2.93	46	175	333	619	7,575	0.59	20	13
21.1	o	87	0.03	0.2	0.04	0.1	0.38	3	9	9	12	12,601	1.95	3	5
Sample 11-114															
1.1	c	1,234	0.02	3	0.6	2.3	0.77	25	108	221	429	8,233	0.31	22	17
2.1	r	75	0.16	1	0.3	0.2	0.10	1	5	13	29	14,571	0.65	2	30
3.1	r	315	4.47	79	10.7	6.0	1.80	18	36	51	111	9,266	0.52	6	6
4.1	r	108	5.66	21	6.1	3.0	1.06	8	9	15	59	10,486	0.67	2	8
5.1	r	233	1.85	7	3.0	1.7	0.50	9	23	42	100	9,152	0.39	2	11
6.1	c	1,177	0.35	5	1.3	2.0	0.62	27	110	209	369	9,342	0.25	4	14
7.1	r	88	1.49	3	0.9	0.6	0.18	2	6	18	72	10,507	0.49	1	37
8.1	c	1,659	1.60	22	4.7	7.4	1.93	60	181	275	436	9,706	0.28	5	7
9.1	c	1,787	4.06	31	10.8	11.1	2.80	69	191	293	464	8,004	0.31	3	7
10.1	r	926	7.33	40	13.5	8.7	4.48	31	73	162	493	11,901	0.83	2	16
11.1	c	824	21	576	9.5	4.3	1.02	22	76	151	309	10,353	0.32	17	14
12.1	c	1,821	0.17	5	1.0	3.2	1.01	42	178	316	567	8,998	0.27	9	14
13.1	r	404	3.63	22	4.8	2.9	1.28	13	38	68	142	13,951	0.63	3	11
14.1	c	1,431	0.02	2	0.9	2.6	0.88	33	136	247	451	8,179	0.29	16	14
15.1	r	67	0.89	3	0.8	0.4	0.19	2	4	14	64	12,321	0.73	2	39

Note: All analyses performed on the SHRIMP-RG ion microprobe at the USGS-Stanford University Microanalytical Center, Stanford, CA following procedure outlined in Mazdab & Wooden (2006).

Table 2-9 Continued

Abundances expressed in ppm.

[a] Spot labeled as grain number. spot number; CL designations: c = dark homogeneous core; o = oscillatory zoned core; mt = mottled core; m = mantle; p = patchy core; r = rim.

CHAPTER 3.
ESTABLISHING THE *P–T–*t PATH OF ECLOGITES IN THE ST. CYR KLIPPE, YUKON-TANANA TERRANE, YUKON, CANADA

Abstract

The St. Cyr klippe, part of the Yukon-Tanana terrane in Yukon, Canada, preserves fresh and retrogressed eclogite hosted within quartzofeldspathic schists. Petrological and mineral chemistry data combined with isochemical phase equilibrium (pseudosection) modeling shows that eclogites at St. Cyr followed a five-stage, clockwise pressure-temperature path. An amphibolite facies, pre-eclogite stage (Stage I) preceded peak pressure (Stage II), which reached up to 3.2 GPa and 610 °C. Retrogression back to amphibolite facies conditions (Stages III and IV) occurred as temperature increased during decompression. These results are consistent with exhumation of ultrahigh-pressure rocks in a subduction zone. U-Pb ion microprobe dating of zircon shows that the protolith of the eclogites formed within the Yukon-Tanana terrane during early, continental arc activity, between 364 and 380 Ma. The rocks were then subducted to mantle depths and metamorphosed to ultrahigh-pressure conditions during the Late Permian, between 267 and 271 Ma. This is the first report of ultrahigh-pressure metamorphism in North America and is unusual for an accretionary orogen.

Introduction

Eclogites and associated high-pressure (HP) and ultrahigh-pressure (UHP) metamorphic rocks play an important role in reconstructions of orogenic processes (Smith, 1984; Ernst, 2001; Hacker et al., 2003; Gilotti, 2013; Hacker et al., 2013; Hermann and Rubatto, 2014). Eclogites preserve mineral assemblages that reflect physical and chemical changes that take place during subduction in continent-continent (Alpine-type) or continent-oceanic (Pacific-type) plate convergence (e.g. Ernst, 2005). By calculating peak metamorphic conditions and characterizing retrograde pressure-

temperature (*P–T*) paths, HP and UHP assemblages can be used to reconstruct the physical and chemical transitions that occur during subduction and exhumation. In combination with geochronological data, this approach allows for the spatial and temporal understanding of the processes involved in the formation and evolution of orogenic belts.

The Yukon-Tanana terrane (YTT) is the largest allochthonous component of the northern Canadian Cordillera, extending from northern British Columbia through the Yukon and into easternmost Alaska. The YTT is a composite of distinct components of arc and back-arc affinity that have been polydeformed and polymetamorphosed over the course of its history (e.g. Colpron et al., 2006a; Nelson et al., 2013). Pacific-type HP assemblages preserved within the YTT extend from southern Yukon to eastern Alaska (Brown and Forbes, 1986; Erdmer et al., 1998). These HP assemblages provide insight into the history of subduction and exhumation within the YTT.

The St. Cyr klippe is one of four known localities within the YTT that record the subduction of a back-arc basin, or basins, outboard of the western margin of Laurentian during the Late Permian (Colpron et al., 2006a; Devine et al., 2006; Nelson et al., 2006; Berman et al., 2007; Nelson et al., 2013). Similar Permian HP metamorphic assemblages are found at Ross River, Faro, and Last Peak (Erdmer and Armstrong, 1989; Creaser et al., 1997; Erdmer et al., 1998). Several studies have attempted to unravel the nature and timing of peak metamorphism at these localities, using conventional thermobarometry and pseudosection modeling (Perchuk et al., 1999; Perchuk and Gerya, 2005; Ghent and Erdmer, 2011) and K-Ar, $^{40}Ar/^{39}Ar$, and U-Pb dating (e.g. Erdmer et al., 1998). Most of these studies were undertaken independently of one another, and so failed to link the age with the metamorphic event that produced it. New methods are available for linking time to the *P–T* history of metamorphic rocks, including *in situ* U-Pb zircon age dating and zircon trace element analysis.

The St. Cyr area consists of variably metamorphosed and deformed, structurally

imbricated units of high-grade Yukon-Tanana arc crust and low-grade oceanic crust (Petrie et al., in preparation a). The St. Cyr klippe hosts well preserved to variably retrogressed eclogite lenses within quartzofeldspathic schists. Eclogite protoliths formed within quartzofeldspathic materials as a part of the Yukon-Tanana composite arc, prior to the *in situ* subduction and metamorphism of both rock units (Petrie et al., in preparation a). The eclogite-bearing quartzofeldspathic host rocks record a Late Permian U-Th zircon age for HP metamorphism in metatonalites (Petrie et al., in preparation a).

Here I present mineral chemistry, petrological observations, metamorphic phase equilibrium calculations, and U-Pb zircon ages for St. Cyr eclogites. Isochemical phase equilibrium calculations are employed to determine the peak metamorphic conditions and the retrograde P–T path of the eclogites (e.g. Holland and Powell, 2010; Massonne, 2013 and references therein). U-Pb geochronology on zircon is used to determine the protolith and metamorphic ages of the eclogites. This study establishes the metamorphic and geochronologic evolution of eclogite in the St. Cyr klippe in an effort to reconstruct the evolution of subduction and exhumation within HP belt of the YTT.

Geologic Setting

The St. Cyr klippe is a 70 km long by 15 km wide, northwest-striking structure that combines a mixture of variably metamorphosed units. The area lies 14 km northeast of Quiet Lake, southwest of the Tintina fault in south-central Yukon (Fig. 3-1). The region consists of a series of northwest-striking imbricate thrust panels that intermix amphibolite and eclogite facies metamorphic rocks of the Yukon-Tanana terrane (YTT) and greenschist facies to serpentinized mafic and ultramafic rocks of the Slide Mountain Ocean terrane (Petrie et al., in preparation a). The YTT and the Slide Mountain Ocean terrane represent Late Devonian to Late Permian arc and back-arc systems that form integral parts of the northern Canadian Cordillera (Fig. 3-1). The Yukon-Tanana arc was built on continental crust rifted from western Laurentia in the Mid- to Late Paleozoic

during the opening of the Slide Mountain Ocean back-arc basin (Nelson et al., 2013 and references therein). The YTT consists of a series of volcanic and volcaniclastic assemblages built upon Neoproterozoic to pre-Early Devonian metasedimentary basement, known as the Snowcap assemblage (Fig. 3-1; Mortensen, 1992; Colpron et al., 2006a; 2006b; Piercey et al. 2002; Piercey et al., 2006; Piercey and Colpron, 2009; Piercey et al., 2012). These rocks have been multiply deformed and metamorphosed to varying degrees, both during the Paleozoic evolution of the arc, as well as Early Mesozoic obduction onto the Laurentian miogeocline (e.g., Colpron et al., 2006). Eclogite bodies in the St. Cyr klippe and three other known localities in the Yukon record Permian subduction of slices of the Yukon-Tanana arc during the subduction of the Slide Mountain back-arc (Erdmer et al., 1998; Devine et al., 2006; Berman et al., 2007; Nelson et al., 2013).

In the study area (Fig. 3-2), eclogite and retrogressed eclogite are found as sub-meter to hundreds of meter scale lenses hosted by quartzofeldspathic schists (Gilotti et al., 2013; Petrie et al., in preparation a). These schists form a coherent, 30 by 6 km, northwest-striking package of metasedimentary and felsic metaigneous rocks, intercalated on the meter to tens of meter scale (Fig. 3-2). Igneous and metamorphic zircons from metatonalites indicate that the felsic igneous rocks are part of the Yukon-Tanana composite arc, and that the host rocks experienced eclogite-facies metamorphism (Petrie et al., in preparation a). These two units thus form slices of coherent arc crust subducted to eclogite facies conditions. Following exhumation from HP metamorphic conditions, the eclogite-bearing unit was tectonically interleaved with unites belonging to the Snowcap assemblage (Gilotti et al., 2013) and a slice of low-grade mafic and ultramafic rocks of unknown terrane affinity. This imbricate stack was then emplaced on a shallow-dipping thrust over low-grade phyllites and marbles of the Finlayson assemblage (Fig. 3-2; Petrie et al., in preparation a).

Petrological, geochemical, geochronological evidence suggests that Permian age eclogites in the YTT form part of a regional HP lithotectonic assemblage (Petrie et al., in preparation). Peak metamorphic conditions within the HP assemblages have been estimated by several authors, including Erdmer and Helmsteadt (1983), Erdmer et al. (1998), and et al. (1999). More recently, Perchuk and Gerya, (2005) used conventional geothermobarometry to calculate peak eclogite facies conditions of 660 °C and 1.5 GPa of an eclogite from Faro. Ghent and Erdmer (2011) utilized documented peak conditions of 550-600 °C and 2.0-2.3 GPa of an epidote-bearing eclogite from Ross River with pseudosection modeling.

Estimates of the timing of the HP metamorphism show that eclogites at Faro, Ross River, and Last Peak are approximately Permian in age based on a series of Late Permian to Triassic K-Ar (Wanless, 1978; Erdmer and Armstrong, 1989) and $^{40}Ar/^{39}Ar$ (Erdmer et al., 1998) cooling ages, and one U-Pb zircon date from Last Peak (269 ± 2 Ma; Creaser et al., 1997). One metamorphic age for an eclogite is known from the St. Cyr klippe, a preliminary analysis by Fallas et al. (1998), in which they used thermal ionization mass spectrometry (TIMS) U-Pb zircon dating to estimate the age of peak metamorphism at 266 ± 0.6 Ma. In the St. Cyr klippe, eclogite facies metamorphism of the host quartzofeldspathic schists was dated at 266 ± 3 Ma, via *in situ* sensitive high-resolution ion microprobe U-Pb analysis of zircon rims (Petrie et al., in preparation a).

Petrography

In the St. Cyr klippe, fresh eclogites contain a peak mineral assemblage of omphacite + garnet + quartz + rutile ± amphibole ± phengite (Petrie et al., in preparation a). Epidote, when present, occurs exclusively as inclusions in garnet, and apatite forms the accessory phase. Ilmenite, titanite, biotite, chlorite, and K-feldspar are retrograde phases. Anhedral to euhedral garnets are typically 100-600 μm in size and coexist with omphacite, quartz, rutile, phengite, and amphibole. Garnet porphyroblasts contain

abundant mineral inclusions, composed of calcic and sodic-calcic amphibole, rutile, quartz, titanite, plagioclase, ilmenite, with minor diopside, augite, phengite, muscovite, and calcite; these inclusions are generally confined to grain cores. Omphacite typically forms grains flattened parallel to the schistosity. Peak amphibole forms brownish-green subhedral, fine- to medium-sized grains in equilibrium with omphacite. Quartz is commonly found as fine-grained, polycrystalline aggregates with undulose- to flat-extinction and 120° triple-junctions. Rutile forms very fine-grained anhedral aggregates or isolated grains. Eclogites show progressive retrogression from fresh eclogite to garnet amphibolite. In weakly to moderately retrogressed samples, matrix omphacite rims are partially transformed to very fine-grained lobate symplectites of either diopside + plagioclase or amphibole + plagioclase. Phengite is commonly replaced by very to extremely fine-grained, blocky symplectites of biotite + plagioclase. Completely retrogressed eclogites consist of amphibole + plagioclase ± garnet ± quartz ± biotite ± ilmenite ± titanite.

Petrography of Eclogite Sample 11-117

Sample 11-117 was chosen for pseudosection modeling because of its well-preserved phengite. The metamorphic mineral assemblage and UTM coordinates for sample 11-117 are given in Table 3-1 and the sample location is shown in Fig. 3-2. Sample 11-117 is a fine-grained, well-preserved eclogite consisting of approximately omphacite 25%, amphibole 25%, garnet 37%, quartz 6%, rutile 3%, phengite 2%, and ≤ 2% plagioclase, K-feldspar, titanite, biotite, and ilmenite (Fig. 3-3). Large, garnet grains, 300-600 μm in diameter, are subhedral to euhedral (Fig. 3-3a). These garnets contain very fine-grained inclusions of omphacite, amphibole, rutile, quartz, plagioclase, phengite, and titanite. In general, omphacite, rutile, and phengite are found throughout the garnet grain, whereas quartz, plagioclase, and titanite are found closer to garnet rims. Small, 50-300 μm garnets are anhedral with irregular shapes and embayed edges.

Brownish-green matrix amphibole is anhedral with lobate grain boundaries, and lacks a grain-shape preferred orientation. The grain-shape preferred orientation of omphacite defines a very weak schistosity. In some cases, omphacite is clearly in equilibrium with matrix amphibole (Fig. 3-3b), but along the majority of omphacite-amphibole grain boundaries there are lobate symplectites of amphibole + plagioclase (Fig. 3-3c). Where isolated from matrix amphibole by quartz, garnet, or another omphacite grain, the edges of omphacite break down to lobate symplectites of clinopyroxene + plagioclase (Fig. 3-3c and d). Sizeable phengite is found sporadically within the matrix and is up to 400 μm long and 500 μm wide (Fig. 3-3e); in places phengite has converted to biotite, blocky symplectites of biotite + plagioclase, or K-feldspar (Fig. 3-3f). In general, biotite forms a barrier between phengite and the outermost garnet rim. Quartz occurs as polycrystalline aggregates with undulose- to flat-extinction and 120° triple-junctions. Titanite and ilmenite form retrograde phases after rutile.

Mineral Chemistry

Mineral chemistry data was collected from sample 11-117 for use in isochemical phase equilibrium modeling. Mineral compositions were determined using a CAMECA SX-100 electron microprobe at the University of California, Davis, California. Analytical conditions include 15 kV acceleration voltage, 5-20 nA beam current, and a beam diameter of 1-10 μm. Garnet was mapped at 80 nA using a 5 μm spot size, while phengite was mapped at 50 nA with a 10 μm spot. Major element concentrations are shown as weight percent (wt.%) oxides. Amphibole nomenclature is after Hawthorne et al. (2012) and pyroxene nomenclature follows Morimoto et al. (1989). Mineral abbreviations are from Whitney and Evans (2010). Clinopyroxene analyses were normalized to four cations per formula unit ($M2M1Si_2O_6$) and the Fe^{2+}/Fe^{3+} ratio was obtained from the charge balance. Cations were assigned to the M1 and M2 sites according to the procedure described in Morimoto et al. (1989).

Omphacite in the matrix decreases from Jd_{39-45} in the core to Jd_{39-40} in the rim. Diopside (Jd_{10}) occurs in symplectites. Amphibole is found as both sodic and calcic phases (Petrie et al., in preparation a). Taramite and katophorite [Si = 6.31-6.38 apfu, Ca = 1.39-1.45 apfu, $^{[A]}$(Na+K) = 0.741-0.83 apfu] are found as matrix grains in equilibrium with omphacite (Table 3-2). Symplectitic amphibole is pargasite with Si = 6.442-6.658 apfu, Ca = 1.50-1.90 apfu, $^{[A]}$(Na+K) = 0.75-0.90 apfu (Table 3-2). Biotite that has replaced phengite in the matrix ranges from Si = 2.70-3.24 apfu, X_{Mg} [Mg/(Mg+Fe)] = 0.54-0.59, and $Ti0_2$ = 0.54-0.59 wt.%. Plagioclase in symplectites is albite-oligoclase with An_{3-16}.

Potassic white mica in the matrix is weakly to moderately zoned (Fig. 3-4; Table 3-2). In general, Si atoms per formula unit (apfu) increase from core to rim, before decreasing sharply at the outer rim, adjacent to K-feldspar or biotite. The cores of white mica are phengite with 3.27 to 3.38 Si apfu. Approaching the rim, the Si-in-phengite values increase to a maximum value of 3.67 Si apfu (Table 3-2). Within approximately 30-40 μm of the rim edge, Si values drop to 3.33-3.47 Si apfu (Table 3-2). At the very edge of the rim adjacent to biotite, Si drops to 3.12 and 3.22 apfu (Table 3-2).

Garnets are almandine-pyrope-grossular solid solutions in the range $Alm_{53-60}Prp_{10-22}Grs_{17-32}Sps_{0.6-4}$ and are complexly zoned (Fig. 3-5 and 3-6). A few grains display sector zoning, which is developed in the intermediate domain between a distinct core and outer rim (Petrie et al., in preparation a). Some grains show increasing grossular content from core to an intermediate zone, before decreasing towards the inner rim. Most garnet grains exhibit a general decrease in grossular and spessartine, and increase in pyrope the core to an inner rim (Fig. 3-5). In these garnets, almandine remains relatively stable (Fig. 3-6). Fig. 5d illustrates the different compositional zones within garnets, which also correspond to the different metamorphic stages described below. The core, zone I, exhibits the highest grossular and spessartine contents, with a corresponding minimum value of pyrope. Grossular and spessartine decrease remarkably from zone I to the

intermediate zone, II-III, while pyrope increases. This trend continues into the inner rim zone, IV (Fig. 3-5d). At the outermost rim (~ 30 μm), grossular exhibits a sharp decrease, while pyrope and spessartine increase (Fig. 3-4 and 3-5). This rim is in textural equilibrium with biotite, pargasite, diopside, and albite. It is possible that the decrease in Ca is due to crossing into the reaction zone of the formation of diopside and Ca-amphibole during exhumation. The increase in Mn and Mg at the outermost garnet rims possibly records the resorption of smaller garnet grains during retrogression, and also the breakdown of phengite.

Si-in-phengite lies between 3.22 and 3.30 apfu in garnet cores (zone I, Fig. 3-5d), similar to the cores of matrix grains. In garnet cores and the intermediate zone (zones I-II, Fig. 3-5d), inclusions are omphacite (Jd_{44-45}; Table 3-2), similar to matrix grains. In the intermediate zone (zone II), Na-amphibole inclusions are taramite [Si = 6.00-6.28 apfu, Ca = 1.30-1.39 apfu, $^{[A]}$(Na+K) = 0.55-0.74 apfu] (Table 3-2). This zone also contains inclusions of albite (An_{7-11}), and Ca-amphibole, including sadanagite and pargasite [Si = 5.87-6.89 apfu, Ca = 1.78-1.79 apfu, $^{[A]}$(Na+K) = 0.67-0.80 apfu]. Rutile is common throughout the garnet, whereas quartz is found from the intermediate zone (zone II), while titanite and plagioclase occur mainly in the vicinity of the rim (zone IV).

P–T Evolution

Calculation Method

The *P–T* evolution of the investigated eclogite was derived from microstructural relationships and isochemical (pseudosection) phase equilibrium modeling. Pseudosection modeling has been applied successfully to document the metamorphic evolution of eclogites from a variety of localities and tectonic settings including Oman (Warren and Waters, 2006; Omrani et al., 2013), the Kokchetav Massif in Kazakhstan (Zhang et al., 2012), the Bohemian Massif in the Czech Republic (Stipska and Powell, 2005; Stipska et al., 2012; Massonne, 2012), the Tromsø nappe of Norway (Janak et al.,

2012), and Ross River, Yukon-Tanana terrane (Ghent and Erdmer, 2011). A pseudosection for sample 11-117 was calculated with the PERPLE_X computer program package (Connolly, 2005; version from November 2013 downloaded from the internet site http://www.perplex.ethz.ch/) for the *P–T* range of 0.5-3.5 GPa and 450-850 °C. The effective bulk rock composition was modified to fit the 10-component system SiO_2-TiO_2-Al_2O_3-MgO-FeO-CaO-Na_2O-K_2O-H_2O-O_2 (Table 3-3). The bulk rock composition was input from major element concentrations analyzed by X-ray fluorescence at the GeoAnalytical Laboratory of Washington State University, Pullman, WA, following conventional procedures. The thermodynamic data set of Holland and Powell (1998, updated 2011) was employed in the calculations. The following solution models were used: phengite, garnet, epidote-clinozoisite, omphacite, talc, and ilmenite after Holland and Powell (1998), feldspar after Fuhrman and Lindsley (1988), and amphibole after Dale et al. (2000) from solution_model.dat file in PERPLE_X. Rutile, titanite, and zoisite are assumed to be end-member compositions. Biotite was ignored, due to the very limited amount present within sample 11-117 (< 1 wt. %). CaO was reduced according to the whole-rock phosphorus content, assuming these elements are bound to apatite.

Phase equilibria were calculated using 3 wt.% H_2O to permit the formation of a free hydrous fluid phase. The presence of a free hydrous fluid phase is formed by the reaction of hydrous minerals to garnet during prograde metamorphism, and is therefore important to determine the *P–T* conditions of the early garnet composition. The oxygen content was estimated to a value of 10% of the iron in the rock being trivalent during metamorphism (e.g. Massonne et al., 2007). Values other than 10% will modify the *P–T* fields and modal contents of amphibole and epidote, as they are the silicates that introduce Fe^{3+} to the PERPLE_X model according to the selected solid-solution models (Massonne et al., 2007).

P–T Pseudosection

The calculated pseudosection for eclogite sample 11-117 (Fig. 3-7) shows a moderate number of *P–T* fields for different phase assemblages. Only H_2O is present over the entire *P–T* range. *P–T* fields of the minerals present in the pseudosection are shown in Fig. 3-8a. Omphacite appears over the majority of the calculated *P–T* range, with the exception of a small field at temperatures lower than ~530 °C and pressures below 3.5 GPa. A SiO_2 phase is stable at temperatures above about 590 °C. Epidote, clinozoisite, and zoisite are stable below approximately 3.1 GPa and 610 °C.

The *P–T* field of garnet was contoured by isopleths for molar fraction of pyrope ($=X_{Mg}$; Fig. 3-8b), and grossular ($=X_{Ca}$) and spessartine ($=X_{Mn}$; Fig. 3-8c). Typically, the content of pyrope increases and grossular decreases with rising temperature, while the content of spessartine decreases with increasing pressure and temperature. The volume percent of garnet increases with rising temperature until approximately 620 °C, where it increases with increasing pressure (Fig. 3-8d). The majority of garnet grew along a two step path during prograde evolution, in which garnet grew at the expense of Ca-amphibole between approximately 1.1-2.0 GPa and below ~ 580 °C, followed by garnet growth at the expense of epidote between about 2.0-2.9 GPa and below ~ 610 °C. The maximum calculated content of garnet is ~ 39 volume percent (vol.%), neglecting the fluid phase. The calculated Si content of potassic white mica increases with rising pressure (Fig. 3-8b), and ranges from 3.09 to 3.74 apfu. The calculated content of potassic white mica is around 2 vol.% at peak conditions stable with garnet, omphacite, Na-amphibole, quartz, and rutile, which is consistent with the small amount of phengite observed. The maximum content of epidote in the *P–T* range of the calculated pseudosection is up to 20 vol.% occurring below about 3.1 GPa and 580 °C. Calculated modes, particularly the maximum *P–T* range for epidote, can be influenced by the Fe^{2+}/Fe^{3+} ratio (i.e. O_2 content) for the bulk rock composition.

P–T Path

The combination of petrography, mineral chemistry, and the pseudosection model produces the *P–T* path of eclogite sample 11-117, shown in Fig. 3-9. The sample displays a five-stage metamorphic evolution, with four stages labeled from I to IV (Fig. 3-9). The early-eclogite stage is defined by the inclusions of pargasite, omphacite, rutile, and phengite in garnet cores (zone I, Fig. 3-5d) indicative of an amphibolite facies assemblage.

Stage I

Using the Mn- and Ca-richest part of the garnet core (zone I, Fig. 3-5d; Table 3-2), and the isopleths of Fig. 3-8c, garnet began to grow at about 1.4 GPa and 500 °C (Stage I, Fig. 3-9). This *P–T* condition lies within the epidote-phengite-amphibole-garnet-omphacite-rutile (+ H_2O) stability field (Fig. 3-7). The calculated Si content of phengite at 1.4 GPa and 500 °C is 3.25 Si apfu. This agrees with the observed phengite inclusions in garnet cores (3.22 to 3.30 Si apfu; Fig. 3-8b; Table 3-2). Garnet cores lack quartz inclusions, as is predicted in the model for initial garnet growth.

The calculated pseudosection predicts approximately 14-16 vol.% epidote to be present during initial garnet formation, yet no epidote was observed in eclogite sample 11-117. Epidote is a common inclusion within garnet in a number of eclogite samples from the St. Cyr area. Because garnet formation consumes hydrous minerals (e.g. Zeh and Millar, 2001; Caddick et al., 2007; Baxter and Caddick, 2013), it is possible that garnet growth consumed all the epidote in sample 11-117. It is also possible that epidote inclusions are present, but they are too small to analyze. Garnet inclusions in eclogite from the St. Cyr area, including sample 11-117, are extremely fine grained; some are on the order of 5 μm or less. These grains are so small that they are impossible to identify using an optical microscope and the electron beam interacts with both the inclusion and the garnet, mixing the signal.

Stage II

Peak *P* conditions are captured by the garnet compositions in the intermediate zone (zone II, Fig. 3-5d) adjacent to the core (Table 3-2). This composition of this garnet is assumed to be in equilibrium with the highest value of Si from within the inner rim of phengite grains (Si = 3.67 apfu). I use this value of phengite, as opposed to the core composition, because the results of Stage I metamorphism show that phengite, with a composition ~ 3.30 Si apfu, was growing at early-eclogite facies conditions prior to garnet growth (Fig. 3-7). Prograde evolution then induced an increase in Si values as phengite continued to grow. The X_{Mg} in garnet and Si-in-phengite isopleths in Fig. 3-8b, with the corresponding compositions of zone II garnet and inner rim phengite, intersect well within the coesite stability field, at approximately 3.2 GPa and 610 °C (Fig. 3-8b and 3-9).

The maximum modal amount of garnet in sample 11-117 equals 37 vol.%, and was estimated from the thin section using ImageJ (Rasband, 1997-2014). We assume the isopleth for the modal content of garnet represents the garnet mode at peak *P* conditions (Fig. 3-8d and 3-9) because textural and chemical observations suggest that most of the smaller garnet grains were resorbed to some extent during exhumation. The intersection of the isopleth for 37 vol.% garnet with the X_{Mg} in garnet and Si-in-phengite isopleths occurs at approximately the same UHP metamorphic conditions (Stage II, Fig. 3-9).

According to the calculated model, peak *P* conditions lie within the phengite-Na-amphibole-garnet-omphacite-coesite-rutile (+ H_2O) stability field (Fig. 3-7). Garnet inclusions within the intermediate zone support this assemblage, which include taramite, omphacite, and rutile (Table 3-2). At peak pressures, the model predicts that coesite would have been a minor component (~ 5 vol.%), which may explain why it was not preserved.

Stage III

The exhumation path is characterized by rising temperatures during decompression. Following peak pressure (Stage II), garnet composition changed steadily during its continued growth with the increase in Mn and Mg and a corresponding decrease in Ca (Table 3-2). Decompression also caused a decrease in the Si value of phengite at grain rims (Table 3-2). Using the isopleths of Si-in-phengite composition and X_{Ca} in garnet (zone III, Fig. 3-5d), Stage III phengite composition grew at conditions of about 2.2 GPa and 630 °C during exhumation (Stage III, Fig. 3-9).

Stage IV

The isopleths for garnet compositions in rims (zone IV, Fig. 3-5d) and decreasing Si-in-phengite near the outer rim places the exhumation path at 1.4 GPa and 740 °C (Fig. 3-9; Table 3-2). These *P–T* conditions coincide with the phengite to K-feldspar reaction in the calculated model (Fig. 3-7, 3-8a, and 3-9). This reaction is observed in sample 11-117 (Fig. 3-3f), so the exhumation path must cross this boundary. This *P–T* condition is in the plagioclase stability field, evidenced by plagioclase inclusions in zones III and IV of garnet. Calculated albite modes are between 2 and 6 vol.% at these conditions, consistent with the low modal amount of plagioclase observed in the sample.

The subsequent retrograde evolution cannot be deduced conclusively from the minerals in the studied eclogite. Nevertheless, a retrograde path along the dashed line in Fig. 3-9 is plausible because it explains several textural and model observations. The presence of ilmenite and diopside + albite symplectites suggests that the path crossed into the stability fields of those minerals (Fig. 3-8a). The very edge of phengite grains adjacent to biotite or K-feldspar record the lowest Si compositions (Si = 3.12-3.22 apfu), which is predicted by the model. The sample preserves rutile, Na-amphibole, and omphacite, which, had the d*P*/d*T* slope been higher, would result in the complete transformation of these minerals into their lower *P–T* -stable counterparts. For example,

according to the pseudosection, Ca-amphibole substitutes for Na-amphibole over a wide range of *P–T* conditions. At 610 °C, Ca-amphibole substitutes for Na-amphibole over the pressure range 1.5-0.7 GPa. Thus, a higher slope would eliminate Na-amphibole in favor of Ca-amphibole (e.g. Massonne et al., 2013).

Geochronology

U-Pb dates of zircon from four eclogite samples 10-89, 11-104, 10-143, and 11-101 from the St. Cyr klippe were obtained to determine the age of the protolith and to establish the age of UHP metamorphism. Sample locations are shown in Fig. 3-2, and UTM coordinates and mineral assemblages are given in Table 3-1. U-Pb data and trace element analyses are shown in Tables 3-4 and 3-5.

Analytical Methods

U–Th–Pb isotopic data were measured using the sensitive high-resolution ion microprobe-reverse geometry (SHRIMP-RG) mass spectrometer at the U.S. Geological Survey – Stanford University ion probe facility, Stanford, California. Zircon grains were separated from 1-3 kg samples by standard physical separation techniques and mounted in 2.54 cm epoxy rounds, which were polished to expose grain interiors. Cathodoluminescence (CL), transmitted light, and reflected light images were used to characterize zircon domains, identify internal growth zones, and select spots for analysis (Fig. 3-16). Calibration of U was based on zircon standard Madagascar Green (MAD; 4196 ppm U; Barth and Wooden, 2010). Isotopic ratios were calibrated by replicate analyses of zircon standard R33 (421 Ma, Black et al., 2004; Mattinson, 2010), which was rerun after every fourth analysis. The analytical routine followed Barth and Wooden (2006, 2010). Uncertainties in the isotopic ratios are reported at the 1σ level. Ages are assigned based on the weighted mean of $^{206}Pb/^{238}U$ ages corrected for common Pb using the ^{207}Pb correction method. Uncertainties in the weighted mean ages discussed below are reported at the 95 % confidence level. The weighted mean ages are equivalent within

uncertainty to concordia ages calculated in Squid 1.13 (Ludwig, 2001). Age calculations and Tera-Wasserburg diagrams (Fig. 3-17) were generated with the Isoplot 3 program of Ludwig (2003).

Trace-element data for Y, REE, and Hf were collected in tandem with the U, Th and Pb analyses. The following peaks were measured: ^{89}Y, ^{139}La, ^{140}Ce, ^{146}Nd, ^{147}Sm, ^{153}Eu, $^{157}Gd^{16}O$, $^{163}Dy^{16}O$, $^{166}Er^{16}O$, $^{172}Yb^{16}O$, $^{90}Zr_2{}^{16}O$, $^{180}Hf^{16}O$, ^{206}Pb, $^{232}Th^{16}O$, $^{238}U^{16}O$. Data reduction of elemental concentrations used zircon standards CZ3 and MAD (Mazdab and Wooden, 2006; Mazdab, 2009). Chondrite-normalised REE plots (Fig. 3-18) use the chondrite REE abundances of Anders and Grevesse (1989) multiplied by a factor of 1.36 (Korotev 1996). Chondrite-normalized values for Pr were calculated by interpolation ($Pr_{(N)} = La_{(N)}^{0.33} \times Nd_{(N)}^{0.67}$). Eu anomalies are based on $Eu_{(N)}/Eu^*$ and $Ce_{(N)}/Ce^*$ with Eu* and Ce* calculated as geometric means (e.g., $Eu^* = (Sm_{(N)} \times Gd_{(N)})^{0.5}$).

Protolith Zircon

Sample 10-89

Sample 10-89 consists of 25% omphacite, 35% garnet, 20% amphibole, 12% rutile, and 8% quartz with accessory retrograde plagioclase, ilmenite, and titanite. Garnets form two habits, those between 50 to 100 μm occur as aggregates of subhedral, blocky grains and those between 100 and 500 μm that form equant, euhedral grains. The larger garnets contain very fine-grained inclusions of clinopyroxene, amphibole, quartz, ilmenite, and rutile. This sample has been weakly retrogressed, exhibited by small patches of very fine-grained symplectites of amphibole + plagioclase formed at the edges of omphacite grains, and titanite after ilmenite. A weak schistosity is defined by the grain-shape preferred orientation of omphacite and amphibole and the planar orientation of very fine-grained aggregates of rutile.

Zircons in sample 10-89 are rounded to subhedral, and preserve CL-dark to pale gray, patchy or sector zoned cores (Fig. 3-10). CL-homogeneous to light-gray rims are present on the majority of the 16 zircons analyzed. Both core and rim analyses, spanning 346-446 Ma (Fig. 3-11; Table 3-4), have characteristic igneous trace element patterns, including steep heavy rare earth element (HREE) patterns (Yb/Gd = 29-64), ΣREE = 227-899, Th/U = 0.2-0.4, an exaggerated Ce anomaly (Ce/Ce* = 3-12), and a weak to moderate Eu anomaly (Eu/Eu* = 1.0-1.4; Fig. 3-12; Table 3-5). Twelve cores and rims give a concordia age of 364 ± 4 Ma (Fig. 3-11), which is interpreted as the age of the mafic protolith for sample 10-89. The two oldest cores were rejected, as the ages are likely due to inheritance.

Sample 11-104

Sample 11-104 is comprised of 45% omphacite, 35% garnet, 15% amphibole, 5% quartz, and 5% rutile; accessory phases include ilmenite and apatite. Garnets are < 600 μm, equant, subhedral to euhedral, and contain very fine-grained inclusions of omphacite, amphibole, quartz, ilmenite, and rutile. Fine-grained symplectites of amphibole + plagioclase after omphacite and retrograde amphibole grains within the matrix found adjacent to cracks show that the sample has been moderately retrogressed. A weakly developed schistosity is defined by the grain-shape preferred orientation of omphacite and the planar orientation of very fine-grained aggregates of rutile.

Zircons from sample 11-104 yielded a bimodal population consisting of sector zoned and oscillatory zoned cores, both with CL-bright rims (Fig. 3-10). Analyses from four sector zoned cores give $^{206}Pb/^{238}U$ ages ranging from 377 to 383 Ma, with a concordia age of 377 ± 4 Ma (Fig. 3-11; Table 3-4). Th/U ratios for the four grains are typical of igneous zircon, ranging from 0.5 to 1.0. Trace element patterns including negative Eu/Eu* and positive Ce/Ce* anomalies between 0.3 and 199-532, respectively, steep HREE patterns (Yb/Gd = 21-32), and ΣREE = 1405-2278 confirm that these

zircons formed during igneous crystallization (Fig. 3-12, Table 3-5). We interpret 377 ± 4 Ma to be the age of the igneous protolith of eclogite sample 11-104.

Metamorphic Zircon

Sample 10-143

Sample 10-143 consists of 35% omphacite, 30% garnet, 20% amphibole, 10% quartz, 4% rutile, and 1% phengite. Accessory minerals include epidote and apatite. Garnets are generally < 500 μm, subhedral to euhedral, and contain very fine-grained inclusions of omphacite, amphibole, plagioclase, epidote, ilmenite, quartz, and rutile. Retrograde microstructures include lobate symplectites of amphibole + plagioclase replacing omphacite, rutile converting to ilmenite, which is in turn converting to titanite, chlorite replacing garnet, and biotite after phengite. A weak schistosity is defined by the grain-shape preferred orientation of omphacite and amphibole.

Zircons from sample 10-143 are rounded to subhedral and preserve sector zoned cores with CL-bright rims (Fig. 3-10). The trace elements from analyses of both the cores and rims of these zircon show a strong depletion of ΣREE (20-236), a pronounced flattening of the HREE pattern (Yb/Gd = 0.5-6) and a lack of a Eu anomaly (Fig. 3-12; Table 3-5). The Th/U ratio ranges from 0.0004 to 0.01. These are all characteristics consistent with the growth or recrystallization of zircon simultaneously with garnet during prograde metamorphism (Rubatto, 2002; Hoskin and Schaltegger, 2003). The $^{206}Pb/^{238}U$ ages range from 259 to 284 Ma with a concordia age of 271 ± 3 Ma (Fig. 3-11), which is interpreted as the age of UHP metamorphism for sample 10-143.

Sample 11-101

Sample 11-101 consists of 45% omphacite, 30% garnet, 10% quartz, 7% amphibole, 5% rutile and 3% ilmenite. Garnets are between 100 and 600 μm, subhedral to euhedral, and contain very fine-grained inclusions of omphacite, amphibole, quartz,

ilmenite, titanite, and rutile. Retrograde microstructures include very fine-grained symplectites of amphibole + plagioclase after omphacite and titanite after ilmenite. A moderately well developed schistosity is defined by the grain-shape preferred orientation of omphacite.

Zircons in sample 11-101 are rounded to subhedral and exhibit sector zoned or patchy cores (Fig. 3-10). Like sample 10-143, the trace elements are consistent with growth during metamorphism, including depleted ΣREE (16-121), a flattened HREE pattern (Yb/Gd = 0.3-1.3), no Eu anomaly, and low Th/U ratios (0.002 to 0.03; Fig. 3-12; Table 3-5). Of 16 analyses, 14 give a concordia age of 267 ± 4 Ma (Fig. 3-11; Table 3-4), which is within error of the metamorphic age determined from sample 10-143.

Discussion

P–T Evolution of St. Cyr Eclogites

P–T conditions were deduced from the solid-solution compositions of phengite and garnet, stable mineral assemblages, garnet inclusions, and the calculated pseudosection. The metamorphic evolution of eclogite sample 11-117 followed a five-stage, clockwise *P–T* path. Omphacite and phengite were already stable when garnet started to grow at approximately 1.4 GPa and 500 °C (Fig. 3-8a; Stage I, Fig. 3-9). Although garnet growth began well within the epidote stability field (Fig. 3-7), epidote was most likely consumed by garnet during subsequent prograde metamorphism. Pseudosection calculations show that UHP conditions were reached at about 3.2 GPa and 610 °C, within the phengite-Na-amphibole-garnet-omphacite-coesite-rutile (+ H_2O) stability field (Fig. 3-7). The highest Si content in phengite was measured near (but not within) the grain rim. This outcome is expected if phengite began growing at shallower crustal levels, and continued to grow during prograde metamorphism. The highest Si-in-phengite (Si = 3.67 apfu) is clearly located in the coesite stability field (Stage II, Fig. 3-9). UHP conditions result even under the assumption of an error in the pressure

determination of ± 0.2 GPa (Massonne et al., 2013). This is the first documentation of UHP metamorphism in North America.

The chemical changes garnet and phengite experienced during continued growth point to decompression accompanied by increasing temperature (Fig. 3-9). The exhumation path reaches a peak temperature of 740 °C at a corresponding pressure of 1.4 GPa. The *P–T* estimate of this stage is compatible with the composition of the inner rim of garnet (zone IV, Fig. 3-5d) and the outer rim of phengite grains. It is also in agreement with the phengite-out reaction (Fig. 3-7 and 3-8a). The final stages of metamorphic evolution are not directly known, although petrological and chemical evidence suggested retrograde evolution similar to that shown on Fig. 3-9. This path agrees with the lowest Si values in potassic white mica found at the very edge of grain rims. This path also explains the preservation of minerals stable at peak metamorphic conditions, such as Na-amphibole and omphacite.

According to the pseudosection, subduction to UHP conditions in the St. Cyr area occurred at a very low thermal gradient of ~ 5 °C/km (Fig. 3-9), coincident with the *P–T* environment of subduction zones (e.g., Zhang et al., 2013). The relatively high temperature during exhumation could have resulted from the ascent of the rocks within a subduction channel due to heating from the hot overlying mantle (e.g. Massonne, 2012). Other factors that may affect the temperature include radiogenic heat production in the surrounding quartzofeldspathic schists, subduction rate, and the ambient mantle temperature.

The protoliths of the eclogite at St. Cyr were subducted and recrystallized from amphibolite prograde through peak metamorphism at UHP conditions consistent with deep subduction to mantle depths on the order of 100 km. Previous work has placed the depth of subduction of Permian eclogites in the YTT at anywhere between 35 to 80 km (Erdmer et al., 1998; Ghent and Erdmer, 2011). The results of this study put the depth of subduction at least 20 km deeper. Provided all Permian age eclogites form one

lithotectonic assemblage, it is possible that a significantly large portion of the Yukon-Tanana arc was subducted to HP and UHP conditions.

Age of Metamorphism in the Yukon-Tanana Terrane

The CL patterns, REE patterns, and U-Pb ages recorded by zircon from eclogites in the St. Cyr klippe indicate two major periods of growth, i.e. a magmatic and metamorphic event. Both the cores and rims of zircons in samples 10-89 and 11-104 to record the magmatic crystallization age of the eclogite protolith between 364 and 380 Ma, based on their REE patterns (Schaltegger et al., 1999; Rubatto, 2002) and high Th/U ratios (Williams, 1998; Rubatto, 2002). Eu anomalies (Fig. 3-10a) are typical of zircons formed in the presence of plagioclase, due to its preferential incorporation within plagioclase (Philpott and Schnetzl, 1968; Rubatto, 2002; Hermann and Rubatto, 2003). Latest Devonian igneous crystallization ages for eclogite protoliths fall mainly within the Ecstall Cycle of Yukon-Tanana arc activity, which corresponds to the oldest igneous activity within the YTT (365 to 390 Ma; Piercey et al., 2006). Similarly aged mafic metavolcaniclastic rocks are found Ecstall belt, northwest British Columbia (Alldrick et al., 2000; Gareau and Woodsworth, 2000; Alldrick, 2001). Tonalitic plutons in the Coast Mountains and isotopic data from the Ecstall belt suggest these assemblages formed in a continental arc setting (Gareau and Woodsworth, 2000).

The REE pattern of zircon in samples 10-143 and 11-101 both exhibit the absence of Eu anomalies, flat, depleted HREE, and low Th/U ratios. These features are characteristic of zircon growth or recrystallization under plagioclase-absent eclogite facies conditions (Rubatto, 2002). Thus, we interpret the age of HP and UHP metamorphism of eclogite in the St. Cyr klippe to be between 267 and 271 Ma. By using *in situ* SHRIMP methods, this study establishes a link between the age of the zircon grain and the trace elements preserved at the time of grain formation. This study is also able to distinguish between zircon formed during magmatic crystallization or HP metamorphism.

Previous dating of St. Cyr eclogite samples yielded a TIMS zircon U-Pb age of 266 ± 0.6 Ma (Fallas et al., 1998), which agrees with our results

The age of metamorphism of the quartzofeldspathic schists that host eclogites in the St. Cyr klippe was documented by Petrie et al. (in preparation a). Metamorphic rims of zircon from one sample also shows the characteristic flat, depleted HREE, low Th/U ratios, and the lack of Eu anomalies (Petrie et al., in preparation a). The metamorphic zircons within the quartzofeldspathic schists give a $^{206}Pb/^{238}U$ age of 266 ± 3 Ma, which is within error of the age of the eclogites they host; confirmation that the eclogite and quartzofeldspathic host rocks experienced a similar HP metamorphic history.

Eclogites at Faro, Ross River, and Last Peak record Late Permian-early Triassic K-Ar and $^{40}Ar/^{39}Ar$ white mica age plateaus in the range 273-236 Ma, with a pronounced peak at ~ 260 Ma, in both eclogite and their quartzofeldspathic host rocks (Wanless, 1978; Erdmer and Armstrong, 1989; Creaser et al., 1997; Erdmer et al., 1998). These ages were assumed to be post eclogite facies metamorphism cooling ages. In combination with our results, the HP and UHP rocks within the YTT could have experienced rapid exhumation to the shallow crust, on the order of ~ 10-17 km/m.y.

Conclusions

Well-preserved eclogites enclosed in quartzofeldspathic schists have been documented in the St. Cyr klippe, Yukon-Tanana terrane of the northern Canadian Cordillera. Eclogites were found to record a five-stage clockwise *P–T* path. Early-eclogite facies conditions give way to peak pressure conditions of about 3.2 GPa and 610 °C, well within the stability field of coesite. These results suggest that the St. Cyr eclogites underwent UHP metamorphism in a subduction zone with a low thermal gradient 5 °C/km. Two retrograde stages record decompression while increasing in temperature, suggesting that the eclogites were exhumed within a subduction channel. Combined with the results from the SHRIMP-RG zircon dating, we conclude that

eclogites have a Mid- to Late Devonian protolith, consistent with their initial formation within the Yukon-Tanana terrane during early, continental arc activity, between 364 and 380 Ma. These rocks subsequently were subducted to mantle depths and metamorphosed to UHP eclogite during the Late Permian, from 267 and 271 Ma. This is the first report of UHP metamorphism in North America, and is a rare example of UHP in an accretionary orogen.

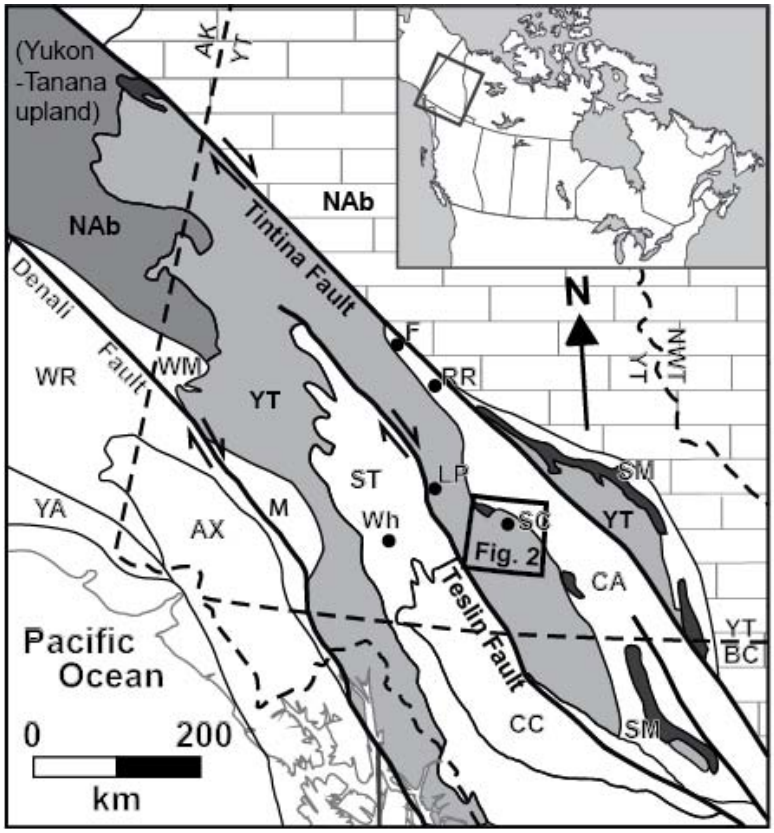

Figure 3-1 Terrane map of the northern Canadian Cordillera. Black box shows the study area (Fig. 3-2; modified from Colpron et al., 2006 and Nelson et al., 2013). F, Faro; LP, Last Peak; RR, Ross River; ST, St. Cyr; Wh, Whitehorse. Terrane abbreviations: AX, Alexander; CA, Cassier; CC, Cache Creek; NAb, North American platform; SM, Slide Mountain; ST, Stikinia; YA, Yukuta; YT, Yukon-Tanana; WM, Windy-McKinley; WR, Wrangellia; M, undivided metamorphic and plutonic rocks.

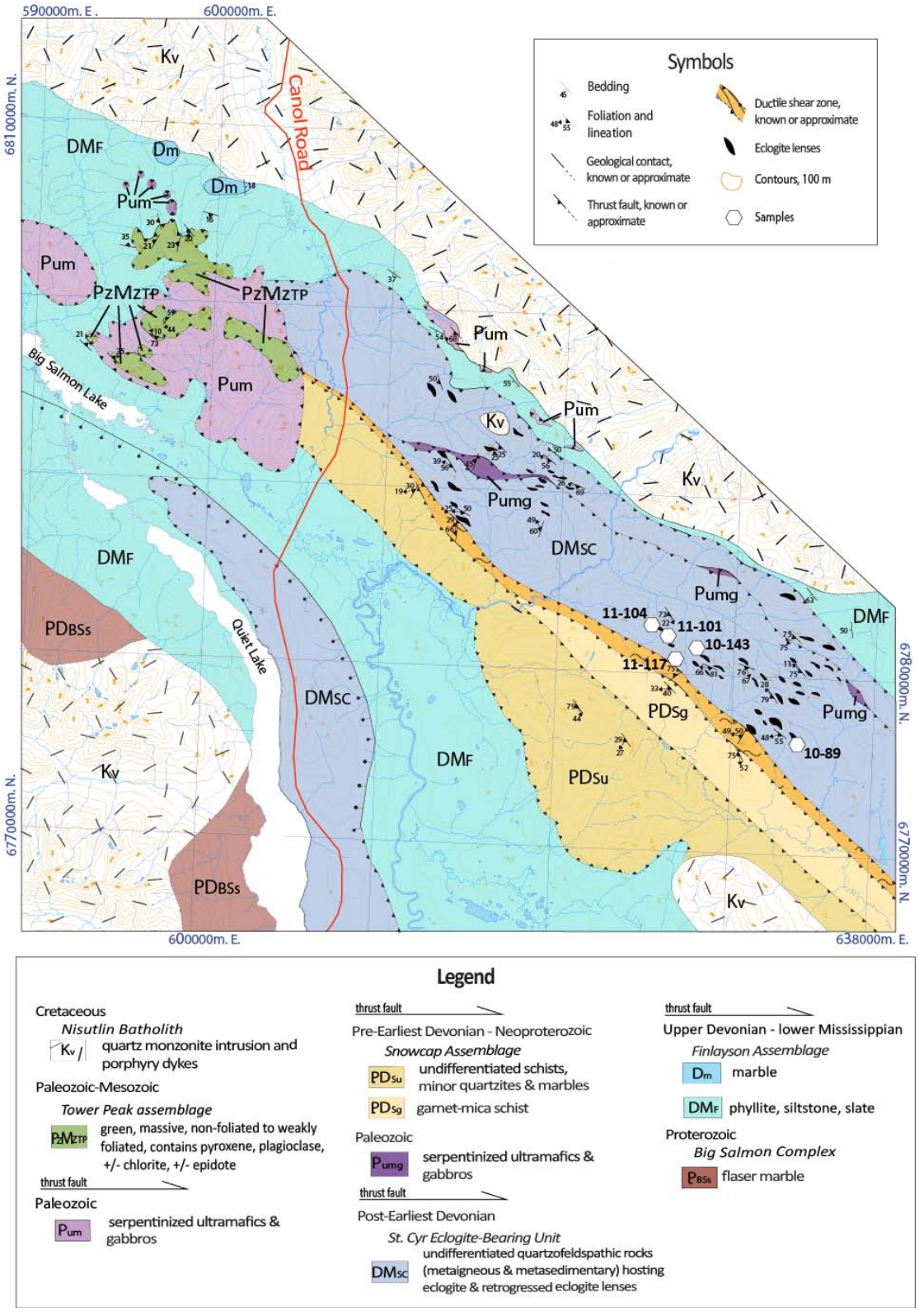

Figure 3-2 Geologic map of the St. Cyr klippe and surrounding region. Modified from Tempelman-Kluit (2012) and Colpron (2006). Based on mapping Isard (2014), this study. Hexagons represent samples used in this study.

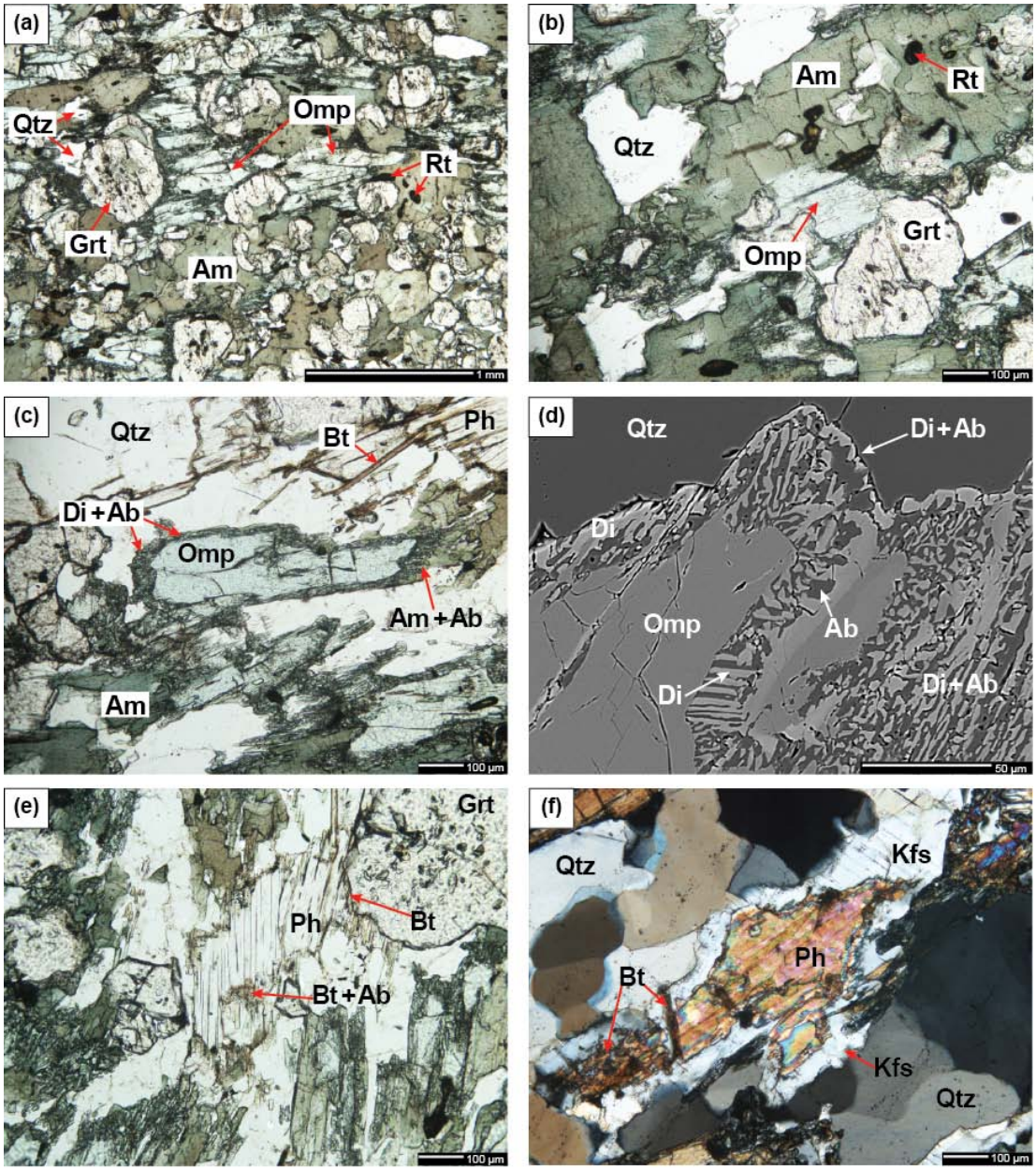

Figure 3-3 Optical photomicrographs and backscattered electron image of eclogite sample 11-117. (a) Optical photomicrograph (plane polarized light) showing the peak assemblage of sample 11-117 consisting of omphacite + garnet + amphibole + quartz + rutile (peak phengite not shown). (b) Optical photomicrograph (plane polarized light) of peak amphibole in equilibrium with omphacite and garnet. (c) Optical photomicrograph (plane polarized light) of omphacite breaking down to symplectites of diopside + plagioclase and amphibole + plagioclase. (d) Electron backscattered image of omphacite converting to diopside + plagioclase. (e) Optical photomicrograph (plane polarized light) of phengite in the matrix. (f) Optical photomicrograph (crossed polarized light) of phengite breaking down to form K-feldspar. Note the textural equilibrium between the biotite replacing phengite and the rim of a garnet grain.

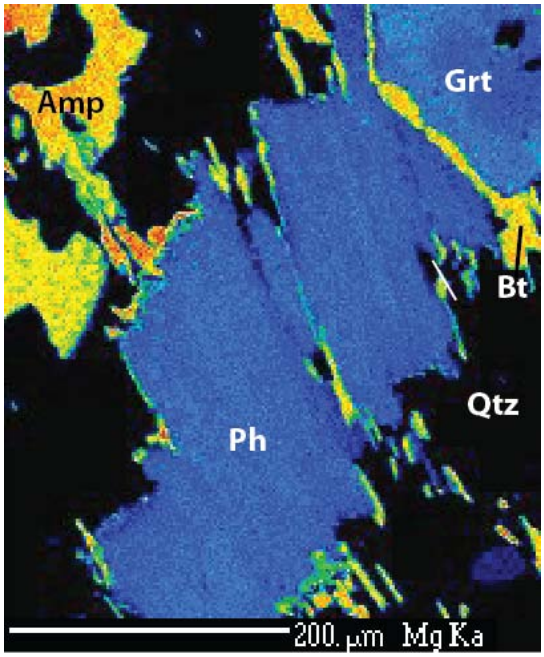

Figure 3-4 Mg X-ray map of phengite from sample 11-117. Warm colors represent higher elemental concentrations and cool colors, lower concentrations. The phengite displays moderate zoning at grain edges.

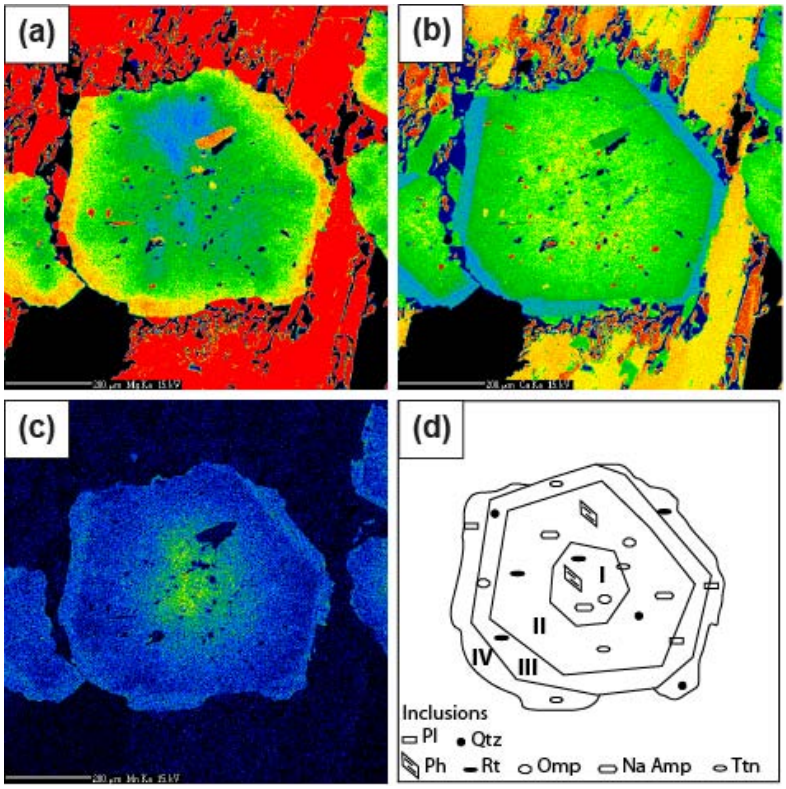

Figure 3-5 X-ray maps garnet from sample 11-117. (a), (b), and (c) are Mg, Ca, and Mn maps, respectively. Warm colors represent higher elemental concentrations and cool colors, lower concentrations. (d) Illustration showing the different compositional zones within the garnets. Roman numerals reflect the stages of metamorphism in Fig. 9.

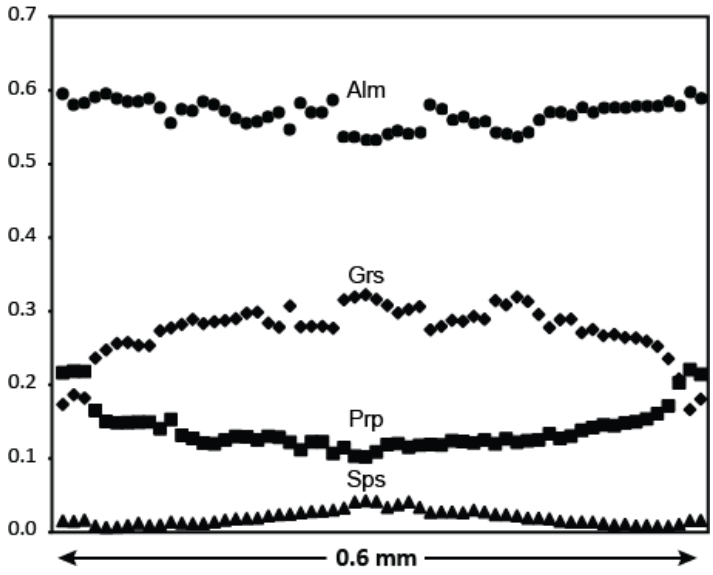

Figure 3-6 Compositional profile across garnet porphyroclast from sample 11-117. See text for details.

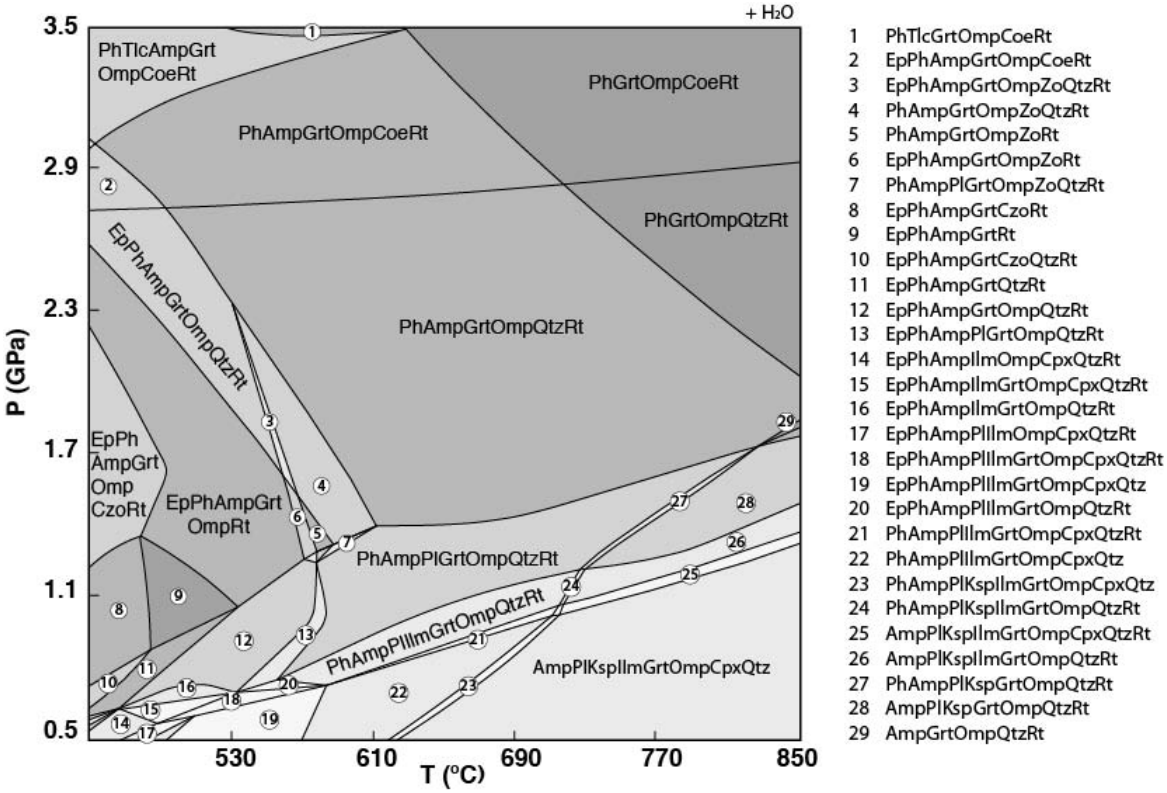

Figure 3-7 *P–T* pseudosection calculated for the modified composition of eclogite sample 11-117. Computer software package PERPLE_X was used for the calculation (see text). Mineral abbreviations follow Whitney and Evans (2010). Bulk composition used in the pseudosection is given in Table 3-3. Amphibole is Ca-rich at high temperatures and low pressures over the displayed *P–T* range. Na-rich amphibole occurs at high pressures, while Na- and Ca- amphibole coexist at moderate pressures. Cpx is diopside. The gray tones are related to the variance (the brighter the lower) of the corresponding mineral assemblage (+ H_2O). Very small *P–T* fields are not labeled.

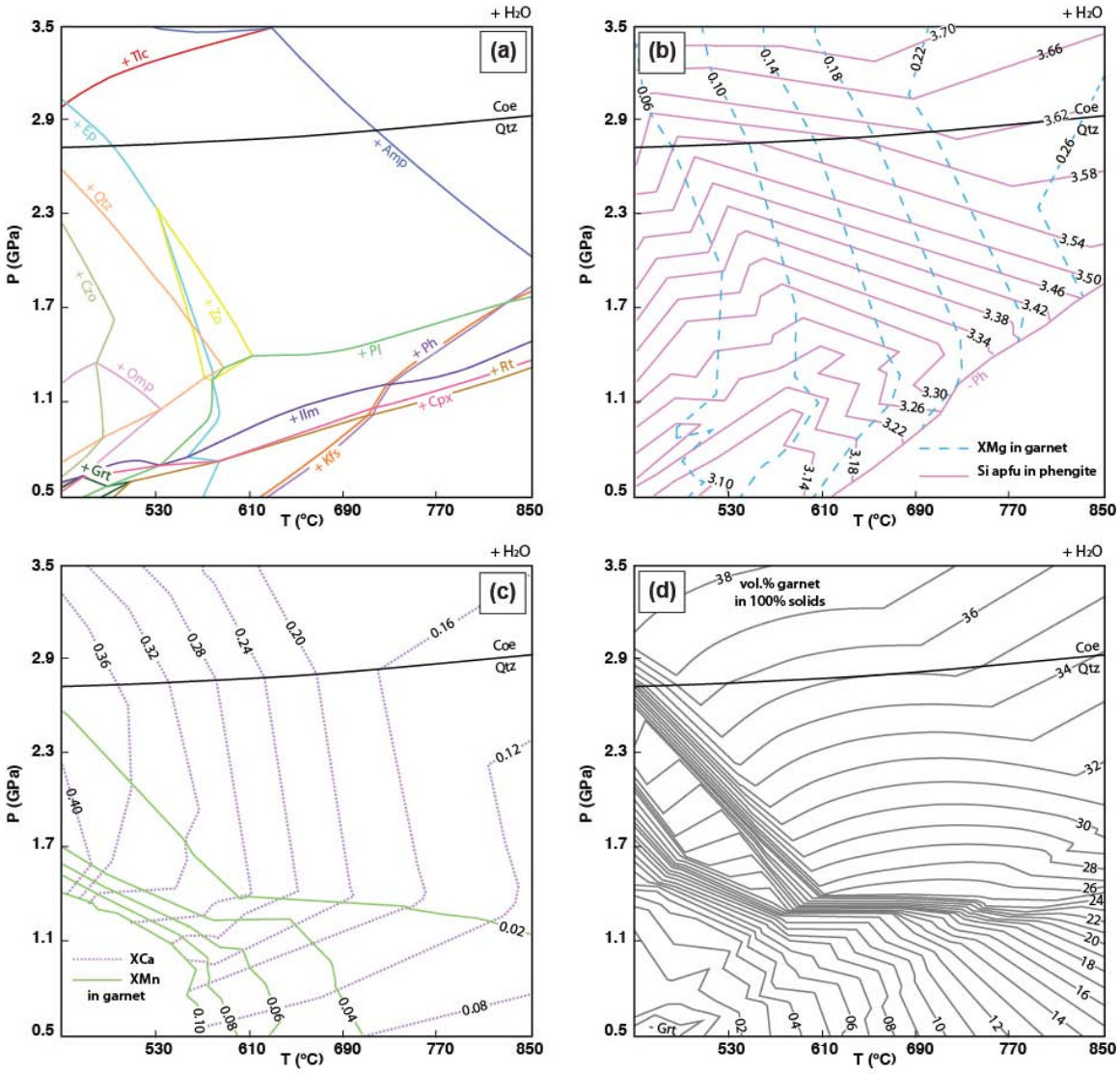

Figure 3-8 Contour diagrams used for interpreting the *P–T* path of eclogite sample 11-117. (a) Boundaries of the *P–T* fields of phases are shown by the various lines taken from Fig. 3-7. Abbreviations as in Fig. 3-7. Contouring of the *P–T* pseudosection of Fig. 3-7 was undertaken by isopleths for the Si apfu content in phengite and the molar fraction of Mg in garnet (b), the molar fractions of Ca and Mn in garnet (c), and the modal content in garnet (d).

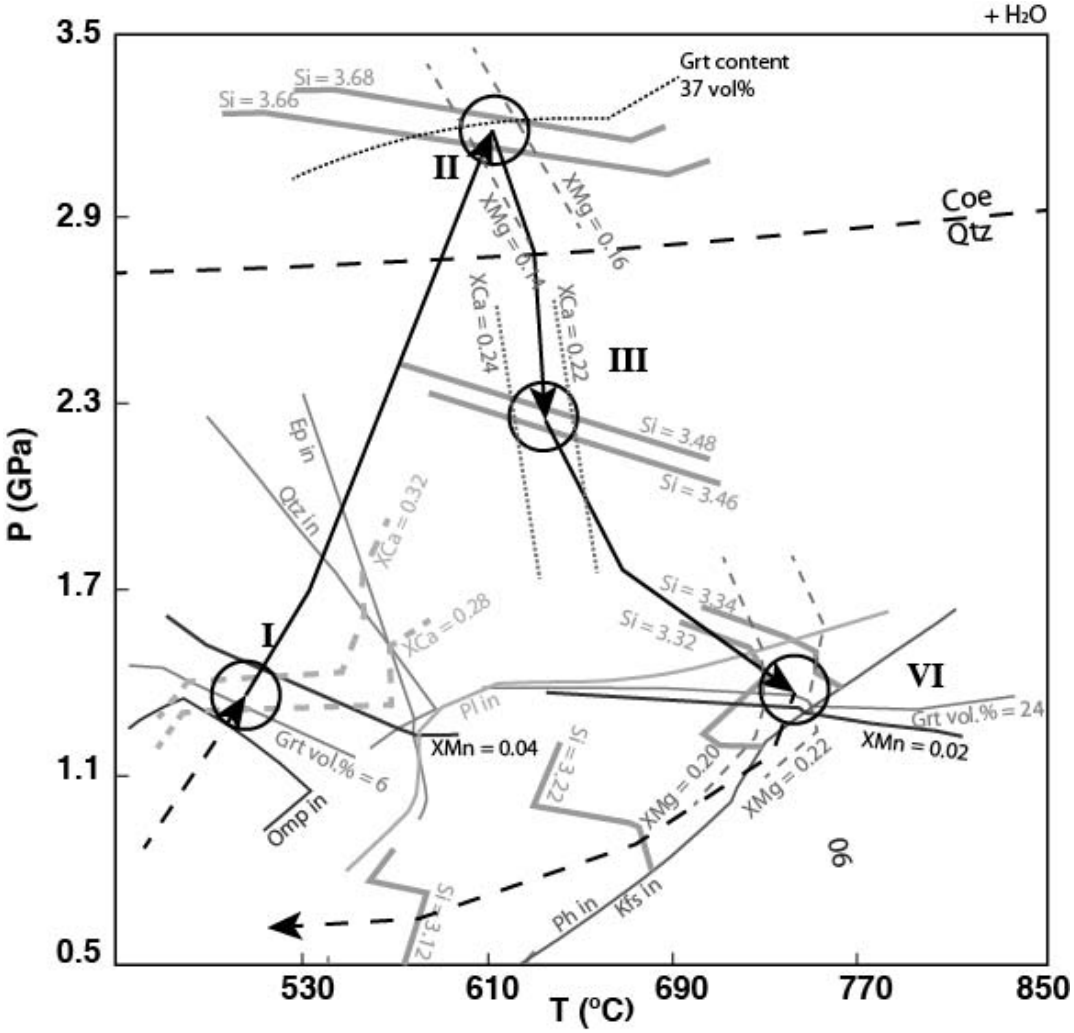

Figure 3-9 *P–T* path for eclogite sample 11-117. Path (shown by the black arrows) derived from the various garnet and phengite Si isopleths displayed in Fig. 3-8. The dotted lines indicate where the *P–T* path is uncertain. Circles mark the beginning of garnet growth, peak *P–T* conditions, and the evolution of the retrograde path. The prograde metamorphic path could have followed a low geothermal gradient.

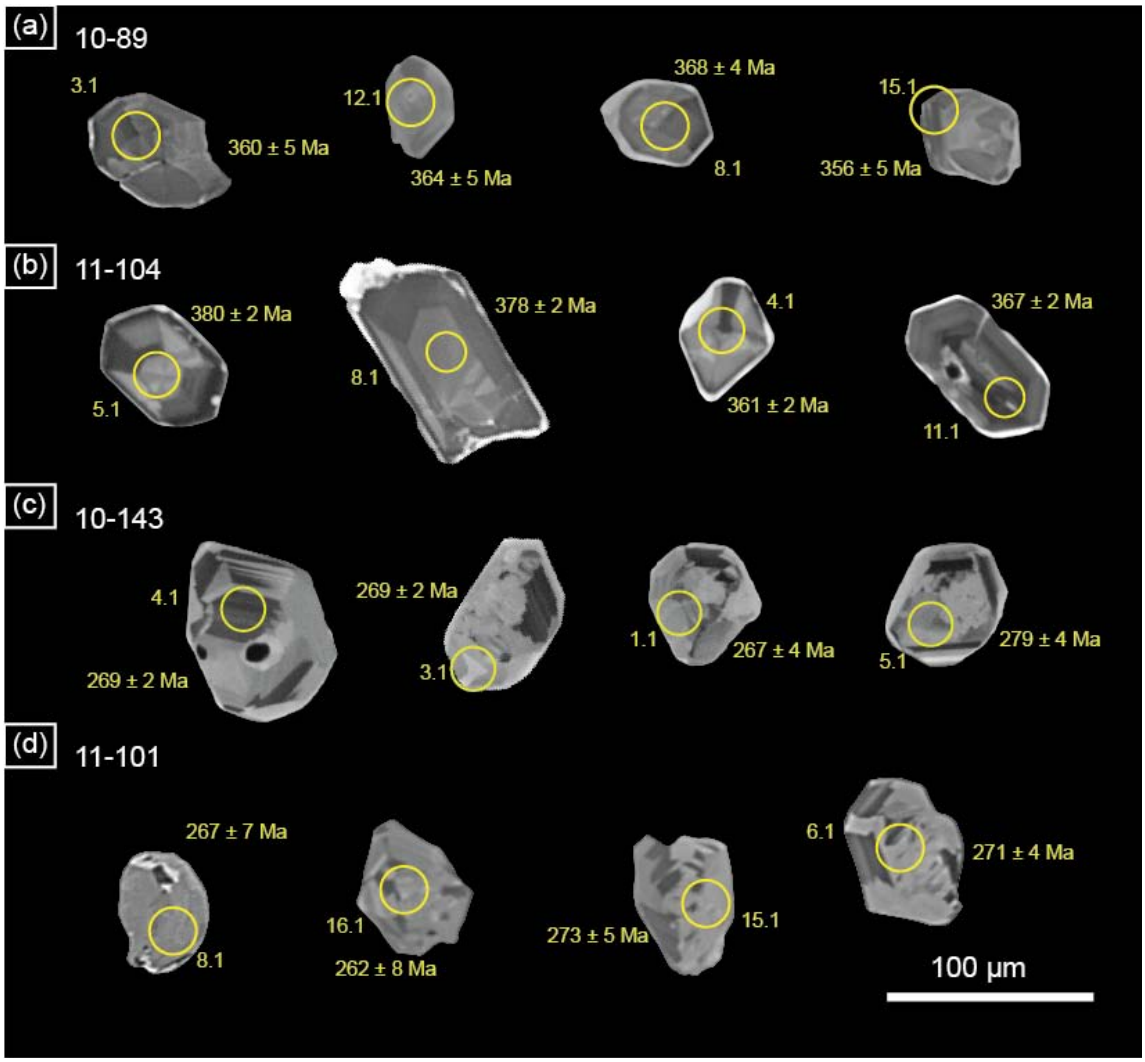

Figure 3-10 Representative cathodoluminescence (CL) images of zircon from eclogites from the St. Cyr klippe. Samples 10-89 (a), 11-104 (b), 10-143 (c), and 11-101 (d). Yellow ellipses indicate sensitive high-resolution ion microprobe reverse-geometry (SHRIMP-RG) U-Pb and trace element analysis spots labeled by grain and spot number.

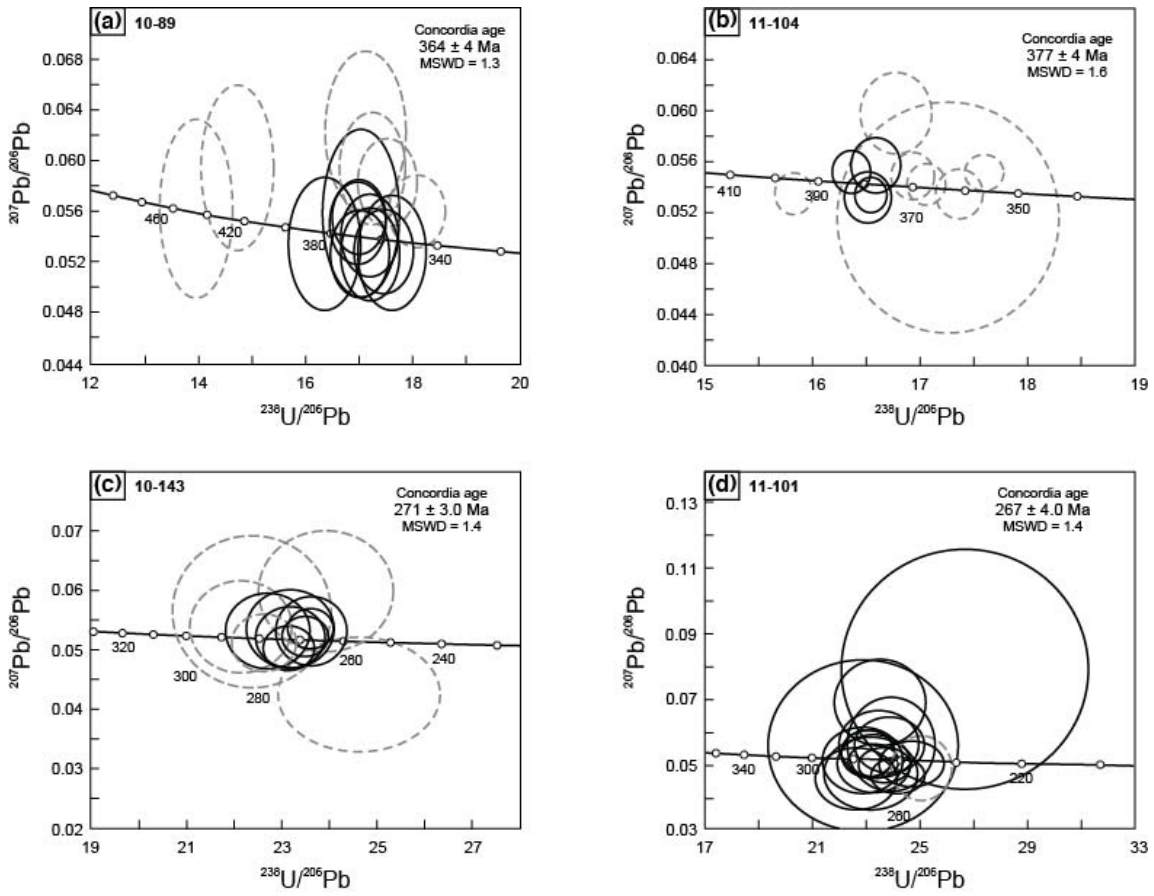

Figure 3-11 Terra–Wasserburg plots of SHRIMP-RG U-Pb data from eclogites from the St. Cyr klippe. Data are 1σ error ellipses uncorrected for common Pb. Eclogite samples 10-89 (a) and 11-104 (b) show protolith crystallization ages, while samples 10-143 (c) and 11-101 (d) show metamorphic crystallization ages. Black ellipses are used in calculating concordia ages. Errors are reported at the 95% confidence level.

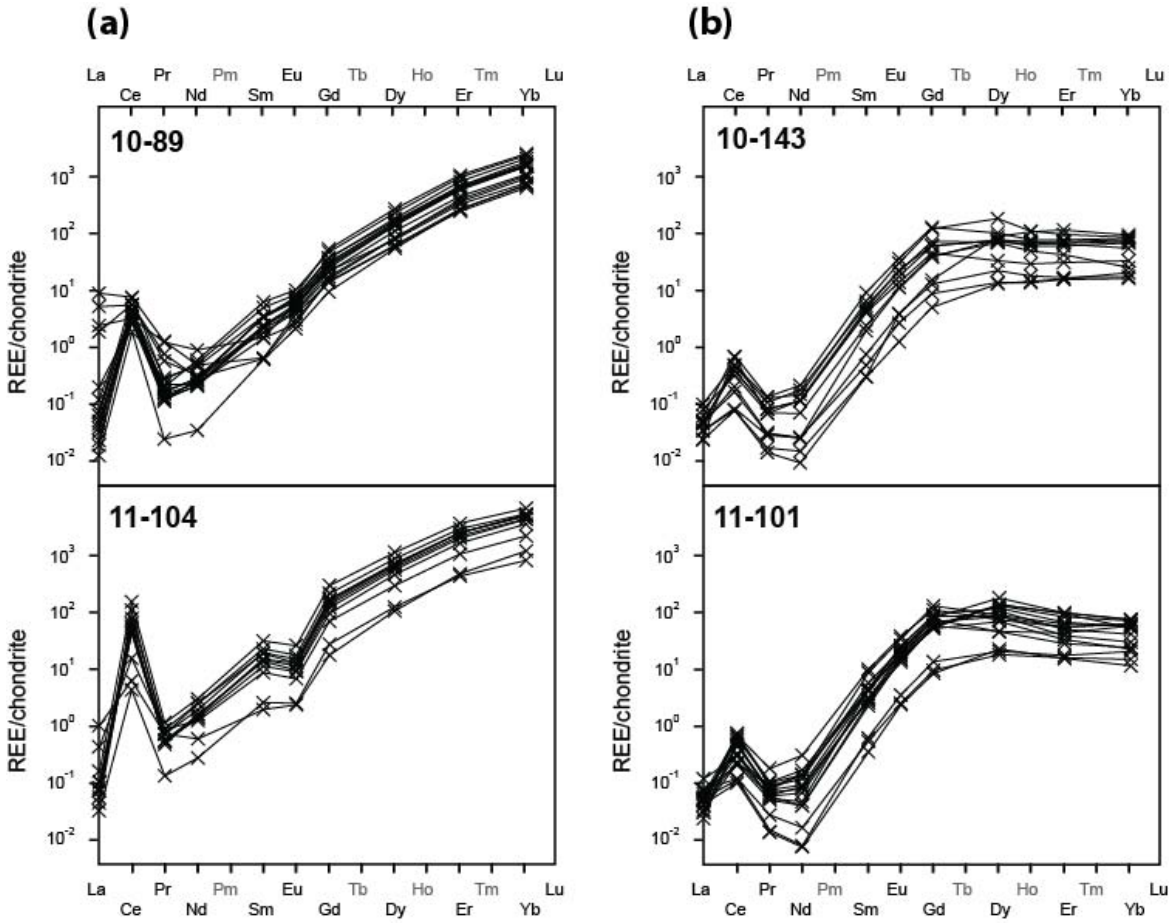

Figure 3-12 Chondrite-normalized REE patterns for different age populations of zircon grains from eclogite samples. Normalization uses chondrite abundances from Anders and Grevesse (1989) multiplied by 1.36 (Korotev, 1996). Ages are divided into igneous crystallization ages (a) and metamorphic ages (b), as discussed in the text.

Table 3-1 Mineral assemblages and locations of samples used in this study

Sample	UTM Coordinates (zone 8N)	Grt	Cpx	Amp	Qtz	Rt	Ph	Pl	Ep	Ap	Ilm	Ttn	Chl	Bt	Ksp
Pseudosection sample															
11-117	0626764, 6780873	pb	m/i/s	m/i/s	m/i	m/i	m/i	i/s			r	r		s/r	r
Geochronology samples															
10-89	0633667, 6776599	pb	m/i	m/i/s	m/i	m/i		s	i		i/r	i/r			
10-143	0627923, 6781477	pb	m/i	m/i/s	m/i	m/i	m	i/s	i/a	a	i/r	r	r	r	
11-101	0626171, 6782297	pb	m/i	i/s	m/i	m/i		s			m/i	i/r			
11-104	0625623, 6782574	pb	m/i	i/s	m/i	m/i		i		a	i/a				

Mineral abbreviations follow those of Whitney and Evans (2010).

Textural abbreviations are: pb = porphyroblast, m = matrix, i = inclusion (in garnet), s = symplectite, a = accessory, r = retrograde phase.

Table 3-2 Representative mineral compositions from sample 11-117

	Grt	Grt	Grt	Grt	Ph	Ph	Ph	Ph
Anal.	core	inter-med.	inner rim	outer rim	core	hi Si	rim	low Si
Anal #	1/29	1/11	1/57	1/3	2/8	1/1	1/1	2/1
SiO_2	38.250	41.482	38.727	38.820	57.232	52.960	48.000	45.346
TiO_2	0.258	0.094	0.071	0.036	0.353	1.477	0.901	0.928
Al_2O_3	21.425	19.670	21.831	21.869	22.885	23.871	30.246	29.052
FeO	24.532	25.186	27.142	27.230	2.382	2.484	2.542	4.575
MnO	1.936	0.600	0.353	0.752	0.000	0.018	0.000	0.034
MgO	2.624	3.880	4.454	5.708	1.577	2.134	2.536	3.659
CaO	11.566	9.803	8.518	6.625	3.141	4.221	0.029	0.028
Na_2O					7.260	5.480	0.664	0.660
K_2O					2.018	3.871	10.066	9.573
BaO							0.409	0.702
Wt % total	100.591	100.715	101.096	101.040	96.848	96.516	95.393	94.557
Oxygen	12	12	12	12	11	11	11	11
Si	2.996	3.235	3.000	2.997	3.671	3.469	3.220	3.121
Ti	0.015	0.006	0.004	0.002	0.017	0.073	0.045	0.048
Al	1.977	1.808	1.993	1.990	1.730	1.843	2.391	2.357
Fe^{3+}	0.001	0.000	0.000	0.013				
Fe^{2+}	1.606	1.642	1.758	1.745	0.128	0.136	0.143	0.263
Mn	0.128	0.040	0.023	0.049	0.000	0.001	0.000	0.002
Mg	0.306	0.451	0.514	0.657	0.151	0.208	0.254	0.375
Ca	0.970	0.819	0.707	0.548	0.216	0.296	0.002	0.002
Na					0.903	0.696	0.086	0.088
K					0.165	0.323	0.861	0.841
Ba							0.011	0.019
X_{Alm}	53.34	55.63	58.55	58.36				
X_{Sps}	4.26	1.34	0.77	1.63				
X_{Prp}	10.17	15.28	17.13	21.81				
X_{Grs}	32.22	27.74	23.54	18.19				

Table 3-2 Continued

Mineral	Omp	Omphacite	Diopside	Amphibole	Amphibole	Amphibole
Anal.	grt incl.	matrix	symplectite	matrix	grt incl.	symplectite
Anal. #	2/1	2/1	5/1	3/1	7/1	9/1
SiO_2	55.120	55.556	53.655	43.129	40.107	44.177
TiO_2	0.110	0.128	0.075	0.932	2.370	0.824
Al_2O_3	9.485	10.040	1.679	15.712	18.011	13.240
FeO	6.635	6.547	11.260	14.231	17.713	14.240
MnO	0.052	0.042	0.177	0.048	0.120	0.120
MgO	8.596	8.142	10.673	9.808	5.989	11.231
CaO	13.914	12.994	21.570	9.062	8.645	9.616
Na_2O	6.294	6.795	1.416	4.317	4.460	4.032
K_2O	0.010	0.000	0.000	0.849	0.305	0.580
BaO						
Wt % total	100.216	100.244	100.505	98.088	97.720	98.060
Oxygen	6	6	6	23	23	23
Si	1.970	1.980	2.005	6.306	5.996	6.442
Ti	0.003	0.003	0.002	0.103	0.267	0.090
Al	0.400	0.422	0.074	2.707	3.173	2.275
Fe^{3+}	0.091	0.081	0.014	0.254	0.182	0.408
Fe^{2+}	0.107	0.114	0.338	1.486	2.032	1.328
Mn	0.002	0.001	0.006	0.006	0.015	0.015
Mg	0.458	0.433	0.595	2.138	1.335	2.441
Ca	0.533	0.496	0.864	1.420	1.385	1.502
Na	0.436	0.470	0.103	1.224	1.293	1.140
K	0.000	0.000	0.000	0.158	0.058	0.108
End Member for Ca-Na Pyroxenes (Morimoto et al., 1988)						
Quad	50.28	47.42				
Jd	41.15	44.87				
Ae	8.57	7.71				
Quad Cpx for Ws-En-Fs plot						
Wo			47.71			
En			32.85			
Fs			19.44			
Name				katophorite	taramite	pargasite

Table 3-3 Whole-rock geochemical data for eclogite sample 11-117

	11-117	modified for pseudosection
SiO_2 (wt. %)	49.31	47.71
TiO_2	2.20	2.13
Al_2O_3	14.24	13.77
FeO*	14.32	13.85
MnO	0.25	0.24
MgO	6.47	6.26
CaO	10.15	9.62
Na_2O	3.19	3.08
K_2O	0.19	0.18
O_2		0.15
H_2O		3.00
P_2O_5	0.16	
Total	100.46	100.00

* Fe reported as total Fe

For O_2 and H_2O, see text.

The modified composition (see text) was used for PERPLE_X calculations.

Table 3-1 U-Pb SHRIMP geochronologic data and apparent ages

Spot[a]	U[b] (ppm)	Th (ppm)	Th/U	$^{206}Pb^{*b}$ (ppm)	$f^{206}Pb_c$ [b]	$^{238}U/^{206}Pb$[c]		$^{207}Pb/^{206}Pb$[c]		$^{206}Pb/^{238}U$[d] (Ma)	
Sample 10-89											
1.1	199	51	0.27	9	<0.01	18.268	(1.5)	.05277	(2.7)	344	(5)
2.1	299	102	0.35	14	0.32	18.124	(1.4)	.05597	(2.1)	345	(5)
3.1	202	55	0.28	10	<0.01	17.496	(1.5)	.05278	(2.6)	359	(5)
4.1	125	33	0.27	6	0.70	17.287	(1.6)	.05935	(3.1)	360	(6)
5.1	82	20	0.25	4	0.24	17.072	(1.9)	.05582	(4.9)	366	(7)
6.1	203	51	0.26	10	0.57	17.569	(1.5)	.05824	(2.4)	355	(5)
7.1	189	57	0.31	9	<0.01	17.246	(1.5)	.05257	(2.9)	364	(5)
8.1	293	99	0.35	15	0.20	17.034	(1.4)	.05552	(2.1)	367	(5)
9.1	87	24	0.28	5	<0.01	16.389	(1.8)	.05340	(4.0)	382	(7)
10.1	232	64	0.29	12	0.14	17.012	(1.4)	.05503	(2.4)	368	(5)
11.1	185	52	0.29	9	<0.01	17.050	(1.5)	.05261	(2.7)	368	(5)
12.1	223	82	0.38	11	0.03	17.236	(1.4)	.05406	(2.5)	363	(5)
13.1	89	19	0.22	5	0.52	14.753	(2.0)	.05941	(4.5)	421	(8)
14.1	87	21	0.25	5	0.04	13.981	(2.1)	.05617	(5.1)	445	(9)
15.1	152	53	0.36	7	<0.01	17.653	(1.6)	.05267	(3.5)	356	(6)
16.1	86	20	0.24	4	1.06	17.158	(1.9)	.06230	(4.2)	361	(7)
Sample 10-143											
1.1	92	0.2	0.003	3.3	0.19	23.619	(1.3)	.05314	(4.5)	267	(3)
2.1	41	0.02	0.0004	1.6	0.24	22.137	(2.0)	.05387	(5.9)	284	(6)
3.1	20	0.03	0.001	0.7	<0.01	24.624	(2.8)	.04249	(9.3)	259	(7)
4.1	201	0.7	0.004	7.4	0.08	23.490	(0.9)	.05225	(2.6)	269	(2)

Table 3-4 Continued

Spot[a]	U[b] (ppm)	Th (ppm)	Th/U	$^{206}Pb*$[b] (ppm)	$f^{206}Pb_c$[b]	$^{238}U/^{206}Pb$[c]		$^{207}Pb/^{206}Pb$[c]		$^{206}Pb/^{238}U$[d] (Ma)	
5.1	78	0.3	0.005	3.0	<0.01-	22.628	(1.2)	.05117	(3.9)	279	(3)
6.1	67	0.2	0.003	2.5	0.04	23.180	(1.3)	.05204	(4.1)	272	(4)
7.1	128	0.6	0.004	4.7	<0.01	23.148	(1.0)	.05027	(3.0)	273	(3)
8.1	19	0.2	0.011	0.7	1.05	23.927	(2.4)	.05985	(6.9)	261	(6)
9.1	43	0.1	0.001	1.6	0.23	23.176	(1.6)	.05352	(5.0)	272	(4)
10.1	46	0.3	0.007	1.8	0.17	22.702	(1.6)	.05317	(4.9)	277	(4)
11.1	13	0.03	0.003	0.5	0.57	22.369	(3.0)	.05642	(9.3)	280	(9)
12.1	166	0.4	0.003	6.0	0.25	23.604	(0.8)	.05357	(2.6)	267	(2)
Sample 11-101											
1.1	21	0	0.005	1	<0.01	23.232	(3.1)	.04761	(9.5)	273	(9)
2.1	78	1	0.007	3	<0.01	25.130	(1.9)	.04922	(8.1)	252	(5)
3.1	26	0	0.002	1	2.21	23.575	(3.0)	.06917	(7.7)	262	(8)
4.1	42	0	0.002	2	<0.01	23.355	(2.5)	.05062	(7.1)	271	(7)
5.1	4	0	0.007	0	3.57	26.742	(7.1)	.07926	(18.8)	228	(17)
6.1	103	1	0.007	4	<0.01	23.335	(1.8)	.05130	(4.2)	271	(5)
7.1	99	1	0.007	4	<0.01	23.742	(1.8)	.05014	(4.3)	266	(5)
8.1	32	0	0.007	1	0.63	23.540	(2.7)	.05664	(7.3)	267	(7)
9.1	28	0	0.003	1	-0.74	22.687	(2.8)	.04597	(8.4)	280	(8)
10.1	64	0	0.004	2	<0.01	24.756	(2.1)	.05049	(5.6)	256	(5)
11.1	5	0	0.007	0	0.54	22.956	(6.4)	.05608	(19.0)	273	(18)
12.1	31	0	0.007	1	<0.01	22.924	(2.8)	.05159	(8.0)	275	(8)
13.1	28	0	0.004	1	0.60	23.924	(2.3)	.05626	(6.2)	262	(6)

Table 3-4 Continued

Spot[a]	U[b] (ppm)	Th (ppm)	Th/U	$^{206}Pb*$[b] (ppm)	$f^{206}Pb_c$[b]	$^{238}U/^{206}Pb$[c]		$^{207}Pb/^{206}Pb$[c]		$^{206}Pb/^{238}U$[d] (Ma)	
14.1	55	0	0.009	2	<0.01	24.243	(1.8)	.04700	(4.8)	262	(5)
15.1	48	1	0.032	2	0.24	23.131	(1.9)	.05366	(5.4)	272	(5)
16.1	16	0	0.002	1	0.62	23.988	(2.9)	.05646	(10.4)	262	(8)
Sample 11-104											
1.1	252	105	0.43	13	0.72	16.77	(0.8)	.0598	(2.2)	371	(3)
1.2	1318	1173	0.92	64	0.18	17.60	(0.4)	.0551	(1.0)	356	(1)
2.1	27	6	0.24	1	<0.01	17.26	(2.4)	.0516	(7.2)	364	(9)
3.1	770	179	0.24	42	<0.01	15.82	(0.5)	.0535	(1.2)	396	(2)
4.1	605	458	0.78	30	<0.01	17.36	(0.5)	.0534	(1.5)	361	(2)
5.1	551	389	0.73	29	<0.01	16.51	(0.5)	.0532	(1.5)	380	(2)
6.1	1273	1286	1.04	66	<0.01	16.54	(0.4)	.0534	(1.1)	379	(1)
7.1	0.5	0.005	0.01	0.03	10.27	15.44	(23)	.1366	(42)	364	(86)
8.1	521	277	0.55	27	0.19	16.59	(0.6)	.0557	(1.6)	377	(2)
9.1	782	395	0.52	41	0.11	16.36	(0.4)	.0552	(1.2)	382	(2)
10.1	669	396	0.61	34	0.11	16.93	(0.5)	.0549	(1.4)	370	(2)
11.1	886	629	0.73	45	0.04	17.06	(0.4)	.0542	(1.2)	367	(2)

Note: All analyses were performed on the SHRIMP-RG ion microprobe at the United States Geological Survey-Stanford University Microanalytical Center, Stanford, CA. Calibration concentrations and isotopic compositions were based on replicate analyses of CZ3 and R33 (419 Ma; Black et al., 2004), respectively. Analytical routine followed Williams (1998). Data reduction utilized Ludwig (2001a).

[a] 1.1 = grain1, spot 1.

Table 3-4 Continued

[b] Pb* denotes radiogenic Pb; Pb_c denotes common Pb; $f^{206}Pb_c = 100*(^{206}Pb_c/^{206}Pb_{total})$

[c] Reported ratios are not corrected for common Pb. Errors are reported in parentheses as percent at the 1 σ level.

[d] Ages calculated from ratios corrected for common Pb using ^{207}Pb for the $^{206}Pb/^{238}U$ ages and ^{204}Pb for the $^{207}Pb/^{206}Pb$ ages. Uncertainties in millions of years reported as 1 σ.

Table 3-2 Zircon trace element data

Spot[a]	CL	Y	La	Ce	Nd	Sm	Eu	Dy	Er	Yb	Hf	Ce/ Ce*	Eu/ Eu*	$Yb_{(N)}$/ $Gd_{(N)}$	T (°C)
Sample 10-143															
1.1	s		222	0.01	0.44	0.11	1.5	2.47	32	39	24	26	10,882	8	1.1
2.2	r		385	0.01	0.06	0.01	0.1	0.39	6	49	42	35	11,611	4	1.8
3.1	r		45	0.01	0.07	0.00	0.1	0.12	2	6	5	7	10,175	4	1.0
4.1	s		166	0.02	0.30	0.04	0.6	1.24	17	37	15	8	11,811	5	1.2
5.1	s		398	0.03	0.47	0.09	1.8	3.59	56	107	35	32	11,383	5	1.1
6.1	s		205	0.01	0.37	0.07	1.2	2.01	26	42	21	25	10,990	7	1.1
7.1	s		271	0.02	0.72	0.14	2.6	4.37	59	57	28	30	10,973	10	1.1
8.1	s		56	0.01	0.15	0.01	0.2	0.40	5	11	5	6	12,339	5	1.3
9.1	s		247	0.01	0.18	0.01	0.5	1.18	16	43	23	20	11,177	6	1.3
10.1	r		95	0.01	0.37	0.07	1.1	1.55	19	17	10	11	11,569	8	1.0
11.1	s		42	0.01	0.07	0.01	0.1	0.27	3	7	5	5	11,906	3	1.3
12.1	s		245	0.01	0.65	0.07	1.3	2.63	27	41	25	28	11,545	21	1.4
Sample 11-89															
1.1	s		681	0.02	3	0.13	0.5	0.39	7	46	134	349	11,963	0.64	41
2.2	s		659	0.02	4	0.14	0.5	0.37	7	47	127	338	11,782	0.63	46
3.1	s		907	0.03	4	0.16	0.7	0.55	10	61	178	466	11,719	0.63	38
4.1	p		491	0.01	2	0.13	0.4	0.33	6	36	97	244	10,850	0.64	41
5.1	s		283	0.00	2	0.02	0.1	0.16	3	18	57	160	12,087	0.87	106
6.1	s		1,028	0.01	3	0.37	1.2	0.77	13	76	208	525	11,509	0.60	63

Table 3-5 Continued

Spot[a]	CL	Y	La	Ce	Nd	Sm	Eu	Dy	Er	Yb	Hf	Ce/ Ce*	Eu/ Eu*	$Yb_{(N)}$/ $Gd_{(N)}$	T (°C)
7.1	s		756	0.01	3	0.17	0.7	0.59	10	55	148	376	12,743	0.68	74
8.1	s		1,238	0.02	6	0.32	1.0	0.65	14	89	235	553	12,105	0.52	52
9.1	p		403	0.06	2	0.14	0.3	0.20	4	28	78	211	10,791	0.54	13
10.1	s		726	0.01	3	0.18	0.6	0.48	8	51	145	391	12,203	0.65	47
11.1	p		713	0.04	4	0.28	0.7	0.50	8	51	141	361	13,939	0.62	23
12.1	s		683	0.01	3	0.16	0.5	0.44	7	47	134	341	11,908	0.70	63
13.1	r		312	1.66	5	0.18	0.1	0.23	4	21	59	157	10,192	1.00	3
14.1	r		278	2.87	6	0.30	0.1	0.29	4	20	53	141	9,311	1.27	2
15.1	r		465	0.59	5	0.20	0.4	0.32	5	28	87	229	7,812	0.75	5
16.1	r		404	0.77	3	0.56	0.3	0.44	6	26	70	174	10,575	1.01	2
Sample 11-101															
1.1	p		130	0.02	0.26	0.06	0.8	1.55	19	28	12	14	10,957	1.20	5
2.2	s		91	0.01	0.43	0.05	0.6	1.31	14	23	7	5	11,831	1.41	12
3.1	s		212	0.02	0.19	0.04	0.6	0.99	16	43	18	16	11,128	0.96	4
4.1	s		220	0.04	0.25	0.02	0.5	1.14	14	45	21	17	11,379	1.36	4
5.1	p		40	0.02	0.09	0.005	0.1	0.26	3	7	4	4	11,541	1.20	4
6.1	s		67	0.01	0.61	0.07	1.1	1.71	20	15	6	5	11,666	1.10	12
7.1	s		107	0.01	0.55	0.10	0.9	1.95	23	28	8	7	11,496	1.28	10
8.1	s		142	0.02	0.49	0.09	1.8	2.61	35	30	13	13	11,433	1.01	8
9.1	s		263	0.01	0.19	0.08	0.8	1.57	21	59	21	16	11,146	1.14	4

Table 3-5 Continued

Spot[a]	CL	Y	La	Ce	Nd	Sm	Eu	Dy	Er	Yb	Hf	Ce/ Ce*	Eu/ Eu*	$Yb_{(N)}$/ $Gd_{(N)}$	T (°C)
10.1	s		126	0.02	0.55	0.19	2.0	2.86	29	24	12	14	11,140	1.15	6
11.1	p		32	0.03	0.10	0.01	0.1	0.19	3	6	3	3	11,482	1.11	3
12.1	s		226	0.02	0.17	0.02	0.5	1.13	15	46	21	12	11,308	1.23	3
13.1	s		167	0.02	0.28	0.03	0.9	1.91	24	39	14	13	11,115	1.26	5
14.1	s		143	0.02	0.37	0.05	0.6	1.45	16	35	11	9	11,580	1.42	7
15.1	s		78	0.01	0.38	0.08	0.8	1.34	15	15	9	13	11,682	1.13	11
16.1	s		36	0.01	0.08	0.00	0.1	0.18	2	8	3	3	12,031	1.39	4
Sample 11-104															
1.1	r		1,253	0.14	13	0.8	1.8	0.53	19	100	230	488	13,224	0.28	25
1.2	o		4,620	0.05	124	1.9	6.5	1.98	79	377	791	1,523	12,688	0.27	344
2.1	r		504	0.01	4	0.2	0.5	0.19	8	41	94	183	10,996	0.29	65
3.1	r		523	0.34	5	0.4	0.4	0.18	5	35	104	267	15,453	0.40	7
4.1	s		3,107	0.03	43	1.2	3.9	1.17	46	242	546	1,078	11,297	0.26	189
5.1	s		2,668	0.02	37	1.0	3.0	0.91	36	206	478	1,007	11,439	0.27	217
6.1	s		3,674	0.02	89	1.5	4.7	1.38	57	290	623	1,211	13,074	0.26	532
7.1	s		30	0.01	0	0.0	0.0	0.01	0.1	3	3	2	13,806	0.55	
8.1	s		3,001	0.03	36	0.9	3.0	1.01	41	230	541	1,118	11,558	0.27	199
9.1	o		2,033	0.02	47	0.9	2.3	0.70	26	155	367	806	12,679	0.27	280
10.1	s		2,444	0.01	53	1.0	2.8	0.75	33	185	445	977	12,444	0.24	419
11.1	o		3,037	0.03	64	1.6	3.8	1.00	45	226	540	1,176	12,842	0.23	254

Table 3-5 Continued

Note: All analyses performed on the SHRIMP-RG ion microprobe at the USGS-Stanford University Microanalytical Center, Stanford, CA following procedure outlined in Mazdab & Wooden (2006).

Abundances expressed in ppm.

[a] Spot labeled as grain # . spot #;

CL designations: s = sector zoned; p = patchy core; o = oscillatory zoned; r = rim.

CHAPTER 4.
METAMORPHIC HISTORY OF ECLOGITE-BEARING QUARTZOFELDSPATHIC ROCKS IN THE ST. CYR KLIPPE, YUKON-TANANA TERRANE, YUKON, CANADA

Abstract

Eclogite-facies rocks are hosted within quartzofeldspathic schists in the St. Cyr klippe in the Yukon-Tanana terrane, Yukon, Canada. A metatonalite in close proximity to eclogite lenses has been studied in detail in an effort to document its high-pressure metamorphic history and to compare the results with those of the eclogites. The metatonalite consists of quartz, plagioclase, epidote, clinozoisite, phengite, garnet, apatite, and paragonite. A *P–T* pseudosection, in the system Na_2O-K_2O-CaO-FeO-O_2-MnO-MgO-Al_2O_3-SiO_2-TiO_2-H_2O for the bulk-rock composition of the studied metatonalite was contoured for isopleths of various parameters, including the Si content of phengite and the molar fractions of garnet components. These results show a clockwise *P–T* path that reaches ultrahigh-pressure conditions. Garnet began to form at 1.4 GPa and 615 °C. Peak pressure conditions were reached at 3.2 GPa, but models return a temperature of 900 °C, which is probably too hot for this tectonic setting. Although the exact retrograde path could not be determined, the subsequent exhumation path passed through conditions between 0.5-1.1 GPa and 450-550 °C. The *P–T* path reflects metamorphism within a subduction zone.

Introduction

In collisional orogens, eclogites and related high-pressure (HP) and ultrahigh-pressure (UHP) assemblages are commonly found as lenses within quartzofeldspathic gneisses and schists. Those assemblages formed in continent-continent (Alpine-type) collisions include the Western Gneiss Region in Norway (Hacker et a., 2003; Butler et al., 2013), the Dora Maira Massif in the western Alps (Beltrando et al., 2010), the Dabie-

Sulu in China (Zhang et al., 2009), and the Kokchetav Massif in Kazakhstan (Schertl and Sobolev, 2013). Examples formed during continent-oceanic (Pacific-type) plate convergence include the Sanbagawa Belt in Japan (Maruyama, 1997), the metamorphic belt in New Caledonia (Brovarone and Agard, 2013), and the As Sifah Unit in Oman (Massonne et al., 2013). A fundamental question in these terranes is whether the HP and UHP rocks and their quartzofeldspathic host share the same pressure-temperature (*P–T*) path, part of the *P–T* path, or if they record completely separate metamorphic histories. This problem arises because many quartzofeldspathic rocks hosting eclogite lack evidence of eclogite facies metamorphism. This discrepancy led to the controversy of '*in situ* versus exotic' metamorphism concerning the relationship between eclogites and their felsic host (Smith, 1984; 1988; Wang and Liou, 1991; Godard, 2001). Today, there is abundant evidence that many of these eclogite-bearing schists and gneisses have experienced the same HP or UHP metamorphism as the eclogites. Coesite inclusions in garnet from schists in the western Alps (Chopin, 1984) and microdiamonds enclosed in zircon from quartzofeldspathic rocks from the Erzgebirge in central Europe (Massonne, 1999), as well as relics of peak eclogite facies mineral armored in garnet, have provided evidence for the shared metamorphic history of mafic rocks and their quartzofeldspathic host (Wei and Powell, 2004, Stipska et al., 2006; Massonne, 2009; Massonne et al., 2013). Although the '*in situ* vs exotic' is currently less of a problem, the metamorphic evolution of many of these quartzofeldspathic host rocks still remains unexplored.

The Canadian Cordillera preserves multiple HP assemblages formed at Pacific-type convergent margins. In Yukon, Canada, four of these localities preserve evidence of the Late Permian subduction of a back-arc beneath a continental arc outboard of the Laurentian margin (Erdmer et al., 1998). Several studies have been undertaken to characterize the *P–T* evolution of the HP mafic assemblages in these localities (Erdmer et al., 1998; Perchuk et al., 1999; Perchuk et al., 2005; Ghent and Erdmer, 2011; Petrie et al., in preparation b), yet the *P–T* evolution of quartzofeldspathic host rocks at these

localities remains relatively unknown.

The St. Cyr klippe hosts the best preserved and most well exposed eclogite-facies rocks of the four Permian localities. The St. Cyr klippe is a complex imbricate fan that consists of slices of eclogite-bearing quartzofeldspathic schists, low-grade mafic and ultramafic rocks, and medium-grade garnet-mica schists (Petrie et al., in preparation a). In the northwestern portion of the St. Cyr area, the imbricates are cut by flat-lying klippen containing a mafic-ultramafic unit and metabasaltic rocks of the overlying Tower Peak assemblage (Fig. 4-2; Isard, 2014). In the St. Cyr klippe, zircon geochronology shows that eclogite-bearing metatonalites were metamorphosed at eclogite facies conditions facies in the Late Permian, consistent with the age of the eclogite facies metamorphism of the mafic rocks (Petrie et al., in preparation a; b). Both metasedimentary and metatonalite schists preserve peak eclogite-facies mineral assemblages (Petrie et al., in preparation a). These results suggest that the eclogite-bearing quartzofeldspathic schists in the St. Cyr klippe were metamorphosed to *P–T* conditions similar to those of the eclogites.

This chapter presents petrological and mineralogical data, in concert with metamorphic phase equilibrium calculations, to elucidate the *P–T* evolution of eclogite-bearing quartzofeldspathic schists in the St. Cyr klippe. Metamorphic phase equilibrium calculations are presented to determine the peak metamorphic conditions and the retrograde *P–T* path of the quartzofeldspathic schists. I compare these results to the previously determined *P–T* path calculated for the eclogites, in order to establish the shared *P–T* history of mafic and quartzofeldspathic rocks in the St. Cyr klippe, and to link time from U-Pb zircon dating to the *P–T* path.

Geologic Setting

The St. Cyr klippe comprises a 70 km long by 15 km wide, northwest-striking structure, located 14 km northeast of Quiet Lake in south-central Yukon (Fig. 4-1). The

region consists of a series of thrust panels that imbricate amphibolite and eclogite facies rocks derived from the Yukon-Tanana terrane with greenschist facies to serpentinized mafic and ultramafic rocks of the Slide Mountain Ocean terrane (Fig. 4-2; Petrie et al., in preparation b). The Yukon-Tanana and Slide Mountain Ocean terranes represent a Late Devonian to Late Permian arc and back-arc system (Fig. 4-1) built on Laurentian continental crust. The Yukon-Tanana arc rifted from western Laurentia in the Mid- to Late Paleozoic, coeval with the opening of the Slide Mountain Ocean back-arc basin (e.g. Colpron et al., 2006a; Nelson et al., 2013 and references therein). The terrane is composed of a series of volcanic and volcaniclastic assemblages built upon pre-Early Devonian metasedimentary continental basement, the Snowcap assemblage (Fig. 4-1; Mortensen 1992; Colpron et al., 2006a; Piercey et al. 2002; Piercey et al., 2006; Piercey and Colpron, 2009; Piercey et al., 2012). These rocks have been polydeformed and polymetamorphosed to varying degrees, during Paleozoic arc evolution and Early Mesozoic obduction (e.g., Colpron et al., 2006b; Berman et al., 2007; Nelson et al., 2013; Staples et al., 2013). Reconstructing the subduction and exhumation history of HP assemblages is critical for our understanding of the metamorphic and tectonic evolution of the Yukon-Tanana terrane.

Permian age eclogite bodies enclosed within quartzofeldspathic schists are found in at least four localities in the Yukon-Tanana terrane (Erdmer et al., 1998; Petrie et al., in preparation a and b). These HP assemblages are thought to record the subduction of a back-arc basin beneath the Yukon-Tanana arc (e.g. Erdmer; 1987; Creaser et al., 1997; Erdmer et al., 1998). At Ross River (Fig. 4-1), eclogites are hosted by quartzofeldspathic garnet-mica and glaucophane-bearing schists (Erdmer, 1987; Erdmer and Armstrong, 1989; Ghent and Erdmer, 2011). At Faro, eclogite is hosted by phengite-bearing glaucophane-garnet-mica schists (Perchuk et al., 1999; Perchuk and Gerya, 2005). The third eclogite locality, Last Peak, host rocks are hornblende-, biotite-, and phengite-bearing schists (Erdmer and Helmstaedt, 1983; Erdmer et al., 1998). At these three

localities, field relationships between the eclogites and surrounding schists suggest that the eclogite and their host co-existed within the Yukon-Tanana arc prior to subduction and HP metamorphism (Erdmer et al., 1998).

Erdmer et al. (1998) attempted to study the *P–T* paths of eclogites from the HP localities. The Ross River eclogites documented peak metamorphic conditions at 500 °C and 1.6 GPa. Ghent and Erdmer (20l1) used pseudosection models to better constrain the *P–T* path of Ross River eclogite, estimating peak conditions at 550-600 °C and 2.0-2.3 GPa. At Faro, Perchuk et al. (1999) calculated eclogite facies conditions at 660 °C and a minimum of 1.5 GPa.

While evidence supports a primary relationship between eclogites and their host rocks prior to eclogite facies metamorphism, the *P–T* path traveled by the eclogite-bearing quartzofeldspathic rocks in the Yukon-Tanana terrane has not been documented. Only Hansen (1992) addressed the *P–T* conditions in eclogite-bearing garnet-epidote-mica schists and gneisses. Hansen (1992) found that schists in an extensive belt on strike with Last Peak preserve evidence of HP metamorphism at 575-750 °C and 9-17 kbar.

The fourth locality, the St. Cyr klippe, preserves fresh and retrogressed eclogite hosted within metasedimentary and metaigneous schists (Petrie et al., in preparation a). Intercalated on the meter to tens of meter scale, these three rock types were originally derived from the Yukon-Tanana arc (Gilotti et al., 2013; Petrie et al., in preparation a). They form a 30 by 6 km, northwest-striking metamorphic package divided into at least two coherent slices by an imbricate panel of low-grade mafic and ultramafic rocks of the Slide Mountain Ocean terrane (Fig. 4-2). The two slices sit structurally above low grade rocks of the Finlayson assemblage, the oldest volcanic and volcaniclastic unit of the YTT, and structurally beneath two units of amphibolite facies, garnet-mica schist, quartzite, and marble in the hanging wall (Fig. 4-2; Gilotti et al., 2013; Petrie et al., in preparation a) that belong to the Snowcap assemblage, the basement of the Yukon-Tanana arc.

Of the four Permian eclogite-bearing localities in the YTT, the St. Cyr klippe provides the best place to investigate the evolution of subduction and exhumation of Yukon-Tanana arc rocks. Eclogite and their host rocks in the St. Cyr klippe are widely distributed and well preserved. The peak and retrograde *P–T* path is well constrained for the eclogites in the St. Cyr klippe. Petrie et al. (in preparation b) documented peak pressure conditions at 3.2 GPa and 610 °C. Field relationships in the St. Cyr area indicate that the eclogites and quartzofeldspathic rocks were intercalated prior to subduction to eclogite-facies conditions (Petrie et al., in preparation b). Metamorphic zircons in the metatonalites corroborate this interpretation, recording eclogite-facies metamorphism at 266 ± 3 Ma (Petrie et al., in preparation a). This age is within error of the age of eclogite facies metamorphism of mafic rocks in the St. Cyr klippe and consistent with documented ages in the other HP localities (Wanless, 1978; Erdmer and Armstrong, 1989; Creaser et al., 1997; Erdmer et al., 1998; Petrie et al., in preparation a; b). The St. Cyr klippe represents an excellent locality to test whether the host rocks share the same metamorphic history as the Permian age eclogites in the YTT.

Lithology and Petrography

Quartzofeldspathic schists in the St. Cyr klippe consist of metamorphosed felsic intrusives and sedimentary rocks, including meta-quartz-diorites, metatonalites, and metatrondhjemites, mica- and garnet-bearing quartzites, garnet-mica schists, and feldspar-quartz-mica schists (Petrie et al., in preparation a). These rocks are fine-grained S and L-S tectonites, variably retrogressed to amphibolite or greenschist facies. Schistosity is defined by the planar alignment of micas or the grain-shape preferred orientation of quartz grains; quartz and plagioclase stretching lineations are common.

Metaigneous schists consist of quartz, plagioclase, garnet, phengite, ± biotite, ± epidote-clinozoisite. Accessory phases include rutile, apatite, and zircon. Phengite is present as coarse, isolated grains and as very fine-grained crystals within plagioclase.

Garnet forms very small porphyroblasts with inclusions of titanite. Garnets are anhedral and grain boundaries show abundant evidence of resorption. Clinozoisite forms medium to fine-grained, anhedral to subhedral grains within the matrix. Coarse-grained plagioclase exhibits highly embayed boundaries adjacent to quartz, as well as albite or deformation twins. When present as a matrix phase, biotite forms coarse pale reddish-brown to dark greenish-brown grains. Retrograde features include titanite after ilmenite or rutile, biotite after phengite, K-feldspar after phengite, and chlorite after biotite and garnet.

Metasedimentary schists are distinguished from metaigneous schists by a higher modal percent of quartz, garnet, and micas, and the absence of K-feldspar. Coarse-grained phengite occurs as a matrix phase. Garnet generally forms isolated, subhedral to rounded porphyroblasts or aggregates of very fine grains within plagioclase. Garnet contains inclusions of quartz, phengite, and biotite. Plagioclase forms elliptical porphyroclasts with embayed or lobate grain boundaries. Titanite forms medium, euhedral grains within the matrix. Quartz, in plagioclase-rich samples, is also preserved as porphyroclasts, surrounded by a finer-grained quartz + mica matrix. Retrograde chlorite and biotite replace fractures in garnet.

Sample Description

Metatonalite sample 12-23 (UTM Zone 8, 0615803, 6792252; Fig. 4-2) was chosen for pseudosection modeling because of its close proximity to an eclogite lens and the abundance of phengite. Dominated by a quartz- (~ 35%) and plagioclase-rich (~ 40%) matrix, sample 12-23 also contains epidote-clinozoisite (~ 8%) and phengite (~12%); accessory minerals include garnet, apatite, and paragonite (Fig. 4-3). Garnet forms very fine (< 100 μm in diameter), neoblastic grains in the matrix, usually associated with quartz (Fig. 4-3). Garnets generally lack inclusions, except for rare, very fine grains of titanite; at least one garnet hosts a small compositionally distinct garnet

inclusion. Chlorite and epidote replace garnet along cracks and rims. Quartz exhibits lobate boundaries, undulose extinction, and subgrains, indicating dynamic recrystallization between approximately 300 and 500 °C (Stipp et al., 2002). Plagioclase porphyroclasts exhibit deformation twins and lobate grain boundaries. Phengite forms coarse matrix grains or fine to very fine, euhedral, non-pleochroic to very pale green grains within plagioclase (Fig. 4-3b). Clinozoisite forms medium-sized porphyroblasts (Fig. 4-3b) that are highly embayed and replaced by fine-grained, lobate symplectites of epidote + plagioclase (Fig. 4-3c and d). The same epidote is found within plagioclase grains. Biotite replaces phengite.

Mineral Chemistry

Mineral chemistry data was collected from sample 12-23 for use in isochemical phase equilibrium analysis. Selected mineral chemistry data are given in Table 4-1. Mineral compositions were determined using a CAMECA SX-100 electron microprobe at the University of California, Davis, CA. Analytical conditions include 15 kV acceleration voltage, 5-20 nA beam current, and a beam diameter of 1-10 μm. Garnet was mapped at 80 nA and a 5 nm spot size, while phengite was mapped at 50 nA and a 10um spot size. Major element concentrations are shown as weight percent (wt.%) oxides. Mineral abbreviations follow Whitney and Evans (2010).

Garnets are almandine-grossular-spessartine solid solutions in the range $Alm_{27-42}Prp_{1-3}Grs_{31-41}Sps_{23-35}$. Garnets exhibit prograde zoning, including a core to rim decrease in Ca and Mn, and an increase in Mg (Fig. 4-4). The core of the garnet in Fig. 4-4 shows that these garnets have overgrown an earlier, compositionally distinct garnet, which are almandine-grossular-rich solid solutions with $Alm_{55}Prp_{8}Grs_{34}Sps_{3}$ (Table 4-1). Large matrix potassic white mica grains are weakly zoned (Fig. 4-5), ranging from 3.13 to 3.28 Si atoms per formula unit (apfu), with one grain showing Si as high as 3.45 apfu. Phengites within plagioclase lack zoning and range from 3.35 to 3.48 Si apfu. Epidote

within lobate symplectites replacing clinozoisite porphyroblasts contain a pistacite component [$Ca_2Al_2Fe^{3+}Si_3O_{12}(OH)$] between 25-29 mol%. Plagioclase is albite (An_{2-3}).

P–T Evolution

Calculation Method

The *P–T* evolution of the investigated metatonalite was derived from microstructural relationships, mineral chemistry, and phase equilibrium modeling. An isochemical phase diagram (pseudosection) was calculated with the PERPLE_X computer program package (Connolly, 2005; version from November 2013 downloaded from the internet site http://www.perplex.ethz.ch/) for the *P–T* range of 0.5-3.5 GPa and 450-950 °C. The effective bulk rock composition was modified to fit the 10-component system SiO_2-TiO_2-Al_2O_3-MnO-MgO-FeO-CaO-Na_2O-K_2O-H_2O-O_2 (Table 4-2). Bulk rock geochemistry was estimated from major element concentrations obtained by X-ray fluorescence at the GeoAnalytical Laboratory of Washington State University, Pullman, WA, following conventional procedures. The calculations utilized the thermodynamic data set of Holland and Powell (1998, updated 2011). The following solution models were applied: phengite, garnet, epidote-clinozoisite, biotite, cordiorite, and ilmenite after Holland and Powell (1998), feldspar after Fuhrman and Lindsley (1988), chlorite after Holland et al. (1998), and paragonite after Chatterjee and Froese (1975) from solution_model.dat file in PERPLE_X. Rutile, titanite, lawsonite, stipnomelane, and zoisite are assumed to be end-member compositions. CaO was reduced according to the whole-rock phosphorus content, assuming these elements are bound to apatite.

Phase equilibria were calculated using 3 wt.% H_2O to permit the formation of a free hydrous fluid phase. A free hydrous fluid phase forms from the reaction of hydrous minerals to form garnet during prograde metamorphism. Therefore, the derivation of the *P–T* conditions of early garnet composition requires a hydrous fluid phase. The oxygen content was set to a value of 10% of the iron in the rock being trivalent during

metamorphism (e.g. Massonne et al., 2007). Deviations from 10% will modify the *P–T* fields and modal contents of epidote, because it is the only silicate that introduces Fe^{3+} to the PERPLE_X model according to the selected solid-solution models (Massonne et al., 2007).

P–T Pseudosection

The calculated pseudosection for metatonalite sample 12-23 (Fig. 4-6) shows a relatively high number of *P–T* fields for different phase assemblages. A SiO_2 phase (either quartz or coesite) and H_2O are the only phases that appear over the whole calculated *P–T* range. The *P–T* fields of the other existing minerals in the pseudosection are given in Fig. 4-7a. Biotite and Fe oxides are the only phases in which their stability fields are purely pressure dependent (Fig. 4-6 and 4-7a). For example, biotite is stable below ~ 2.1 GPa and 900 °C. Plagioclase is stable over the majority of the calculated *P–T* range, with the exception of a small field at temperatures higher than about 850 °C (Fig. 4-7a). Phengite is unstable at temperatures below approximately 680 °C and pressures below about 1.4 GPa (Fig. 4-7a). Hematite is stable in two ranges, one at conditions between 2.1-2.7 GPa and temperatures in excess of ~ 700 °C and a second at pressures above 1.9 GPa and temperatures below ~ 650 °C.

The *P–T* field of garnet was contoured for molar fraction of pyrope (=X_{Mg}), grossular (=X_{Ca}) and almandine (=X_{Fe}; Fig. 4-7b). In general the contents of grossular decrease and pyrope increase with increasing temperature and decreasing pressure. The content of almandine is temperature dependent at temperatures below about 600 °C and pressure dependent at higher temperatures (Fig. 4-7b), and generally decreases with increasing temperature. The content of spessartine is generally pressure dependent. The isopleths of grossular and pyrope wrap around the lawsonite-in phase boundary (temperatures below ~ 750 °C and pressures above ~ 1.4 GPa), such that they decrease with increasing pressure. At pressures below ~ 1.7 GPa, the volume percent of garnet

increases with increasing pressure, while at higher pressures, garnet content increases with increasing temperature (Fig. 4-7c). The maximum calculated amount of garnet is ~ 4.6 volume percent (vol.%), neglecting the fluid phase.

The calculated amount of potassic white mica is approximately 14 vol.% at peak conditions stable with garnet, coesite, epidote, paragonite, and rutile, which is consistent with the content of phengite observed in the sample (~ 10 %). The calculated Si content of potassic white mica increases with rising pressure (Fig. 4-8b), ranging from 3.08 to 3.85 apfu in this particular pseudosection space. Across the lawsonite-in phase boundary, the content of phengite decreases with increasing pressure and decreasing temperature. Paragonite contents were calculated at ~ 11 vol.%, which does not agree with the minor amount of paragonite observed in the sample (~ 1 %), but can be accounted for by the conversion of paragonite to plagioclase upon decompression. The maximum amount of epidote in the *P–T* range of the calculated pseudosection is about 4 vol.%, which contrasts with the higher (~ 8%) amount of epidote observed. This discrepancy can be accounted for because both content and the maximum *P–T* range for epidote can be influenced by the Fe^{2+}/Fe^{3+} ratio (i.e. O_2 content) for the calculated bulk rock composition.

P–T Path

I use petrography, mineral chemistry, the pseudosection model and the garnet and phengite isopleths shown in Fig. 4-7 to derive the *P–T* path of metatonalite sample 12-23, shown in Fig. 4-8. The sample displays a three-stage metamorphic evolution, labeled from I to III (Fig. 4-8). The prograde evolution prior to Stage I likely passed through amphibolite facies conditions.

Stage I

According to the intersecting isopleths for the Mg, Ca, and Fe content of a small garnet inclusion in a larger porphyroblast (Fig. 4-5; Table 4-1), initial garnet growth

occurred at approximately 1.4 GPa and 615 °C (Stage I, Fig. 4-8). This *P–T* condition occurs within the epidote-phengite-plagioclase-garnet-paragonite-biotite-quartz-rutile field (+ H_2O; Fig. 4-6). The calculated amount of garnet at these conditions is ~ 1.20 vol.%, consistent with the small modal amount of garnet observed in metatonalite sample 12-23, where garnet is a minor phase. The calculated Si content of phengite at the *P–T* conditions of Stage I is approximately 3.34 apfu. This Si content is higher than the majority of measured Si contents in matrix phengite, most of which range 3.13-3.28 Si apfu (Table 4-1). Si = 3.34 apfu agrees well with the measured Si values in very fine-grained phengite found within plagioclase grains (Table 4-1). It is possible that this stage records the initial formation of the fine-grained phengite, after the initial formation of the larger matrix grains.

Stage II

Peak *P–T* conditions are captured by the garnet compositions in the intermediate zone of garnet, approximately 15 μm away from the garnet inclusion (Fig. 4-4). This composition of garnet is taken to be in equilibrium with the highest value of Si from a fine-grained phengite (Si = 3.48 apfu; Table 4-1) and a matrix phengite (Si = 3.45 apfu; Table 4-1) because this intermediate zone represents the initiation of a second stage of garnet growth after the resorption of the first stage, which is represented by the garnet inclusion. The breakdown of the first garnet and the addition of a fluid phase may have been the catalyst driving the growth of the fine-grained phengite with high Si contents. This suggests that the fine-grained phengite formed during peak metamorphism, whereas the majority of the matrix phengite formed at lower *P–T* conditions during prograde evolution. The X_{Ca} and X_{Fe} isopleths from the intermediate zone of the garnet intersect with the maximum phengite Si values within the coesite stability field, at approximately 3.2 GPa and 900 °C (Fig. 4-7b, c, and 4-8; Table 4-1).

According to pseudosection, peak *P–T* conditions lie within the epidote-phengite-

plagioclase-garnet-paragonite-coesite-rutile stability field (+ H_2O; Fig. 4-6). Relict epidote-clinozoisite porphyroblasts attest to its stability at HP and UHP conditions. The maximum calculated amount of garnet in sample 12-23 (~ 5 vol.%) is consistent with the predicted amount of garnet in equilibrium with phengite given the bulk composition of the rock and the stability of clinozoisite; however, garnet must have been resorbed during exhumation.

Stage III

The exhumation path is not well preserved in sample 12-23; however, a retrograde path similar to what is shown in Fig. 4-8 is plausible in that it explains the preserved mineral assemblage and the composition of garnet rims. Using the isopleths for X_{Mg} and X_{Fe} of the garnet rim (Table 4-1) and the calculated garnet modal content of 0.30 vol.%, which is approximately the observed modal content of garnet (< 1%), the exhumation path intersects the broad region shown in Fig. 4-8 (Stage III). This intersection occurs between about 0.5-1.1 GPa and 450-550 °C, assuming that the garnet rim is in equilibrium with the retrograde assemblage. These *P–T* conditions are consistent with the observed retrograde mineral assemblage, in which biotite and titanite are stable, and garnet is replaced by epidote and chlorite.

Discussion

P–T Evolution of St. Cyr Eclogite-Bearing Metatonalites

P–T conditions were deduced from the varying compositions of phengite and garnet, in conjunction with stable mineral assemblages and the calculated pseudosection model. The results show that metamorphic evolution of an eclogite-bearing metatonalite sample from the St. Cyr klippe followed a three stage, clockwise *P–T* path. According to the calculated pseudosection and garnet and matrix phengite compositions, phengite was already stable when garnet began to grow at approximately 1.4 GPa and 615 °C (Fig. 4-

7a, 4-8; Stage I). The prograde path up to this stage is obscured by subsequent metamorphism, but must have passed through amphibolite facies conditions.

Pseudosection calculations show that peak UHP conditions were reached at about 3.2 GPa and 900 °C (Fig. 4-6 and 4-8). Maximum values of Si in phengite, measured in both matrix and fine-grained phengite, ranged from 3.45 to 3.48 apfu. These values intersected the Ca and Fe compositions of the intermediate zone of garnet grains within the coesite stability field of epidote-phengite-plagioclase-garnet-paragonite-coesite-rutile. We use the intermediate zone of garnet, as opposed to the core composition, because it is presumed that after the growth of the inclusion, crystallization of the new garnet composition occurred during prograde metamorphism, just prior to peak conditions. This interpretation is supported by the calculated modal volume of garnet (Fig. 4-7c), which shows that the majority of garnet growth occurred at pressures below ~ 2 GPa, and is compatible with isopleths of the core composition.

The calculated pseudosection predicts that rutile is present over the majority of the modeled *P–T* range (Fig. 4-6). However, the maximum calculated modal amount of rutile is 0.14 vol. %, which may explain the absence of rutile in sample 12-23. The model also shows that epidote-group minerals remained stable throughout the majority of garnet growth, and was most likely the factor that retarded the amount of garnet that could have formed during prograde metamorphism.

UHP conditions result even under the assumption of an error in the pressure determination of ± 0.2 GPa (Massonne et al., 2013). According to the calculated pseudosection, burial to UHP conditions of the rocks in the St. Cyr klippe occurred along a very low geotherm (5 °C/km; Fig. 4-8). These conditions are similar to the *P–T* conditions expected if burial occurred within a subduction zone (e.g., Wei and Powell, 2004; Ghent et al., 2009; Ghent and Erdmer, 2011; Massonne and Toulkeridis, 2012; Faryad et al., 2013; Massonne et al., 2013).

The exact exhumation path is not directly known, nevertheless, petrological and chemical evidence suggest a retrograde evolution similar to that shown on Fig. 4-8. This path is compatible with the composition of garnet rims and the preserved mineral assemblage. The majority of garnet is replaced by chlorite and epidote, yet a few have preserved their rims and these rims appear to be in equilibrium with the retrograde assemblage. The preservation of matrix and very fine-grained phengite suggests that the exhumation path never crossed into the phengite-out stability field. At peak metamorphic conditions, paragonite has a calculated modal content of 6 vol.%. Because there are trace amounts left in the sample, it is most likely that the retrograde path intersected that of the paragonite-out *P–T* field. Furthermore, two separate epidote-group minerals are present in sample 12-23, clinozoisite porphyroblasts and symplectitic epidote (Fig. 4-3c and d). Clinozoisite grains are highly embayed, suggesting that at some point along the retrograde path the sample passed through the epidote-clinozoisite-out phase boundary. During continued exhumation, the path may have once again crossed into the epidote stability field, causing the formation of the symplectite-epidote. This is supported by the propensity of symplectitic epidote to replace clinozoisite (Fig. 4-3).

Evolution of UHP Metamorphism in the St. Cyr Klippe

The derived *P–T* path for the metatonalite shows that eclogite-bearing quartzofeldspathic host rocks in the St. Cyr klippe reached peak UHP conditions at 3.2 GPa (Fig. 4-8). Petrie et al. (in preparation a and b) showed structural, metamorphic, and geochronological evidence that indicates the *in situ* metamorphism of eclogite and their host in the St. Cyr klippe. Petrie et al. (in preparation b) also showed that the eclogites reached peak UHP metamorphic conditions at 3.2 GPa. According to the calculated pseudosection, garnet growth in the metatonalites began at approximately 1.4 GPa, which coincides with the initial phase of garnet growth within the eclogites (Petrie et al., in preparation b). Thus our study confirms the previously determined metamorphic

pressures derived for the eclogites, and suggests that the two units were metamorphosed together at the same pressures, at least along the prograde path.

While peak pressures achieved by the eclogite and their host support their shared metamorphic history, predicted temperatures are conflicting. First, the temperature of initial garnet growth is 615 °C, as apposed to 500 °C for garnet in the eclogites (Petrie et al., in preparation b). Second, the eclogites followed a clockwise *P–T* path, that reached peak pressure conditions at 610 °C (Petrie et al., in preparation b). According to the calculated pseudosection for the metatonalite, the peak temperature was 900 °C. This temperature is not only 160 °C higher than the maximum temperature recorded by the eclogites, it is also not geologically reasonable given the accretionary tectonic setting. Numerical modeling and natural examples have shown that under normal Pacific-type subduction zone geothermal gradients, < 10 °C/km, the majority of HP and UHP assemblages will reach peak temperatures between 400-700 °C (Peacock 1987; 1990; Gerya and Stockhert, 2006). Higher temperature UHP assemblages, those that experience 700-900°C, are only known to form at Alpine-type convergent margins, where they can spend longer residence times at mantle conditions (Li and Gerya, 2009). At 3.2 GPa and a 5 °C/km geotherm, as derived for the eclogites (Petrie et al., in preparation b), peak temperatures predicted in the host rocks in the St. Cyr klippe are predicted to be between 550-650 °C.

If the host rocks and the eclogites share the same *P–T* history, the temperature recorded by the eclogites at peak pressure conditions of 610 °C is more likely to be the same temperature the experienced by the metatonalite host. If the metatonalite did experience peak pressure conditions at 610 °C, the sample would have crossed into the lawsonite stability field (Fig. 4-6), yet no lawsonite is present in the sample. In general, lawsonite is stable at very low temperatures and high pressures, but according to the pseudosection (Fig. 4-6), it is stable at temperatures in excess of 700 °C in the metatonalitic bulk composition. Lawsonite converts to clinozoisite between 400-500 °C

(Whitney and Davis, 2006) and, following the *P–T* path derived for the eclogite (Petrie et al., in preparation b), the sample would cross into the stability field of lawsonite above 550 °C (Fig. 4-8), making it unlikely that lawsonite would form. Upon exhumation, the sample would pass back through the epidote-clinozoisite stability field, removing any lawsonite that may have formed at peak pressure. Because the eclogite and host metatonalite share peak pressure conditions and a prograde path, a peak temperature of 610 °C for the metatonalite sample is much more plausible than a peak temperature of 900 °C.

Finally, although the exhumation path for the eclogites is established, the path from the peak conditions of Stage II to the retrograde conditions of Stage III (Fig. 4-8) cannot be derived for the studied metatonalite using the calculated model. However, the petrologic evolution of sample 12-23 is consistent with the *P–T* path derived from the eclogites, in which the rocks experience an increase in temperature to 740 °C along a clockwise exhumation path (Fig. 4-8). Following this path, the sample crosses multiple stability fields, and still preserves phengite, two phases of epidote, and paragonite.

Conclusions

An eclogite-bearing metatonalite from the St. Cyr klippe in the Yukon-Tanana terrane, Yukon, Canada, was investigated in an effort to document the metamorphic evolution of host rocks and to determine if they share the same metamorphic history as the eclogites. Using the bulk-rock composition of the metatonalite, a *P–T* pseudosection was constructed and contoured for molar fractions of garnet and the Si content in phengite. The resulting model predicts that the metatonalite was metamorphosed at ultrahigh-pressure conditions along a three-stage, clockwise path. Garnet began to form at 1.4 GPa and 615 °C. Peak conditions were reached at 3.2 GPa and 900 °C, although this temperature is unrealistic given the tectonic setting. The results of the model do not allow for the derivation of the exact exhumation path, however, garnet rim compositions,

the presence of titanite, and the garnet to chlorite reaction show that cooling occurred at relatively high *P–T* conditions, in excess of 0.5 GPa between 450-550 °C. The *P–T* path reflects metamorphism within a subduction zone, with burial occurring along a very low geothermal gradient ~ 5 °C/km. The *P–T* path predicted by the calculated pseudosection for the metatonalite suggests that the eclogites and their quartzofeldspathic host share a HP and UHP metamorphic history, but in detail, the paths are not the same. This discrepancy is probably an artifact of the modeling and the lack of preservation of the UHP relicts.

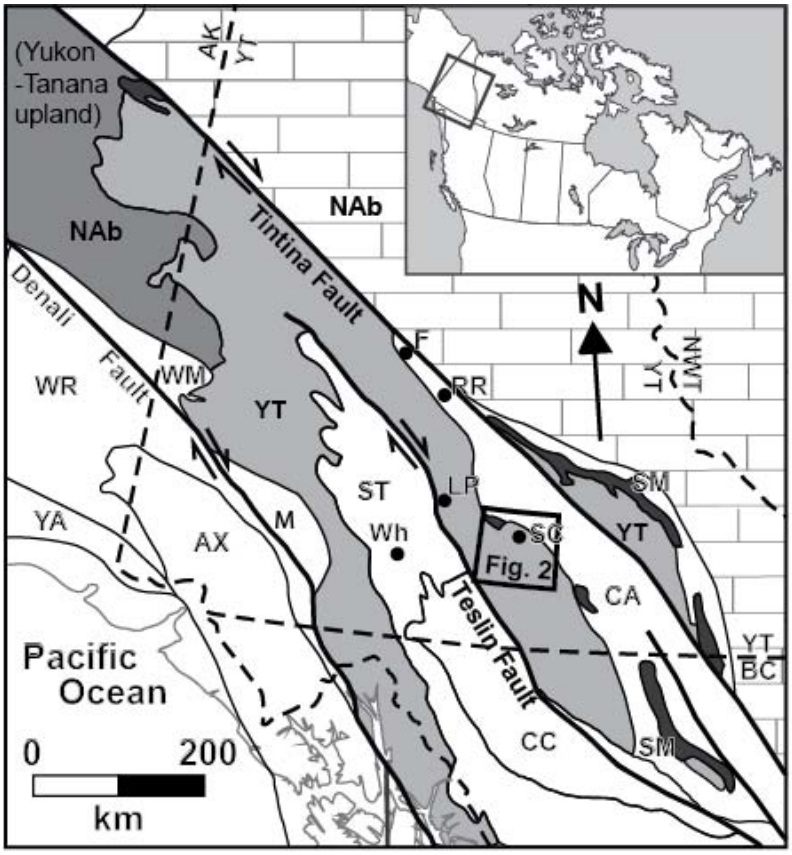

Figure 4-1 Terrane map of the northern Canadian Cordillera. Black box shows the study area (Fig. 3-2; modified from Colpron et al., 2006 and Nelson et al., 2013). F, Faro; LP, Last Peak; RR, Ross River; ST, St. Cyr; Wh, Whitehorse. Terrane abbreviations: AX, Alexander; CA, Cassier; CC, Cache Creek; NAb, North American platform; SM, Slide Mountain; ST, Stikinia; YA, Yukuta; YT, Yukon-Tanana; WM, Windy-McKinley; WR, Wrangellia; M, undivided metamorphic and plutonic rocks.

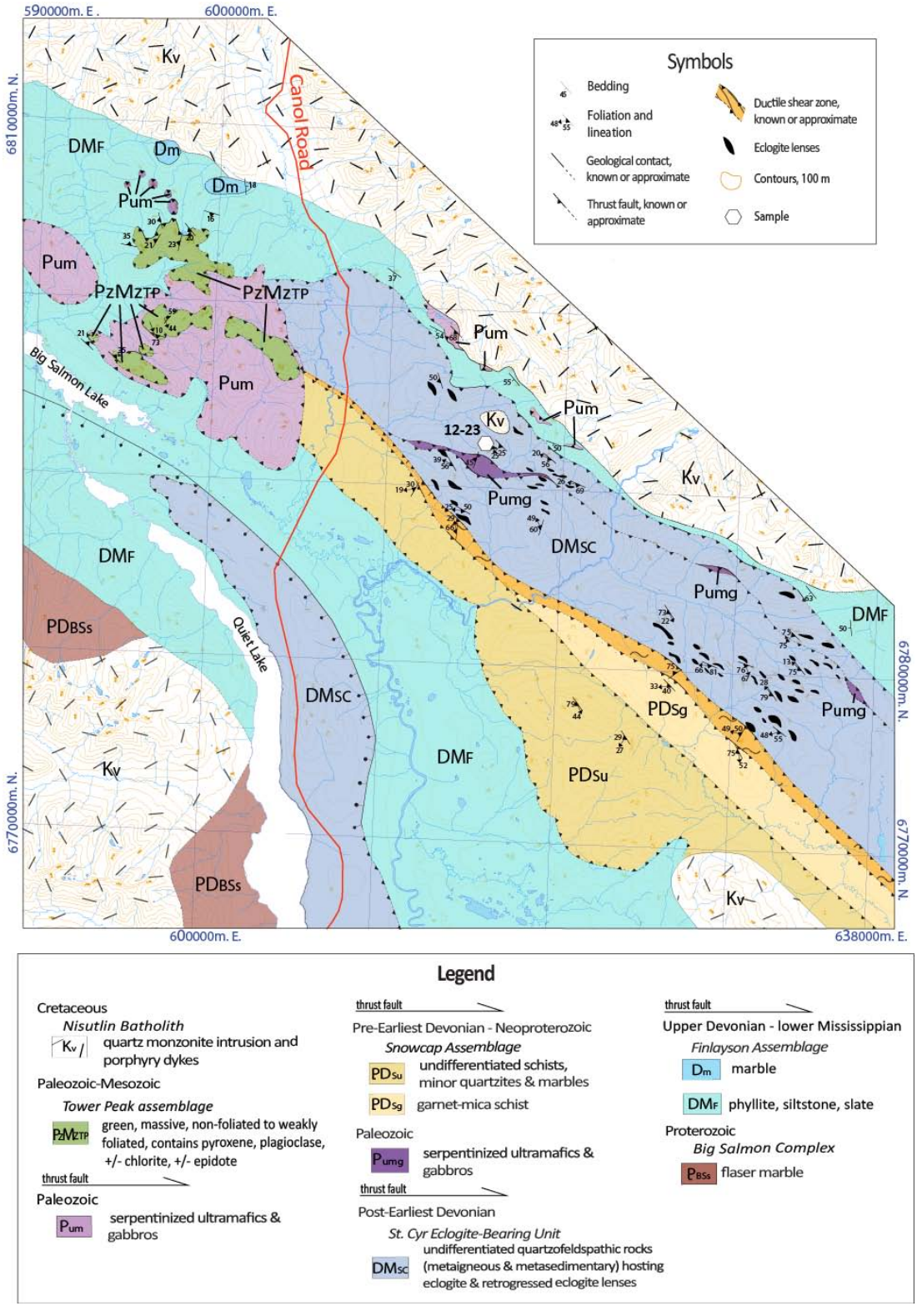

Figure 4-2 Geologic map of the St. Cyr klippe and surrounding region. Modified from Tempelman-Kluit (2012) and Colpron (2006). Based on mapping Isard (2014), this study. The hexagon represents metatonalite sample 12-23 used in this study.

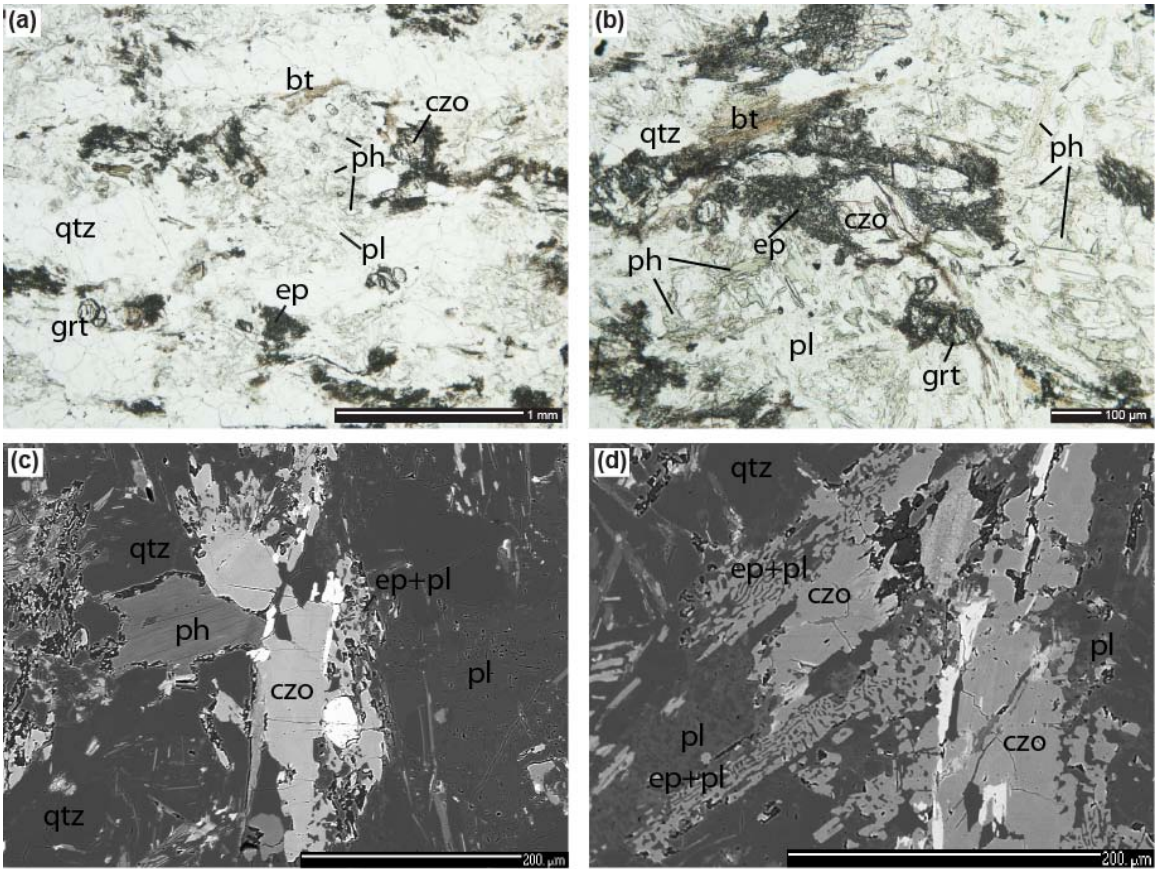

Figure 4-3 Optical photomicrographs and backscattered electron images of metatonalite sample 12-23. (a) Optical photomicrograph (plane polarized light) of plagioclase with inclusions of fine blades of phengite, small garnets, quartz, and lobate symplectites of epidote + plagioclase. (b) Optical photomicrograph (plane polarized light) of clinozoisite porphyroblast replaced by lobate symplectites of epidote + plagioclase and pale green phengite within plagioclase. (c) Backscattered electron image of a matrix phengite grain and clinozoisite grains converting to epidote + plagioclase. (c) Backscattered electron image of a matrix clinozoisite grains converting to lobate symplectites of of epidote + plagioclase symplectites.

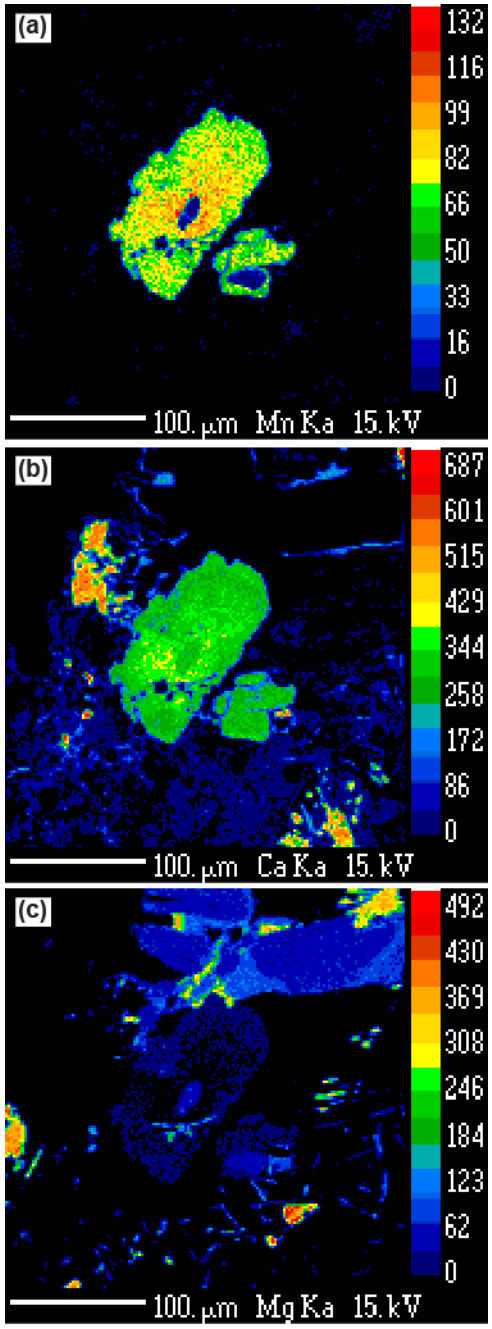

Figure 4-4 Garnet X-ray maps from sample 12-23. (a), (b), and (c) are Mn, Ca, and Mg maps, respectively. Warm colors represent higher elemental concentrations and cool colors, lower concentrations. The older garnet inclusion is visible as is dark blue (a), dark green (b), or bright blue (c) oval in the center of the larger host grain.

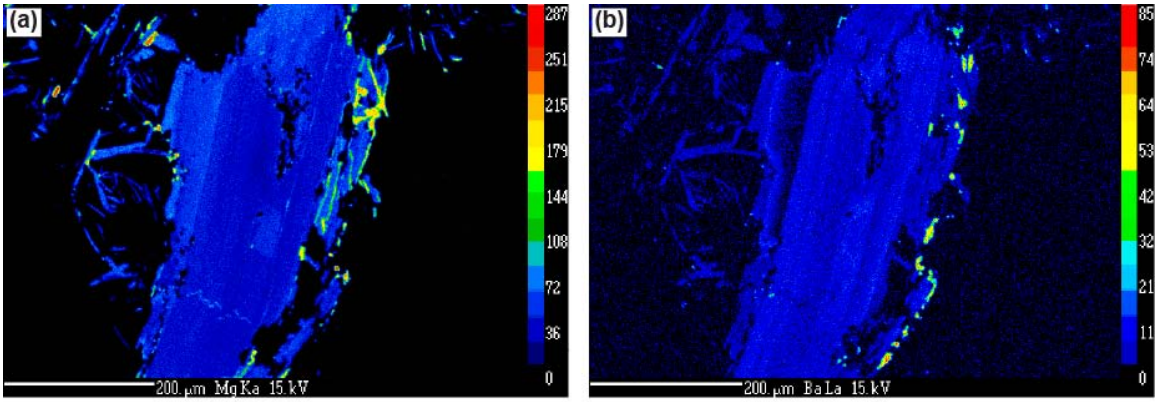

Figure 4-5 X-ray maps of phengite from sample 12-23. The maps show weak to moderate zoning on the edges of phengite grains. Mg (a) and Ba (b). High Mg corresponds with high Si due to the celadonite solid solution. Warm colors represent higher elemental concentrations and cool colors, lower concentration.

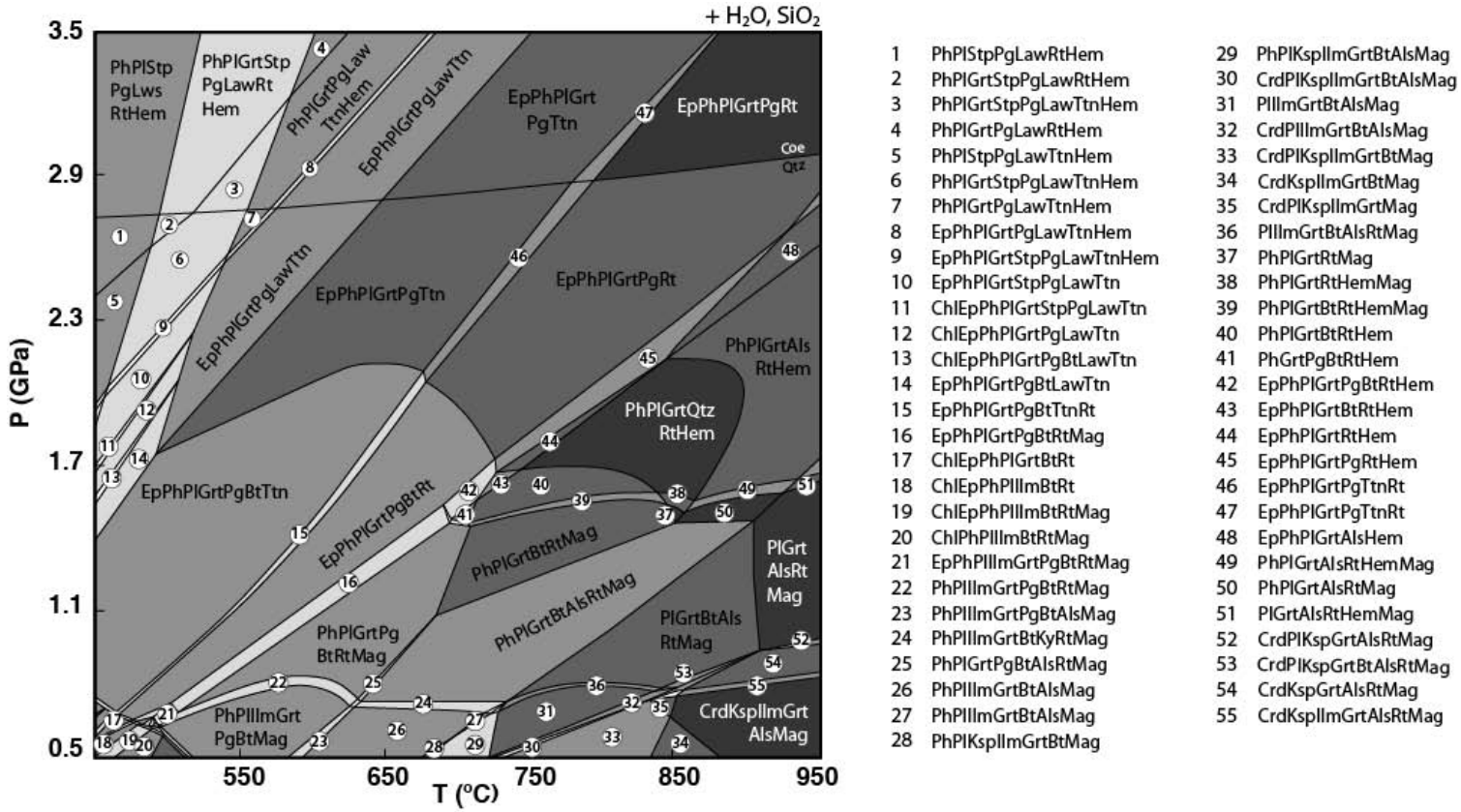

1	PhPlStpPgLawRtHem	29	PhPlKspIlmGrtBtAlsMag
2	PhPlGrtStpPgLawRtHem	30	CrdPlKspIlmGrtBtAlsMag
3	PhPlGrtStpPgLawTtnHem	31	PlIlmGrtBtAlsMag
4	PhPlGrtPgLawRtHem	32	CrdPlIlmGrtBtAlsMag
5	PhPlStpPgLawTtnHem	33	CrdPlKspIlmGrtBtMag
6	PhPlGrtStpPgLawTtnHem	34	CrdKspIlmGrtBtMag
7	PhPlGrtPgLawTtnHem	35	CrdPlKspIlmGrtMag
8	EpPhPlGrtPgLawTtnHem	36	PlIlmGrtBtAlsRtMag
9	EpPhPlGrtStpPgLawTtnHem	37	PhPlGrtRtMag
10	EpPhPlGrtStpPgLawTtn	38	PhPlGrtRtHemMag
11	ChlEpPhPlGrtStpPgLawTtn	39	PhPlGrtBtRtHemMag
12	ChlEpPhPlGrtPgLawTtn	40	PhPlGrtBtRtHem
13	ChlEpPhPlGrtPgBtLawTtn	41	PhGrtPgBtRtHem
14	EpPhPlGrtPgBtLawTtn	42	EpPhPlGrtPgBtRtHem
15	EpPhPlGrtPgBtTtnRt	43	EpPhPlGrtBtRtHem
16	EpPhPlGrtPgBtRtMag	44	EpPhPlGrtRtHem
17	ChlEpPhPlGrtBtRt	45	EpPhPlGrtPgRtHem
18	ChlEpPhPlIlmBtRt	46	EpPhPlGrtPgTtnRt
19	ChlEpPhPlIlmBtRtMag	47	EpPhPlGrtPgTtnRt
20	ChlPhPlIlmBtRtMag	48	EpPhPlGrtAlsHem
21	EpPhPlIlmGrtPgBtRtMag	49	PhPlGrtAlsRtHemMag
22	PhPlIlmGrtPgBtRtMag	50	PhPlGrtAlsRtMag
23	PhPlIlmGrtPgBtAlsMag	51	PlGrtAlsRtHemMag
24	PhPlIlmGrtBtKyRtMag	52	CrdPlKspGrtAlsRtMag
25	PhPlGrtPgBtAlsRtMag	53	CrdPlKspGrtBtAlsRtMag
26	PhPlIlmGrtBtAlsMag	54	CrdKspGrtAlsRtMag
27	PhPlIlmGrtBtAlsMag	55	CrdKspIlmGrtAlsRtMag
28	PhPlKspIlmGrtBtMag		

Figure 4-6 *P–T* pseudosection calculated for the modified composition of metatonalite sample 12-23. Computer software package PERPLE_X was used for the calculation (see text). Mineral abbreviations follow Whitney and Evans (2010). Bulk composition used in the pseudosection is given in Table 4-2. The gray tones are related to the variance (the brighter the lower) of the corresponding mineral assemblage (+ H_2O). Very small *P–T* fields are not labeled. The bulk rock composition used in this pseudosection is given in Table 4-2.

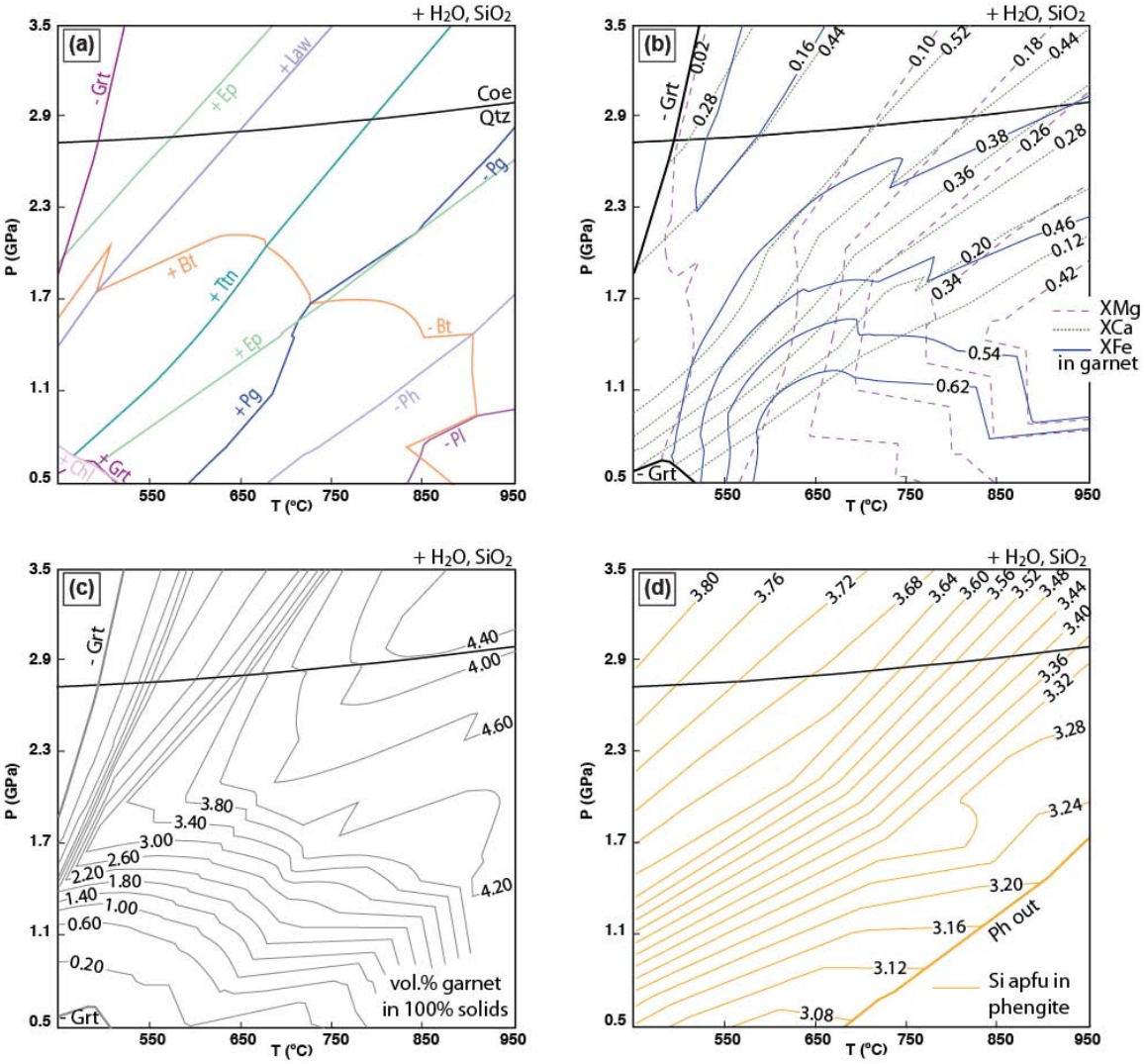

Figure 4-7 Contour diagrams used for interpreting the *P–T* path of eclogite sample 12-23. (a) Boundaries of the *P–T* fields of relevant phases are shown by the various lines taken from Fig. 4-6. Abbreviations as in Fig. 4-6. Contouring of the *P–T* pseudosection of Fig. 4-6 was undertaken by isopleths for the molar fraction of Mg, Ca, and Fe in garnet (b), the modal content in garnet (c), and the Si apfu content in phengite (d).

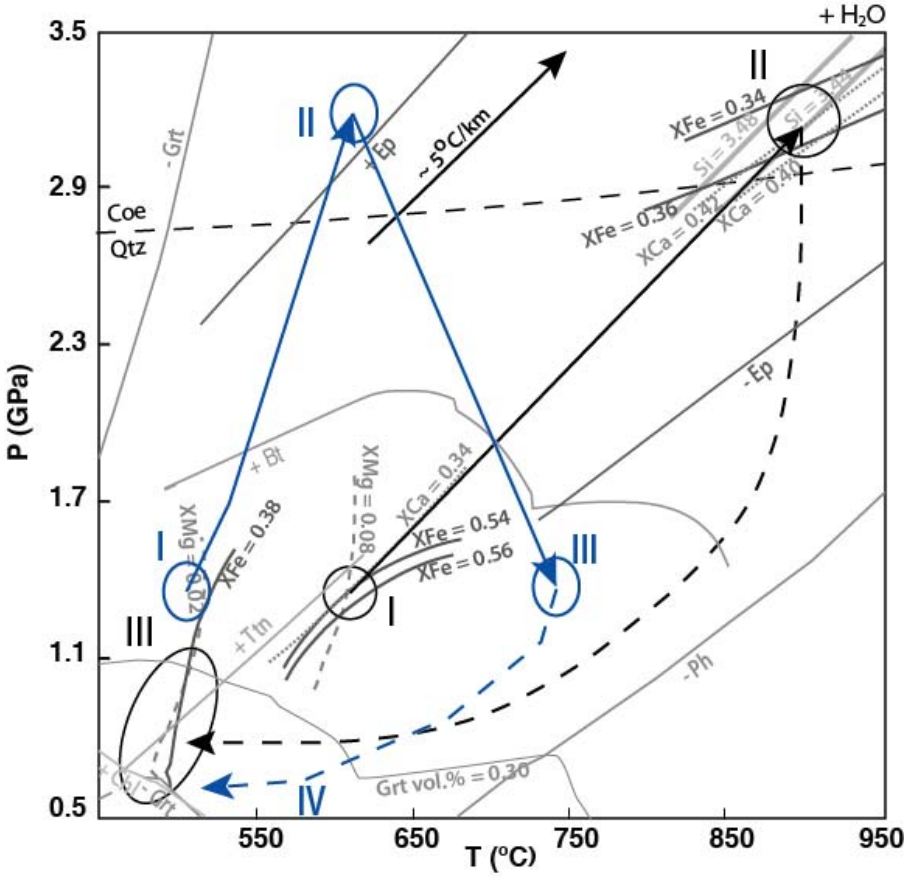

Figure 4-8 *P–T* path for metatonalite sample 12-23. Path (shown by the black arrows) derived from the various garnet and Si-in-phengite isopleths displayed in Fig. 4-7. The dotted lines indicate where the *P–T* path is uncertain. Circles mark the beginning of garnet growth, peak *P–T* conditions, and the evolution of the retrograde path. Eclogite path (blue) modified after Petrie et al. (in preparation b).

Table 4-1 Representative mineral composition from metatonalite sample 12-23

Mineral	Grt	Grt	Grt	Ph	Ph	Ph	Ph
Mineral Analysis	Grt Incl.	inter-mediate	rim	matrix	within Pl	matrix	within Pl
Analysis #	5/8	5/11	5/4	1/8	8/1	4/1	11/1
SiO_2	38.172	38.332	38.212	51.304	52.889	47.435	50.952
TiO_2	0.077	0.076	0.144	0.612	0.099	0.129	0.145
Al_2O_3	21.506	21.326	21.277	27.675	26.894	33.053	27.231
FeO	15.962	12.672	16.932	1.280	2.224	1.807	2.458
MnO	11.537	15.466	10.289	0.015	0.008	0.038	0.069
MgO	0.501	0.312	0.604	1.135	2.356	2.250	2.526
CaO	12.635	12.443	12.748	0.032	0.112	0.000	0.471
Na_2O				0.334	3.257	0.208	2.516
K_2O				11.065	7.421	10.773	8.329
BaO				2.373	0.665	1.057	0.643
Wt % total	100.390	100.627	100.206	95.825	95.925	94.960	95.340
Oxygen	12	12	12	11	11	11	11
Si	3.024	3.036	3.032	3.450	3.481	3.207	3.404
Ti	0.005	0.005	0.009	0.031	0.005	0.007	0.007
Al	2.008	1.990	1.990	2.193	2.086	2.491	2.144
Fe^{2+}	1.057	0.839	1.123	0.072	0.122	0.102	0.137
Mn	0.774	1.037	0.691	0.001	0.000	0.002	0.004
Mg	0.059	0.037	0.071	0.114	0.231	0.227	0.252
Ca	1.072	1.056	1.084	0.002	0.008	0.000	0.034
Na				0.044	0.416	0.027	0.326
K				0.949	0.623	0.929	0.710
Ba				0.063	0.017	0.028	0.017
X_{Alm}	35.69	28.26	37.83				
X_{Sps}	26.12	34.94	23.28				
X_{Prp}	2.00	1.24	2.41				
X_{Grs}	36.19	35.56	36.49				

Table 4-2 Whole-rock geochemical data for eclogite sample 12-23

	12-23	modified for pseudosection
SiO_2 (wt. %)	73.45	72.902
TiO_2	0.21	0.204
Al_2O_3	14.26	14.154
FeO*	1.58	1.568
MnO	0.05	0.047
MgO	0.76	0.754
CaO	1.80	1.686
Na_2O	4.32	4.288
K_2O	1.39	1.380
O_2		0.017
H_2O		3.00
P_2O_5	0.08	
Total	97.89	100.00

* Fe reported as total Fe

For O_2 and H_2O, see text.

The modified composition (see text) was used for PERPLE_X calculations.

CHAPTER 5.

CONCLUSIONS

High-pressure (HP) and ultrahigh-pressure (UHP) metamorphic rocks record subduction zone processes and are important for understanding the geodynamics of collisional orogenesis. HP and UHP rocks are found in a variety of geological settings including as blocks within tectonic mélange, ductilely deformed thin nappes, and coherent slices of continental crust. The Yukon-Tanana terrane (YTT), a major allochthonous component of the Canadian Cordillera in Yukon and Alaska, preserves multiple localities of eclogite-facies assemblages. Some localities preserve Mid-Mississippian retrogressed eclogite that occur within tectonic mélanges. Other localities preserve Permian age eclogites in contact with metasedimentary and metaigneous quartzofeldspathic host rocks. One such locality, the St. Cyr klippe, was previously characterized as a tectonic mélange hosting eclogite blocks. This association led early workers to assume that the eclogites were part of the Slide Mountain Ocean assemblage. However, the host quartzofeldspathic schists share lithological and metamorphic relationships with the YTT, not the Slide Mountain Ocean assemblage. Thus, the eclogites and their host rocks in the St. Cyr klippe comprise a crustal component of the Yukon-Tanana arc.

The purpose of this study was to test the hypothesis that the eclogites and their quartzofeldspathic host rocks in the St. Cyr klippe are a fragment of Yukon-Tanana crust subducted to eclogite-facies conditions. Field mapping was used to determine if the eclogites were part of a tectonic mélange or are coherent slices of hanging wall Yukon-Tanana arc crust. U-Pb zircon geochronology was used to determine the protolith and metamorphic ages of the eclogites and quartzofeldspathic host rocks. Phase equilibrium modeling was used to reconstruct the pressure-temperature (*P–T*) evolution of eclogites and host rocks in the St. Cyr klippe to establish the metamorphic and geochronologic evolution eclogite-facies assemblages in the YTT.

The St. Cyr klippe is composed of variably metamorphosed and deformed, units of Yukon-Tanana continental arc crust structurally imbricated with slices of mafic and ultramafic units. Sub-meter to hundreds of meter scale lenses of well-preserved eclogite and retrogressed eclogite are hosted within quartzofeldspathic schists derived from the YTT. SHRIMP-RG zircon dating shows that the mafic protolith of the eclogites formed ca. 364 and 380 Ma, while the protolith of the metatonalites were intruded at ca. 333-334 Ma. The eclogites formed during early, continental arc activity, and the metatonalites formed during the Little Salmon Cycle of the Klinkit phase of Yukon-Tanana arc activity. Trace element signatures of metamorphic zircon in both the eclogites and metatonalites indicate their formation during eclogite facies conditions ca. 266-271 Ma. Phase equilibrium modeling shows that the eclogite and metatonalites reached peak pressure condition of 3.2 GPa, consistent with UHP metamorphism. Comparison of pseudosection models and petrography of the samples support the shared metamorphic history of the eclogites and their quartzofeldspathic host. Pseudosection results suggest that the St. Cyr eclogite-bearing unit underwent UHP metamorphism in a subduction zone with a low thermal gradient 5 °C/km.

The results of this study define four events in the history of the YTT. Beginning in the Mid- to Late Devonian, east-directed subduction of Panthalassa initiated beneath the western North American margin (Fig. 5-1a; Devine et al., 2006; Berman et al., 2007). This coincides with the formation of the protolith to the eclogites as a mafic pluton formed in a continental arc setting. During the Latest Devonian-Early Mississippian, slab rollback of Panthalassa oceanic crust initiated the opening of a back-arc or back-arcs (Fig. 5-1b; Devine et al., 2006; Berman et al., 2007). The YTT was rifted from the western margin of North America, coincident with the formation of the Finlayson arc assemblage (Colpron et al., 2006a; Piercey et al., 2006). During the Early Mississippian, continued subduction, and slab rollback off the western margin of the Yukon-Tanana arc coincided with continued spreading in the back-arc, the formation of the Klinkit arc

assemblage, and the formation of Mississippian HP rocks (Fig. 5-1c; Devine et al., 2006; Piercey et al., 2006; Berman et al., 2007). At this time, tonalites were intruded into the arc and form a metaigneous component in the St. Cyr klippe. By the Mid-Permian, east-directed subduction of Panthalassa had ceased, and continued east-directed convergence initiated westward subduction of the back-arc beneath the Yukon-Tanana arc (Fi. 5-1d; Devine et al., 2006; Berman et al., 2007). During the Mid- to Late Permian, portions of the Yukon-Tanana arc were entrained into the subduction zone, carried to mantle conditions (Fig. 5-1), and exhumed. Structural imbrication likely occurred during exhumation from the subduction channel, as well as during thrusting of the YTT back onto North America in the Mesozoic, creating the complex imbricate stack that is the St. Cyr klippe.

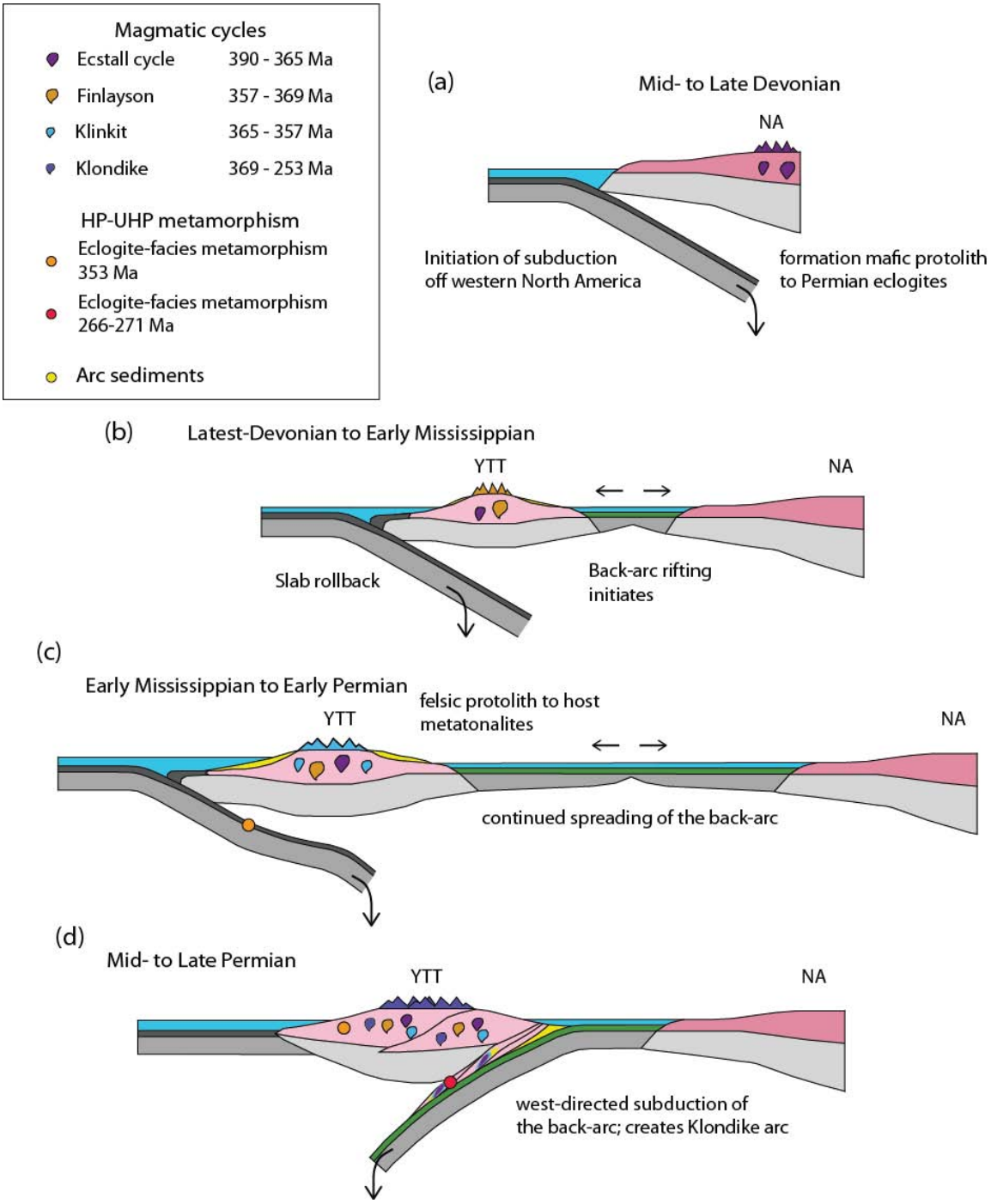

Figure 5-1 Tectonic cartoon for the Devonian to Late Permian evolution of the eclogite-facies assemblages in the St. Cyr klippe, YTT. Modified after Devine et al. (2006) and Berman et al. (2007).

REFERENCES

Aalto, K.R., 1981. Multistage melange formation in the Franciscan Complex, northernmost California; Geology, v. 9, p. 602-607.

Aalto, K.R., 2014. Examples of Franciscan Complex mélanges in the northernmost California Coast Ranges, a retrospective; International Geology Review, v. 56, p. 555-570.

Agard, P., Yamato, P., Jolivet, L., and Burov, E., 2009. Exhumation of oceanic blueschists and eclogites in subduction zones; Timing and mechanisms; Earth-Science Reviews, v. 92, p. 53-79.

Alldrick, D.J., 2001. Geology and mineral deposits of the Ecstall greenstone belt, northwest British Columbia (NTS 103H/103I); Geological Fieldwork 2000: B.C. Ministry of Energy and Mines, Paper 2001-1, 279-305.

Alldrick, D.J. and Gallagher, C.S., 2000. Geology and mineral potential of the Ecstall VMS Belt (NTS 103H, 103I); Geologic Fieldwork 1999: B.C. Ministry of Energy and Mines, Paper 2001-1, 249-265.

Anders, E., and Grevesse, N., 1989. Abundances of the elements: meteoritic and solar; Geochimica Et Cosmochimica Acta, v. 53, p. 197-214.

Andersen, T.B., Jamtveit, B., Dewey, J.F., and Svensson, E., 1991. Subduction and eduction of continental crust: major mechanisms during continent-continent collision and orogenic extensional collapse, a model based on the south Norwegian Caledonides; Terra Nova, v. 3, p. 303-310.

Anderson, E.D., and Moecher, D.P., 2009. Formation of high-pressure metabasites in the southern Appalachian Blue Ridge via Taconic continental subduction beneath the Laurentian margin; Tectonics, v. 28.

Armbruster, T., Bonazzi, P., Akasaka, M., Bermanec, V., Chopin, C., Giere, R., Heuss-Assbichler, S., Liebscher, A., Menchetti, S., Pan, Y., and Pasero, M., 2006. Recommended nomenclature of epidote-group minerals; European Journal of Mineralogy, v. 18, p. 551-567.

Barth, A.P., and Wooden, J.L., 2006. Timing of magmatism following initial convergence at a passive margin, southwestern US Cordillera, and ages of lower crustal magma sources; Journal of Geology, v. 114, p. 231-245.

Barth, A.P. and Wooden, J.L., 2010. Coupled elemental and isotopic analyses of polygenetic zircons from granitic rocks by ion microprobe, with implications for melt evolution and the sources of granitic magmas; Chemical Geology, v. 277, p. 149-159.

Baxter, E.F. and Caddick, M.J., 2013. Garnet growth as a proxy for progressive subduction zone dehydration; Geology, v. 41, 643-646.

Beltrando, M., Compagnoni, R., and Lombardo, B., 2010. (Ultra-) High-pressure metamorphism and orogenesis; An Alpine perspective: Gondwana Research, v. 18, p. 147-166.

Berman, R.G., Ryan, J.J., Gordey, S.P., and Villeneuve, M., 2007. Permian to Cretaceous polymetamorphic evolution of the Stewart River region, Yukon-Tanana terrane, Yukon, Canada: P-T evolution linked with in situ SHRIMP monazite geochronology; Journal of Metamorphic Geology, v. 25, p. 803-827.

Black, L.P., Kamo, S. L., Allen, C.M., Davis, D.W., Aleinikoff, J.N., Valley, J.W., Mundil, R., Campbell, I.H., Korsch, R.J., Williams, I.S., and Foudoulis, C., 2004. Improved $^{206}Pb/^{238}U$ microprobe geochronology by the monitoring of a trace-element-related matrix effect; SHRIMP, ID-TIMS, ELA-ICP-MS and oxygen isotope documentation for a series of zircon standards; Chemical Geology, v. 205, p. 115-140.

Blake, M.C., and Jones, D.L., 1974. Origin of Franciscan melanges in northern California; in: Modern and ancient geosynclinal sedimentation, (ed.) Dott, R.H., and Shaver, R.H.; Society of Economic Paleontologists and Mineralogists Special Publication 19, p. 345-357.

Boyer, S.E., and Elliott, D., 1982. Thrust Systems; AAPG Bulletin-American Association of Petroleum Geologists, v. 66, p. 1196-1230.

Brown, E.H. and Forbes, R.B., 1986. Phase petrology of eclogitic rocks in the Fairbanks district, Alaska; in: Blueschists and eclogites (eds Evans, B. W. and Brown, E. H.), Geological Society of America Memoir, v. 164, 155-168.

Brovarone, A.V., and Agard, P., 2013. True metamorphic isograds or tectonically sliced metamorphic sequence? New high-spatial resolution petrological data for the New Caledonia case study; Contributions to Mineralogy and Petrology 166, 451-469.

Butler, J.P., Jamieson, R.A, Steenkamp, H.M, and Robinson, P., 2013. Discovery of coesite-eclogite from the Nordoyane UHP domain, Western Gneiss Region, Norway: field relations, metamorphic history, and tectonic significance; Journal of Metamorphic Geology, v. 31, p. 147-163.

Caddick, M.J., Bickle, M.J., Harris, N.B.W., Holland, T., Horstwood, M.S.A., Parrish, R.R. and Ahmad, T., 2007. Burial and exhumation history of a Lesser Himalayan schist: Recording the formation of an inverted metamorphic sequence in NW India; Earth and Planetary Science Letters, v. 264, 375-390.

Carswell, D.A., Bruckner, H.K., Cuthbert, S.J., Mehta, K., and O'Brien, P.J., 2003. The timing of stabilization and exhumation rate for ultrahigh-pressure rocks in the Western Gneiss Region of Norway; Journal of Metamorphic Geology, v. 21, p. 601-612.

Chatterjee, N.D., Froese, E., 1975. A thermodynamic study of pseudo-binary join muscovite-paragonite in the system $KAlSi_3O_8$-$NaAlSi_3O_8$-Al_2O_3-SiO_2-H_2O; American Mineralogist, v. 60, p. 985-993.

Chopin, C., 1984. Coesite and pure pyrope in high-grade blueschists of the western Alps: a first record and some consequences; Contributions to Mineralogy and Petrology v. 86, p. 107-118.

Chopin, C., 2003. Ultrahigh-pressure metamorphism: tracing continental crust into the mantle; Earth and Planetary Science Letters, v. 212, p. 1-14.

Clift, P., and Vannucchi, P., 2004. Controls on tectonic accretion versus erosion in subduction zones: Implications for the origin and recycling of the continental crust; Reviews of Geophysics, v. 42.

Coleman, R.G., Lee, D.E., Beatty, L.B., and Brannock, W.W., 1965. Eclogites and eclogites - their differences and similarities; Geological Society of America Bulletin, v. 76, p. 483-508.

Colpron, M., 2006. Tectonic assemblage map of Yukon-Tanana and related terranes in Yukon and northern British Columbia (1:1,000,000 scale); Yukon Geologic Survey, Open File 2006-1.

Colpron, M., Nelson, J.L., and Murphy, D.C., 2006a. A tectonostratigraphic framework for the pericratonic terranes of the northern Canadian Cordillera; in: Paleozoic Evolution and Metallogeny of Pericratonic Terranes at the Ancient Pacific Margin of North America, Canadian and Alaskan Cordillera, (ed.) Colpron, M., and Nelson, J.L.; Canadian Geologic Survey, Special Paper 45, p. 1-23.

Colpron, M., Mortensen, J.K., Gehrels, G.E., and Villeneuve, M., 2006b. Basement complex, Carboniferous magmatism and Paleozoic deformation in Yukon-Tanana terrane of central Yukon: Field, geochemical and geochronological constraints from Glenlyon map area; in: Paleozoic Evolution and Metallogeny of Pericratonic Terranes at the Ancient Pacific Margin of North America, Canadian and Alaskan Cordillera, (ed.) Colpron, M., and Nelson, J.L.; Geological Association of Canada, Special Paper 45, p. 131-151.

Colpron, M., Nelson, J.L., and Murphy, D.C., 2007. Northern Cordilleran terranes and their interactions through time; GSA Today, v. 17, p. 4-10.

Connolly, J.A.D., 2005. Computation of phase equilibria by linear programming: A tool for geodynamic modeling and its application to subduction zone decarbonation; Earth and Planetary Science Letters v. 236, p. 524-541.

Corfu, F., Hanchar, J.M., Hoskin, P.W.O., and Kinny, P., 2003. Atlas of zircon textures; in (ed.) Hanchar, J.M., and Hoskin, P.W.O.; Reviews in Mineralogy and Petrology, Zircon, Volume 53, p. 469-500.

Creaser, R.A., Erdmer, P., Stevens, R.A., and Grant, S.L., 1997. Tectonic affinity of Nisutlin and Anvil assemblage strata from the Teslin tectonic zone, northern Canadian Cordillera; Constraints from neodymium isotope and geochemical evidence; Tectonics, v. 16, p. 107-121.

Creaser, R.A., Goodwin-Bell, J.A.S., and Erdmer, P., 1999. Geochemical and Nd isotopic constraints for the origin of eclogite protoliths, northern Cordillera: implications for the Paleozoic tectonic evolution of the Yukon-Tanana terrane; Canadian Journal of Earth Sciences, v. 36, p. 1697-1709.

Dale, J., Holland, T. and Powell, R., 2000. Hornblende-garnet-plagioclase thermobarometry: a natural assemblage calibration of the thermodynamics of hornblende; Contributions to Mineralogy and Petrology, v. 140, p. 353-362.

Devine, F., Carr, S.D., Davis, W.J., Smith, S., and Villeneuve, M., 2006. Geochronological and geochemical constraints on the origin of the Klatsa metamorphic complex: Implications for Early Mississippian high-pressure metamorphism within Yukon-Tanana terrane; in: Paleozoic Evolution and Metallogeny of Pericratonic Terranes at the Ancient Pacific Margin of North America, Canadian and Alaskan Cordillera, (ed.) Colpron, M., and Nelson, J.L.; Canadian Geological Association, Special Paper 45, p. 107-130.

Dusel-Bacon, C., Hopkins, M.J., Mortensen, J.K., Dashevsky, S.S., Bressler, J.R., and Day, W.C., 2006. Paleozoic tectonic and metallogenic evolution of the pericratonic rocks of east-central Alaska and adjacent Yukon; in: Paleozoic Evolution and Metallogeny of Pericratonic Terranes at the Ancient Pacific Margin of North America, Canadian and Alaskan Cordillera, (ed.) Colpron, M., and Nelson, J.L.; Canadian Geological Association, Special Paper 45, p. 25-74.

Enami, M., 1998. Pressure-temperature path of Sanbagawa prograde metamorphism deduced from grossular zoning of garnet; Journal of Metamorphic Geology, v. 16, p. 97-106.

Erdmer, P., 1987. Blueschist and eclogite in mylonitic allochthons, Ross River and Watson Lake areas, southeastern Yukon; Canadian Journal of Earth Sciences, v. 24, p. 1439-1449.

Erdmer, P., 1992. Eclogitic rocks of the St. Cyr klippe, Yukon, and their tectonic significance; Canadian Journal of Earth Sciences, v. 29, p. 1296-1304.

Erdmer, P., and Helmstaedt, H., 1983. Eclogite from central Yukon - a record of subduction at the western margin of ancient North America; Canadian Journal of Earth Sciences, v. 20, p. 1389-1408.

Erdmer, P., and Armstrong, R.L., 1989. Permo-Triassic isotopic dates for blueschist, Ross River area, Yukon; in: Yukon Geology, Volume 2, Exploration and Geological Services Division, Yukon, Indian and Northern Affairs Canada, p. 33-36.

Erdmer, P., Ghent, E., Archibald, D., and Stout, M., 1998. Paleozoic and Mesozoic high-pressure metamorphism at the margin of ancestral North America in central Yukon; Geological Society of America Bulletin, v. 110, p. 615-629.

Ernst, W.G., 1988. Tectonic history of subduction zones inferred from retrograde blueschist P-T paths; Geology, v. 16, p. 1081-1084.

Ernst, W.G., 2001. Subduction, ultrahigh-pressure metamorphism, and regurgitation of buoyant crustal slices - implications for arcs and continental growth; Physics of the Earth and Planetary Interiors, v. 127, p. 253-275.

Ernst, W.G., 2005. Alpine and Pacific styles of Phanerozoic mountain building: subduction-zone petrogenesis of continental crust; Terra Nova, v. 17, p. 165-188.

Ernst, W.G., 2006. Preservation/exhumation of ultrahigh-pressure subduction complexes; Lithos, v. 92, p. 321-335.

Ernst, W.G., 2010. Subduction-zone metamorphism, calc-alkaline magmatism, and convergent-margin crustal evolution; Gondwana Research, v. 18, p. 8-16.

Evans, B.W., Hattori, K., and Baronnet, A., 2013. Serpentinite: What, Why, Where?; Elements, v. 9, p. 99-106.

Fallas, K.M., 1997. Preliminary constraints on the structural and metamorphic evolution of the St. Cyr Klippe, south-central Yukon; LITHOPROBE Slave-Northern Cordillera Lithospheric Evolution (SNORCLE) Transect Meeting Report, March 7-9, 1997, University of Calgary, v. 56, p. 90-95.

Fallas, K.M., Erdmer, P., Archibald, D.A., Heaman, L.M., and Creaser, R.A., 1998. The St. Cyr Klippe, south-central Yukon: an outlier of the teslin tectonic zone?; LITHOPROBE Slave-Northern Cordillera Lithospheric Evolution (SNORCLE) Transect Meeting Report, March 6-8, 1998, Simon Fraser University, p. 131-138.

Fallas, K.M., Erdmer, P., Creaser, R.A., Archibald, D.A., and Heaman, L.M., 1999. New terrane interpretation for the St. Cyr Klippe, south-central Yukon; LITHOPROBE Slave-Northern Cordillera Lithospheric Evolution (SNORCLE) Transect Meeting Report, March 5-7, 1999, University of Calgary, v. 69, p. 130-137.

Faryad, S. W., Jedlicka, R., and Collett, S., 2013. Eclogite facies rocks of the Monotonous unit, clue to Variscan suture in the Moldanubian Zone (Bohemian Massif); Lithos, v. 179, p. 353-363.Fuhrman, M.L., Lindsley, D.H., 1988. Ternary-feldspar modeling and thermometry; American Mineralogist v. 73, p. 201-215.

Fuhrman, M.L., and Lindsley, D.H., 1988. Ternary-feldspar modeling and thermometry; American Mineralogist, v. 73, p. 201-215.

Gareau, S.A. and Woodsworth, G.J., 2000. Yukon-Tanana terrane in the Scotia-Quaal belt, Coast Plutonic Complex, central-western British Columbia; in: Tectonics of the Coast Mountains in SE Alaska and Coastal British Columbia (ed.) Stowell, H.H. and McClelland, W.C., Geological Society of America, Special Paper, v. 343, p. 23-43.

Gerya, T., and Stockhert, B., 2006. Two-dimensional numerical modeling of tectonic and metamorphic histories at active continental margins; International Journal of Earth Sciences, v. 95, p. 250-274.

Ghent, E., and Erdmer, P., 2011. Very high-pressure epidote eclogite from Ross River area, Yukon, Canada, records deep subduction; in: Ultrahigh-Pressure Metamorphism: 25 Years after the Discovery of Coesite and Diamond, (ed.) Dobrzhinetskaya, L.F., Faryad, S.W., Wallis, S. and Cuthbert, S., Elsevier, Burlington, p. 441–457.

Ghent, E., Tinkham, D., and Marr, R., 2009. Lawsonite eclogites from the Pinchi Lake area, British Columbia-new P-T estimates and interpretation; Lithos, v. 109, p. 248-253.Gilotti, J.A., 2013. The Realm of Ultrahigh-Pressure Metamorphism; Elements, v. 9, p. 255-260.

Gilotti, J.A., 2013. The realm of ultrahigh-pressure metamorphism; Elements, v. 9, p. 255-260.

Gilotti, J.A., McClelland, W.C., Petrie, M.B., and van Staal, C., 2013. Interpreting subduction polarity from eclogite-bearing slices in accretionary orogens - a cautionary note from the Yukon-Tanana terrane; Abstracts, Geological Society of America, Annual Meeting, Denver, Colorado.

Gilotti, J.A., McClelland, W.C., and Wooden, J.L., 2014. Zircon captures exhumation of ultrahigh-pressure terrane, north-east Greenland Caledonides; Gondwana Research, v. 25, p. 235-256.

Godard, G., 2001. Eclogites and their geodynamic interpretation: a history; Journal of Geodynamics v. 32, p. 165-203.

Harley, S.L., and Carswell, D.A., 1990. Experimental studies on the stability of eclogite facies mineral paragenesis; in: Eclogite Facies Rocks (ed.) Carswell, D.A.: New York, Chapman and Hall, p. 53-82.

Hacker, B.R., Andersen, T.B., Root, D.B., Mehl, L., Mattinson, J.M., and Wooden, J.L., 2003. Exhumation of high-pressure rocks beneath the Solund Basin, Western Gneiss Region of Norway; Journal of Metamorphic Geology, v. 21, p. 613-629.

Hacker, B.R., Gerya, T.V., and Gilotti, J.A., 2013. Formation and Exhumation of Ultrahigh-Pressure Terranes; Elements, v. 9, p. 289-293.

Hansen, V.L., 1992. P-T evolution of the Teslin suture zone and Cassiar tectonites, Yukon, Canada: evidence for A- and B-type subduction; Journal of Metamorphic Geology, v. 10, p. 239-263.

Hawthorne, F.C., Oberti, R., Harlow, G.E., Maresch, W.V., Martin, R.F., Schumacher, J.C., and Welch, M.D., 2012. Nomenclature of the amphibole supergroup; American Mineralogist, v. 97, p. 2031-2048.

Hermann, J. and Rubatto, D., 2003. Relating zircon and monazite domains to garnet growth zones: age and duration of granulite facies metamorphism in the Val Malenco lower crust; Journal of Metamorphic Geology, v. 21, p. 833-852.

Holland, T.J.B., Powell, R., 1998. An internally consistent thermodynamic data set for phases of petrological interest; Journal of Metamorphic Geology, v. 16, p. 309-343.

Holland, T., Baker, J., Powell, R., 1998. Mixing properties and activity-composition relationships of chlorites in the system MgO-FeO-Al_2O_3-SiO_2-H_2O; European Journal of Mineralogy, v. 10, p. 395-406.

Holland, T. and Powell, R., 2011. An improved and extended internally consistent thermodynamic dataset for phases of petrological interest, involving a new equation of state for solids; Journal of Metamorphic Geology, v. 29, p. 333-383.

Hoskin, P.W.O., and Schaltegger, U., 2003. The composition of zircon and igneous and metamorphic petrogenesis; in (ed.) Hanchar, J.M., and Hoskin, P.W.O., Reviews in Mineralogy and Petrology, Zircon, v. 53, p. 27-62.

Isard, S.J., 2014. Origin of the Tower Peak unit, St. Cyr area, Canadian Cordillera [MS thesis]; Iowa City, University of Iowa, 130 p.

Isard, S.J., and Gilotti, J.A., 2013. Geology and jade prospects of the northern St. Cyr klippe (NTS 105F/6), Yukon; Yukon Exploration and Geology.

Janak, M., Ravna, E.J.K., and Kullerud, K., 2012. Constraining peak P-T conditions in UHP eclogites: calculated phase equilibria in kyanite- and phengite-bearing eclogite of the Tromso Nappe, Norway; Journal of Metamorphic Geology, v. 30, p. 377-396.

Kleinschmidt, G., Heberer, B., and Laeufer, A.L., 2008. Pre-Alpine sector-zoned garnets in the southeastern Alps; Zeitschrift Der Deutschen Gesellschaft Fur Geowissenschaften, v. 159, p. 565-573.

Korotev, R.L., 1996. A self-consistent compilation of elemental concentration data for 93 geochemical reference samples; Geostandards Newsletter, v. 20, p. 217-245.

Li, Z., and Gerya, T., 2009. Polyphase formation and exhumation of high-to ultrahigh-pressure rocks in continental subduction zone: Numerical modeling and application to the Sulu ultrahigh-pressure terrane in eastern China; Journal of Geophysical Research-Solid Earth, v. 114.

Liou, J.G., Ernst, W.G., Zhang, R.Y., Tsujimori, T., and Jahn, B.M., 2009. Ultrahigh-pressure minerals and metamorphic terranes - The view from China; Journal of Asian Earth Sciences, v. 35, p. 199-231.

Liou, J.G., Zhang, R.Y., Liu, F., Zhang, Z., and Ernst, W.G., 2012. Mineralogy, petrology, U-Pb geochronology, and geologic evolution of the Dabie-Sulu classic ultrahigh-pressure metamorphic terrane, East-Central China; American Mineralogist, v. 97, p. 1533-1543.

Liu, F.L., Liou, J.G., and Xu, Z., 2005. U-Pb SHRIMP ages recorded in the coesite-bearing zircon domains of paragneisses in the southwestern Sulu terrane, eastern China: New Interpretation; American Mineralogist, v. 90, p. 790–800.

Liu, L., Zhang, J., Green, H.W. II, Jin, Z., and Bozhilov, K.N., 2007. Evidence of former stishovite in metamorphosed sediments, implying subduction to > 350 km; Earth and Planetary Science Letters, v. 263, p. 180-191.

Liu, F.L., Gerdes, A., Liou, J.G., and Liu, P.H., 2009. Unique coesite-bearing zircon from allanite-bearing gneisses: U-Pb, REE and Lu-Hf properties and implications for the evolution of the Sulu UHP terrane, China; European Journal of Mineralogy, v. 21, p. 1225-1250.

Liu, F.L., and Liou, J.G., 2011. Zircon as the best mineral for P-T-time history of UHP metamorphism: A review on mineral inclusions and U-Pb SHRIMP ages of zircons from the Dabie-Sulu UHP rocks; Journal of Asian Earth Sciences, v. 40, p. 1-39.

Ludwig, K.R., 2001. Squid 1.02: a user's manual; Berkeley Geochronology Center Special Publication No. 2, Berkeley, USA, 19 p.

Ludwig, K.R., 2003. User's manual for Isoplot 3.00: a geochronological toolkit for Microsoft Excel; Berkeley Geochronology Center Special Publication No. 4, Berkeley, USA, 70 p.

Maruyama, S., 1997. Pacific-type orogeny revisited: Miyashiro-type orogeny proposed; Island Arc 6, p. 91-120.

Maruyama, S., Liou, J.G., and Terabayashi, M., 1996. Blueschists and eclogites of the world and their exhumation; International Geology Review, v. 38, p. 485-594.

Massonne, H.-J., 1999. Experimental aspects of UHP metamorphism in pelitic systems; International Geology Review, v. 41, p. 623-638.

Massonne, H.-J., 2009. Hydration, dehydration, and melting of metamorphosed granitic and dioritic rocks at high- and ultrahigh-pressure conditions; Earth and Planetary Science Letters, v. 288, p. 244-254.

Massonne, H.-J., 2012. Formation of Amphibole and Clinozoisite-Epidote in Eclogite owing to Fluid Infiltration during Exhumation in a Subduction Channel; Journal of Petrology, v. 53, p. 1969-1998.

Massonne, H.-J., 2013. Constructing the Pressure-Temperature Path of Ultrahigh-Pressure Rocks; Elements, v. 9, p. 267-272.

Massonne, H.-J., and Toulkeridis, T., 2012. Widespread relics of high-pressure metamorphism confirm major terrane accretion in Ecuador: A new example from the Northern Andes; International Geology Review, v. 54, p. 67-80.

Massonne, H.-J., Willner, A.P., Gerya, T., 2007. Densities of metapelitic rocks at high to ultrahigh pressure conditions: What are the geodynamic consequences?; Earth and Planetary Science Letters, v. 256, p. 12-27.

Massonne, H.-J., Opitz, J., Theye, T., Nasir, S., 2013. Evolution of a very deeply subducted metasediment from As Sifah, northeastern coast of Oman; Lithos, v. 156, p. 171-185.

Matsumoto, M., Wallis, S., Aoya, M., Enami, M., Kawano, J., Seto, Y., and Shimobayashi, N., 2003. Petrological constraints on the formation conditions and retrograde P-T path of the Kotsu eclogite unit, central Shikoku; Journal of Metamorphic Geology, v. 21, p. 363-376.

Mattinson, J.M., 2010. Analysis of the relative decay constants of U-235 and U-238 by multi-step CA-TIMS measurements of closed-system natural zircon samples; Chemical Geology, v. 275, p. 186-198.

Mottana, A., Carswell, D.A., Chopin, C., and Oberhansli, R., 1990. Eclogite facies mineral paragenesis; in: Eclogite Facies Rocks (ed.) Carswell, D.A.: New York, Chapman and Hall, p. 14-52.

Mazdab, F.K., 2009. Characterization of flux grown trace-element-doped titanite using the high mass resolution ion microprobe (SHRIMP-RG); Canadian Mineralogist, v. 47, p. 813-831.

Mazdab, F.K., and Wooden, J.L., 2006. Trace element analysis in zircon by ion microprobe (SHRIMP-RG): Technique and applications; Geochimica Et Cosmochimica Acta, v. 70.

Meschede, M., 1986. A method of discriminating between different types of mid-ocean ridge basalts and continental tholeiites with the Nb-Zr-Yb diagram; Chemical Geology, v. 56, p. 207-218.

Morimoto, N., 1989. Nomenclature of pyroxenes; Canadian Mineralogist, v. 27, p. 143-156.

Mortensen, J.K., 1990. Geology and U-Pb geochronology of the Klondike District, west-central Yukon Territory; Canadian Journal of Earth Sciences, v. 27, p. 903-914.

Mortensen, J.K., 1992. Pre-mid-Mesozoic tectonic evolution of the Yukon-Tanana terrane, Yukon and Alaska; Tectonics, v. 11, p. 836-853.

Murphy, D.C., Mortensen, J.K., Piercey, S.J., Orchard, M.J., and Gehrels, G.E., 2006. Mid-Paleozoic to early Mesozoic tectonostratigraphic evolution of the Yukon-Tanana and Slide Mountain terranes and affiliated overlap assemblages, Finlayson Lake massive sulphide district, southeastern Yukon; in: Paleozoic Evolution and Metallogeny of Pericratonic Terranes at the Ancient Pacific Margin of North America, Canadian and Alaskan Cordillera, (ed.) Colpron, M., and Nelson, J.L.; Geological Association of Canada, Special Paper 45, p. 75-105.

Nelson, J.L., 1993. The Sylvester allochthon: Upper Paleozoic marginal-basin and island-arc terranes in northern British Columbia; Canadian Journal of Earth Sciences, v. 30, p. 631-643.

Nelson, J.L., and Friedman, R., 2004. Superimposed Quesnel (Late Paleozoic-Jurassic) and Yukon-Tanana (Devonian-Mississippian) arc assemblages, Cassiar Mountains, northern British Columbia: Field, U-Pb, and igneous petrochemical evidence; Canadian Journal of Earth Sciences, v. 41, p. 1201-1235.

Nelson, J.L., Colpron, M., Piercey, S.J., Dusel-Bacon, C., Murphy, D.C., and Roots, C.F., 2006. Paleozoic tectonic and metallogenetic evolution of pericratonic terranes in Yukon, northern British Columbia and eastern Alaska; in: Paleozoic Evolution and Metallogeny of Pericratonic Terranes at the Ancient Pacific Margin of North America, Canadian and Alaskan Cordillera, (ed.) Colpron, M., and Nelson, J.L.; Geological Association of Canada, Special Paper 45, p. 323-360.

Nelson, J.L., Colpron, M., and Israel, S., 2013. The Cordillera of British Columbia, Yukon, and Alaska: Tectonics and Metallogeny; Society of Economic Geologists, Inc., Special Publication 17, p. 53-109.

Peacock, S.M., 1987. Creation and preservation of subduction-related inverted metamorphic gradients; Journal of Geophysical Research-Solid Earth and Planets, v. 92, p. 12763-12781.

Peacock, S.M., 1990. Numerical-simulation of metamorphic pressure-temperature-time paths and fluid production in subducting slabs; Tectonics, v. 9, p. 1197-1211.

Pearce, J.A., and Cann, J.R., 1973. Tectonic setting of basic volcanic rocks determined using trace element analysis; Earth and Planetary Science Letters, v. 19, p. 290-300.

Omrani, H., Moazzen, M., Oberhaensli, R., Tsujimori, T., Bousquet, R., and Moayyed, M., 2013. Metamorphic history of glaucophane-paragonite-zoisite eclogites from the Shanderman area, northern Iran; Journal of Metamorphic Geology, v. 31, p. 791-812.

Perchuk, A.L., Gerya, T.V., 2005. Subsidence and exhumation dynamics of eclogites in the Yukon-Tanana terrane, Canadian cordillera: Petrological reconstructions and geodynamic modeling; Petrology v. 13, p. 253-266.

Perchuk, A., Philippot, P., Erdmer, P., Fialin, M., 1999. Rates of thermal equilibration at the onset of subduction deduced from diffusion modeling of eclogitic garnets, Yukon-Tanana terrane, Canada, Geology, v. 27, p. 531-534.

Petrie, M.P., Gilotti, J.A., McClelland, W.C., van Staal, C.R., in preparation-a. Establishing the P-T-t path of eclogites in the St. Cyr imbricate zone, Yukon, Canada.

Petrie, M.P., Gilotti, J.A., McClelland, W.C., van Staal, C., Isard, S.J., in preparation-b. Geologic setting of high-pressure assemblages in the St. Cyr klippe, Yukon-Tanana terrane, Yukon, Canada.

Philpott, J. and Schnetzl, C., 1968. Europium anomalies and genesis of basalt; Chemical Geology, v. 3, p. 5-13.

Piercey, S.J., and Colpron, M., 2009. Composition and provenance of the Snowcap assemblage, basement to the Yukon-Tanana terrane, northern Cordillera: Implications for Cordilleran crustal growth; Geosphere, v. 5, p. 439-464.

Piercey, S.J., Mortensen, J.K., Murphy, D.C., Paradis, S., and Creaser, R.A., 2002. Geochemistry and tectonic significance of alkalic mafic magmatism in the Yukon-Tanana terrane, Finlayson Lake region, Yukon; Canadian Journal of Earth Sciences, v. 39, p. 1729-1744.

Piercey, S.J., Nelson, J.L., Colpron, M., Dusel-Bacon, C., Simard, R.L., and Roots, C.F., 2006. Paleomagmatism and crustal recycling along the ancient Pacific margin of North America, northern Cordillera; in: Paleozoic Evolution and Metallogeny of Pericratonic Terranes at the Ancient Pacific Margin of North America, Canadian and Alaskan Cordillera, (ed.) Colpron, M., and Nelson, J.L.; Geological Association of Canada, Special Publication 45, p. 281-322.

Piercey, S.J., Murphy, D.C., and Creaser, R.A., 2012. Lithosphere-asthenosphere mixing in a transform-dominated late Paleozoic backarc basin: Implications for northern Cordilleran crustal growth and assembly; Geosphere, v. 8, p. 716-739.

Pigage, L.C., 2004. Bedrock geology compilation of the Anvil District (parts of NTS 105K/2, 3, 5, 6, 7 and 11), central Yukon; Yukon Geological Survey, Bulletin 15, 103 p.

Roots, C.F., Nelson, J.L., Simard, R.-L., and Harms, T.A., 2006. Continental fragments, mid-Paleozoic arcs and overlapping late Paleozoic arc and Triassic sedimentary rocks in the Yukon-Tanana terrane of northern British Columbia and southern Yukon; in: Paleozoic Evolution and Metallogeny of Pericratonic Terranes at the Ancient Pacific Margin of North America, Canadian and Alaskan Cordillera, (ed.) Colpron, M., and Nelson, J.L.; Geological Association of Canada, Special Paper 45, p. 153-177.

Rasband, W.S., 1997-2014. ImageJ, U. S. National Institutes of Health, Bethesda, Maryland, USA, http://imagej.nih.gov/ij/

Rubatto, D., 2002. Zircon trace element geochemistry: partitioning with garnet and the link between U-Pb ages and metamorphism; Chemical Geology, v. 184, p. 123-138.

Rubatto, D., and Hermann, J., 2007. Zircon behavior in deeply subducted rocks; Elements, v. 3, p. 31-35.

Rumble, D., Wang, Q.C., and Zhang, R.Y., 2000. Stable isotope geochemistry of marbles from the coesite UHP terrains of Dabieshan and Sulu, China; Lithos, v. 52, p. 79-95.

Schaltegger, U., Fanning, C.M., Gunther, D., Maurin, J.C., Schulmann, K. and Gebauer, D., 1999. Growth, annealing and recrystallization of zircon and preservation of monazite in high-grade metamorphism: conventional and in-situ U-Pb isotope, cathodoluminescence and microchemical evidence; Contributions to Mineralogy and Petrology, v. 134, p. 186-201.

Schertl, H.P., and Sobolev, N.V., 2013. The Kokchetav Massif, Kazakhstan: "Type locality" of diamond-bearing UHP metamorphic rocks; Journal of Asian Earth Sciences, v. 63, p. 5-38.

Shirahata, K., and Hirajima, T., 1995. Chemically sector-zoned garnet in Sanbagawa schists: its mode of occurrence and growth timing; Journal of Mineralogy, Petrology and Economic Geology, v. 90, p. 69-79.

Silver, E.A., and Beutner, E.C., 1980. Penrose Conference report: Mélanges; Geology, v. 8, p. 32-34.

Simard, R.L., Dostal, J., and Roots, C.F., 2003. Development of Late Paleozoic volcanic arcs in the Canadian Cordillera: an example from the Klinkit Group, northern British Columbia and southern Yukon; Canadian Journal of Earth Sciences, v. 40, p. 907-924.

Smith, D.C., 1984. Coesite in clinopyroxene in the Caledonides and its implications for geodynamics; Nature, v. 310, p. 641–644.

Smith, D.C., 1988. A review of the peculiar mineralogy of he "Norwegian eclogite province," with crystal chemical, petrological, geochemical, and geodynamical notes and an extensive bibliography; in: (ed.) Smith, D.C., Eclogites and Eclogite-Facies Rocks, Elsevier, Amsterdam, pp. 1-206.

Staples, R.D., Gibson, H.D., Berman, R.G., Ryan, J.J., and Colpron, M., 2013. A window into the Early to mid-Cretaceous infrastructure of the Yukon-Tanana terrane recorded in multi-stage garnet of west-central Yukon, Canada; Journal of Metamorphic Geology, v. 31, p. 729-753.

Stipp, M., Stunitz, H., Heilbronner, R., and Schmid, S. M., 2002. The eastern Tonale fault zone: a 'natural laboratory' for crystal plastic deformation of quartz over a temperature range from 250 to 700 degrees C; Journal of Structural Geology, v. 24, no. 12, p. 1861-1884.

Stipska, P., and Powell, R., 2005. Constraining the P-T path of a MORB-type eclogite using pseudosections, garnet zoning and garnet-clinopyroxene thermometry: an example from the Bohemian Massif; Journal of Metamorphic Geology, v. 23, p. 725-743.

Stipska, P., Pitra, P., Powell, R., 2006. Separate or shared metamorphic histories of eclogites and surrounding rocks? An example from the Bohemian Massif; Journal of Metamorphic Geology, v. 24, p. 219-240.

Stipska, P., Chopin, F., Skrzypek, E., Schulmann, K., Pitra, P., Lexa, O., Martelat, J.E., Bollinger, C., and Zackova, E., 2012. The juxtaposition of eclogite and mid-crustal rocks in the Orlica-Snieznik Dome, Bohemian Massif; Journal of Metamorphic Geology, v. 30, p. 213-234.

Sun, S.-s., and McDonough, W.F., 1989. Chemical and isotopic systematics of oceanic basalts: implications for mantle composition and processes; Geological Society, London, Special Publications, v. 42, p. 313-345.

Tempelman-Kluit, D.J., 1977. Quiet Lake (105F) and Finlayson Lake (105G) map areas, Yukon; Geological Survey of Canada, Open File 486, map scale 1:250,000.

Tempelman-Kluit, D.J., 1979. Transported cataclasite, ophiolite and granodiorite in Yukon: evidence of arc-continent collision; Geological Survey of Canada, Paper, Volume 79-14, p. 27.

Tempelman-Kluit, D.J., 2012. Geology of Quiet Lake and Finlayson Lake map areas, south-central Yukon - An early interpretation of bedrock stratigraphy and structure; Geological Survey of Canada, Open File 5487.

von Huene, R., Ranero, C.R., and Vannucchi, P., 2004. Generic model of subduction erosion; Geology, v. 32, p. 913-916.

Wain, A., 1997. New evidence for coesite in eclogite and gneisses: Defining an ultrahigh-pressure province in the Western Gneiss Region of Norway; Geology, v. 25, p. 927-930.

Wang, X., and Liou, J.G., 1991. Regional ultrahigh-pressure coesite-bearing eclogitic terrane in central China: Evidence from country rocks, gneiss, marble, and metapelites; Geology, v. 19, p. 933–936.

Wanless, R.K., Stevens, R.D., Lachance, G.R., Delabio, R.N., 1978. Age determinations and geological studies: K-Ar isotopic ages; Report 13, Geological Survey of Canada Paper 77-2.

Warren, C.J., and Waters, D.J., 2006. Oxidized eclogites and garnet-blueschists from Oman: P-T path modeling in the NCFMASHO system; Journal of Metamorphic Geology, v. 24, p. 783-802.

Wei, C.J., Powell, R., 2004. Calculated phase relations in high-pressure metapelites in the system NKFMASH (Na_2O-K_2O-FeO-MgO-Al_2O_3-SiO_2-H_2O); Journal of Petrology, v. 45, p. 183-202.

Wheeler, J.O., and McFeely, P., 1991. Tectonic map of the Canadian Cordillera and adjacent parts of the USA; Geological Society of Canada, A Series Map 1712A.

Wheeler, J.O., Brookfield, A.J., Gabrielse, H., Monger, J.W.H., Tipper, H.W., and Woodsworth, G.J., 1991. Terrane map of the Canadian Cordillera; Geological Survey of Canada, Map 1713A, 1:2,000,000.

Whitney, D. L., and Davis, P. B., 2006, Why is lawsonite eclogite so rare? Metamorphism and preservation of lawsonite eclogite, Sivrihisar, Turkey: Geology, v. 34, p. 473-476.

Whitney, D.L., and Evans, B.W., 2010. Abbreviations for names of rock-forming minerals; American Mineralogist, v. 95, p. 185-187.

Williams, I.S., 1998. U-Th-Pb geochronology by ion microprobe; in: Applications of Microanalytical Techniques to Understanding Mineralizing Processes, Review in Economic Geology (eds McKibben, M.A., Shanks, I. and Ridley, W.I.), p. 1-35.

Zeh, A. and Millar, I.L., 2001. Metamorphic evolution of garnet-epidote-biotite gneiss from the Moine Supergroup, Scotland, and Geotectonic Implications; Journal of Petrology, v. 42, v. 529-554.

Zhang, R.Y., Hirajima, T., Banno, S., Cong, B., and Liou, J.G., 1995. Petrology of ultrahigh-pressure rocks from the southern Sulu region, eastern China; Journal of Metamorphic Geology, v. 13, p. 659–675.

Zhang, R.Y., Liou, J.G., and Ernst, W.G., 2009. The Dabie-Sulu continental collision zone: A comprehensive review; Gondwana Research, v. 16, p. 1-26.

Zhang, R.Y., Liou, J.G., Omori, S., Sobolev, N.V., Shatsky, V.S., Iizuka, Y., Lo, C.H., and Ogasawara, Y., 2012. Tale of the Kulet eclogite from the Kokchetav Massive, Kazakhstan: Initial tectonic setting and transition from amphibolite to eclogite; Journal of Metamorphic Geology, v. 30, p. 537-559.

Zhang, R.Y., Lo, C.H., Chung, S.L., Grove, M., Omori, S., Iizuka, Y., Liou, J.G., and Tri, T.V., 2013. Origin and Tectonic Implication of Ophiolite and Eclogite in the Song Ma Suture Zone between the South China and Indochina Blocks; Journal of Metamorphic Geology, v. 31, p. 49-62.

Zhang, R.Y., Liou, J.G. and Ernst, W.G., 2009. The Dabie-Sulu continental collision zone: A comprehensive review. Gondwana Research v. 16, p. 1-26.